Hypersonic Laminar-Turbulent Transition on Circular Cones and Scramjet Forebodies

Progress in Aerospace Sciences, vol. 40, no. 1-2, Feb. 2004, pp. 1-50.
Final printed version available from www.sciencedirect.com

Steven P. Schneider*
School of Aeronautics and Astronautics
Purdue University
West Lafayette, IN 47907-1282

Revised version, November 13, 2003

Abstract

Laminar-turbulent transition in hypersonic boundary layers has a dramatic effect on heat transfer, skin friction, and separation. This effect is critical to reentry vehicles and airbreathing cruise vehicles, yet the physics of the transition process is not yet well enough understood to be used for predictive purposes. The literature for transition on circular cones and scramjet forebodies is reviewed, from an experimental point of view. Ground experiments, emphasized here, nearly always suffer from ambiguity caused by operating in the presence of high levels of facility noise. Measurements of the instabilities leading to transition reduce much of this ambiguity, and thus these instability measurements are emphasized. A number of transition measurements have also provided good control of extraneous effects, and several of these measurements are compared in detail.

Small bluntness always delays transition on smooth cones at zero angle of attack, while large bluntness creates a change in mechanism that again moves transition forwards. For smooth cones at angle of attack with small or negligible bluntness, transition is always leeside-forward and windside-aft,

*Associate Professor. Associate Fellow, AIAA.

although the movement with angle of attack is tunnel and geometry dependent. For cones with large bluntness, transition becomes windside forward and leeside aft. In both cases, nosetip roughness may be involved in the trend reversal. Reliable prediction of the trend reversal conditions is one of many topics requiring additional research. The limited existing database for transition on scramjet-vehicle forebodies is also reviewed, along with the literature for transition in the compression corners that are often a part of such forebody designs.

Contents

1 Nomenclature

AOA	angle of attack
e^N	integrated amplification of instabilities from onset to transition; a common correlating parameter
$F = \omega\nu_e/U_e^2$	nondimensional frequency
k	roughness height
L	body length, generally along surface
M_e	Mach number at the boundary layer edge
M_∞	Freestream Mach number
P_t	total pressure
r_n or R_N	nose radius
Re_b	Reynolds number based on freestream conditions and average leading edge thickness
Re_k	Reynolds number based on conditions in the undisturbed boundary layer at the roughness height, $Re_k = U_k\rho_k k/\mu_k$
Re_R	Reynolds number based on nose radius
Re_T	Reynolds number at transition, based on arc length from the leading edge, and local conditions at the boundary layer edge. May be onset or end, depending on the source
$(Re_t)_\delta$	Reynolds number based on the end of transition and local edge conditions
$Re_{T,s}$	Re_T for the smooth-wall case
Re/m	unit Reynolds number per meter, usually in the freestream
Re_∞	freestream unit Reynolds number
Re_e	unit Reynolds number at the boundary layer edge
s	arc length along surface from stagnation point
RV	reentry vehicle
T_e	temperature at the boundary layer edge
T_t	stagnation temperature
T_w	wall temperature
T_{aw}	adiabatic wall temperature
x	streamwise distance along surface from stagnation point
x_k	streamwise distance to roughness element
x_s	streamwise location of the tip of the cone, cm
X_{onset} or x_T	arc length to transition onset
X_{end}	arc length to end of transition
z, ZA	height above wall
α	angle of attack, deg.
$\delta_k^\star$	displacement thickness at roughness element
$\nu = \mu/\rho$	kinematic viscosity
θ_c	half angle of cone, deg.

2 Introduction

2.1 Aerothermal Design Issues

Laminar-turbulent transition in high-speed boundary layers is important for prediction and control of heat transfer, skin friction, and other boundary layer properties, yet the mechanisms leading to transition are still poorly understood [1]. The Defense Science Board found that boundary-layer transition was one of two technical areas which needed further development before a demonstrator version of the National Aerospace Plane could be justified [2]. Other applications hindered by this lack of understanding include ballistic and lifting reentry vehicles [3, 4, 5], high-speed missiles ([6], [7]), and high-speed reconnaissance aircraft.

A visual example of Mach-4.3 transition is shown in Fig. 1, which shows a magnified portion of a shadowgraph obtained in the Naval Ordnance Lab ballistics range [8]. The sharp cone model is near zero angle of attack, at a freestream Reynolds number of 2.66×10^6/inch. The previously unpublished image is from Shot 6728, and the length of the 5-deg. half-angle cone is 9.144 inches [9]. The full photograph was obtained from Dan Reda by Ken Stetson, and is now available from the author. The cone is traveling from left to right through still air. The lower surface boundary layer is turbulent, and acoustic waves radiated from the turbulent eddies can be seen passing downstream at the Mach angle. On the upper surface, the boundary layer is intermittently turbulent, with two turbulent spots being visible in the image, interspersed among laminar regions. Larger waves can be seen in front of the turbulent spots, with smaller levels of acoustic noise being radiated from the turbulence within the spots. The acoustic noise is not present above the laminar regions. Similar phenomena are expected at hypersonic speeds, although suitable images are not at hand.

The high heating rates caused by the turbulence are illustrated in Figure 2, which presents computations and measurements of the surface heat transfer during the Reentry-F test of a ballistic reentry vehicle [10, Figure 8]. The vehicle was a 13-ft. beryllium cone that reentered at a peak Mach number of about 20 and a total enthalpy of about 18 MJ/kg. The cone half-angle was 5-degrees, the angle of attack was near zero, and the graphite nosetip had an initial radius of 0.1 inches [11]. The symbols show the flight data. The computations were carried out using a variable-entropy boundary-layer code that includes equilibrium chemistry effects. They start with laminar flow at the nose, and initiate instantaneous transition at $z/L = 0.625$, to give best agreement with the flight data. Here z is the axial distance along the cone, and

L is the cone length. Agreement is good for both the laminar and turbulent regions, once the transition location is known. Harris Hamilton from NASA Langley, who conducted the computations, says that typical accuracies are 20-25% for the turbulent boundary layer, and 15-20% for the laminar layer; error bars are sketched on the figure according to these estimates. Similar results are reported in Ref. [12]. Transition onset causes the rise in heating at $z/L = 0.65$. Present empirical correlations for the onset and extent of transition are uncertain by a factor of 3 or more [11]. Thus, our computational capabilities for laminar and turbulent heating in attached flows are fairly good; the uncertainty in prediction of the overall heating is now often dominated by the uncertainty in predicting the location of transition (depending on other factors such as the altitudes and Reynolds numbers that are of interest). The effect of transition on the thermal protection system also depends on many different design-specific factors (see, for example, Ref. [5]).

Sandia National Laboratory also has considerable experience with the design and testing of hypersonic reentry vehicles. Dave Kuntz from Sandia stated that their experience is similar, although he was not aware of any comparable data that could be released (private communication, March 1999). The uncertainties for transition on boost-glide reentry vehicles are even larger, due to the limited amount of flight data on non-ballistic vehicles [13].

2.2 Boundary-Layer Transition

The transition process is initiated through the growth and development of disturbances originating on the body or in the freestream. Environmental disturbances include atmospheric turbulence, entropy spottiness, particulates, and electrostatic discharges [14]. The receptivity mechanisms by which the disturbances enter the boundary layer are influenced by roughness, waviness, bluntness, curvature, Mach number, and so on. The growth of the disturbances is determined by the instabilities of the boundary layer. These instabilities are in turn affected by all the factors determining the mean boundary layer flow, including Mach number, cross-stream and streamwise curvature, pressure gradient, temperature, and so on [15]. Relevant instabilities include the concave-wall Görtler instability [16], the first and second mode streamwise-instability waves described by Mack [17], and the 3D crossflow instability [18, 19]. The first appearance of turbulence is associated with the breakdown of the instability waves, which is determined by various secondary effects [20]. The local spots of turbulence grow downstream through an intermittently-turbulent region whose length is dependent on the local flow conditions and on the rate at which spots are generated [21]. Only after the turbulent boundary layer has

become fully developed does it appear to become independent of the precise mechanism by which it was formed [22].

In view of the dozens of parameters influencing transition, classical attempts to correlate the transition 'point' with one or two parameters such as Reynolds number and Mach number will necessarily be very limited in accuracy and reliability. Such simple correlations can only work for cases that are highly similar to those previously tested [11]. Even comparisons between transition in different ground-test datasets are usually ambiguous and uncertain, due to variations in the many factors that can affect transition, some of which are often unknown or uncontrolled.

However, for simple shapes the outlook for reliable estimation methods appears promising. For example, for 2D boundary layers, correlations between transition and the integrated growth of the linear instability waves have shown promising agreement with experiment [23]. Although these e^N correlations neglect all receptivity and secondary instability effects, they seem to work fairly well for a variety of conditions where the environmental noise is generally low and most of the wave growth is linear. Initial comparisons to dissimilar flight data are promising [24]. For streamwise-vortex instabilities such as stationary crossflow, the nonlinear parabolized-stability-equation methods may be necessary for a useful first approximation [25].

2.3 Need for Accurate Simulations of the Transition Mechanisms

Reed et al. [26] discuss progress on issues such as instability studies, nose bluntness, and angle-of-attack effects, from theoretical, computational, and experimental points of view. Direct simulations of transition [27] and the recently developed Parabolized Stability Equations [28, 29] have made it possible to compute details of the transition mechanisms and instabilities. However, experimental measurements of these mechanisms are extremely rare in high-speed flows. Experimental work that quantifies not only the location of transition but also the mechanisms involved is needed in order to improve these modern theories, whose accuracy depends on a proper simulation of the transition mechanisms.

Unambiguous progress in characterizing the mechanisms of low-speed transition has been made through the use of low-noise wind tunnels with disturbance levels comparable to those in flight, and the study of the development of controlled perturbations. However, conventional hypersonic wind tunnels suffer from high levels of noise, due to radiation from the turbulent boundary

layers on the nozzle walls. These high noise levels can cause transition to occur at arc-length Reynolds numbers that are an order of magnitude lower than in flight [30, 11]. Within conventional facilities, transition tends to occur later in larger tunnels, and transition Reynolds numbers tend to increase with unit Reynolds number [31, 32, 33].

In addition, the mechanisms of transition that would be observed in small-disturbance environments can be changed or bypassed altogether in high-noise environments; these changes in the mechanisms change the parametric trends in transition [31]. For example, linear instability theory suggests that the transition Reynolds number on a 5 degree half-angle cone should be 0.7 of that on a flat plate, but noisy tunnel data showed that the cone transition Reynolds number was about twice the flat plate result. Only when quiet tunnel results were obtained was the theory verified [34]. The flat plate is anomalously affected by tunnel noise, as compared to the round cone [35]. This can be critical, since design usually involves consideration of the trend in transition when a parameter is varied. Clearly, transition measurements in conventional ground-test facilities are generally not reliable predictors of flight performance, except perhaps for roughness-dominated flows [31].

Measurements of transition location alone provide an incomplete picture, due to a lack of information regarding the cause of transition. Transition data is highly ambiguous in most cases, due in part to these various effects of tunnel noise. Tunnel noise is itself very complex, consisting of vorticity, acoustic, and entropy disturbances, and a Fourier spectrum with all three spatial components [31]. Any change in tunnel configuration or test condition will change tunnel noise, and no two tunnels will have the same noise level. The sensitivity of transition to the details of this tunnel noise remain uncertain and controversial, and even quiet tunnels are not free of noise. Since transition nearly always originates from amplification of this poorly understood tunnel noise, transition measurements nearly always occur under poorly controlled conditions. Transition can also shift due to small, undetected, and poorly controlled factors, such as small angles of attack (for a near-symmetric vehicle) and small surface roughness flaws. Stetson argues that *'one should not expect a transition Reynolds number obtained in any wind tunnel, conventional or quiet, to be directly relatable to flight',* since the wind tunnel cannot duplicate the atmospheric environment or the boundary-layer profiles ([36]; see also [37]). Measurements of the details of the transition processes are needed to sort out these factors, but these instability measurements are much more difficult than transition-location measurements, and so they are seldom carried out.

Despite these difficulties, hypersonic development programs go on, and designers require predictions of transition. Transition measurements in con-

ventional tunnels remain of some use for design, since in nearly all cases they provide a lower bound for transition on a smooth body in flight. Although the extrapolation of these transition data to flight involves a large uncertainty, they are often the only basis for an initial prediction, and limited resources often preclude a more thorough study. With these reservations in mind, transition data will be presented here despite these uncertainties. *However, only the study of controlled disturbances in a controlled quiet environment can produce unambiguous data suitable for development of reliable theory.* Reliable predictive methods will have to be based on estimates of the flight disturbance environment.

The first successful supersonic wind tunnel with low noise at high Reynolds number was developed only in the early 1980's [30, 38], although the JPL supersonic tunnel was running quiet at low Reynolds numbers in the middle 1960's [39]. Development of low-noise facilities has been very difficult, since the test-section wall boundary-layers must be kept laminar in order to avoid high levels of eddy-Mach-wave acoustic radiation from the normally-present turbulent boundary layers. Each nozzle development is a very expensive experiment in supersonic/hypersonic laminar flow control. A Mach 3.5 tunnel was the first to be successfully developed at NASA Langley [40]. Langley then developed a Mach 6 quiet nozzle, which was used as a starting point for a new Purdue nozzle [41, 42]. Unfortunately, this Langley nozzle was removed from service due to a space conflict. It was not immediately reassembled due to the ongoing development of a more capable Mach-8 quiet tunnel [38]; however, this effort was unsuccessful, due in large part to the high temperatures required to reach Mach 8. Since the new Purdue Mach-6 Ludwieg tube is not yet quiet at substantial Reynolds numbers [43], there is at present no operational high-Reynolds-number hypersonic quiet tunnel, anywhere in the world.

2.4 Stability Experiments and Computations

A necessary step in the further development of mechanism-based methods is accurate computation of the actual instability-wave growth. At high speeds, this is a major challenge. At low speeds, such computations were slow to become validated (e.g., Ref. [44]); this validation is more critical at high speeds, where there are many more physical factors whose influence must be properly taken into account. However, even in noisy conventional tunnels, there are few measurements of the instability mechanisms causing transition. Of these instability measurements, few have been carried out with calibrated instruments and well-documented conditions, so that a fairly reliable comparison to computations can be carried out. Rather, existing stability experiments have

mainly served to *discover* the stability phenomena, confirm the fundamental aspects of the theoretical predictions, and supply preliminary quantitative information. While such experiments have been an important step forward, the requirements for *code validation* experiments are much more stringent (e.g. Refs. [45] and [46]). Even for the surface pressure distribution under cold-flow conditions, accurate validated results remain to be obtained [47].

NATO Research and Technology Organization Working Group 10 was an international group organized to evaluate technologies for propelled hypersonic flight. The transition members of NATO RTO Working Group 10 felt that the following elements should be present in code-validation experiments for hypersonic transition [48]:

1. Detailed and reliable measurements of the transition mechanisms.

2. Accurate knowledge of the mean flow. Repeated checks of boundary layer symmetry, instrumentation calibrations, tunnel flow nonuniformity effects, repeatability, etc. Accurate agreement with computation of mean flow. This requires repeated tunnel entries and cooperation between experiments and computations.

3. Linear instability comparisons require calibrated measurements of the fluctuations at a known position in the eigenfunction. It seems possible that these might be carried out in conventional tunnels using ensemble averaging of controlled disturbances.

4. Nonlinear secondary breakdown effects are dependent on small fluctuations combining with the primary instability. It seems doubtful that these can be repeatably and successfully studied except in quiet tunnels, since even controlled secondary disturbances may be swamped by tunnel noise. For similar reasons, receptivity experiments may also require quiet flow.

These specifications are updated from Ref. [49], which gives additional suggestions, and shows the long-term importance of a coordinated approach.

Unfortunately, these specifications are extremely difficult to meet at hypersonic speeds. Although experimental efforts continue (e.g., Ref. [50]), all existing data fall short. Despite these shortcomings, it seems valuable to assess the best existing datasets in detail, as both a determination of the state of the art, and as a means of finding the improvements that are needed.

2.5 Variation in Definitions of Transition Location

Hypersonic transition from fully laminar to fully developed turbulent flow occurs over a finite spatial extent. The arclength from onset to completion can equal the arclength from the nose to onset, so this finite extent can be substantial [51]. However, much of the extant literature reduces the raw data to an analysis of the transition 'point'. In addition, methods of transition detection include surface pitot pressures, surface heat transfer rates, surface temperature distributions, and schlieren and shadowgraph images, to name only the most common. Thus, analyses of the transition 'point' are dependent on the experimental apparatus used, and on the way in which the data were reduced. Pages 153-167 of Ref. [33] compare some 14 different methods of detecting transition 'location'. In general, the beginning of the transitional or intermittent region is near the minimum in the surface pitot pressure or the minimum in the surface heat transfer rate; the middle of the transition region is near the maximum in wall temperature, in sublimation rate, or in hot-wire voltage fluctuations; and the end of transition is near the peak in the surface pitot pressure or surface heat-transfer rate. These generalizations may be problem-specific; see Fig. 4a of Ref. [52] for a case where the peak in heat transfer is only about 2/3 of the way to fully-developed turbulent heating. The variation in definitions of transition 'point' is yet another reason for ambiguity in the comparison of different data sets. In the present paper, an attempt will be made to compare only data obtained using the same method.

2.6 Additional Previous Reviews

A book reviewing the experimental literature has yet to appear, although several books review various aspects of the theory [53, 54, 55]. Good reviews of the early literature appear in Refs. [56] and [57]. Morkovin reviewed the literature several times [58], perhaps most comprehensively in Ref. [59], which contains 345 references and still makes excellent reading even after some 34 years. Most of Pate's results are reviewed in Refs. [33], although the later review in Ref. [60] contains new information, especially about work not done at AEDC. The 1975 report of the transition study group still makes excellent reading, after nearly 3 decades, and much of the work proposed there still remains to be accomplished [49].

2.7 Scope and Organization of Present Review

The general prediction of transition based on simulations of the transition mechanisms is a very complex and difficult problem. There are several known receptivity mechanisms, several different known forms of instability waves, many different parameters that affect the mean flow and therefore modify the stability properties, and many known nonlinear breakdown mechanisms. The parameter space is large, and many papers have been published on the topic. The author's personal collection from 18 years of focused work includes more than 2600 papers on stability or transition, and more than 1000 on the supersonic or hypersonic case. A comprehensive review of the hypersonic case alone would fill a much-needed monograph. In such a complex and extensive field, errors and omissions are inevitable in a work of this type; nevertheless, the author would appreciate having them drawn to his attention so they can be corrected in the future.

The present article will attempt to complement the existing literature by emphasizing experimental work. It will be limited to circular cones and generic scramjet forebodies, and will focus on ground experiments, as data from flight and the ballistic range were reviewed in Ref. [11]. Circular cones are representative of the noses of many types of missiles. The effects of ablation, blowing, and roughness will be treated only in passing. The discussion is generally limited to hypersonic flows, but supersonic data are occasionally included when particularly relevant.

The topics that were selected for discussion could be organized in many different ways. The author has chosen to discuss the stability results before the transition results, because stability precedes transition, as disturbances propagate downstream. The simpler geometries are treated first, followed by those judged to be generally more complex. The reader is assumed to have a general familiarity with introductory material available in previous reviews and in textbooks ([61, Chap. 5],[62, Sec. 7.4.3]).

3 Transition on Circular Cones

The blunt cone at small angle of attack is generic for ballistic reentry vehicles, and may also be generic for hypersonic rocket-powered missiles of shorter range. Considerable flight data exists for ballistic RV's, which makes it possible to compare future prediction methods to flight. Although many transition measurements have been made on sharp and blunt cones at zero angle of attack (AOA), and on sharp cones at AOA, there are not many transition measure-

ments on blunt cones at AOA, and there are few stability measurements, even on sharp cones at zero AOA. Real vehicles always have some bluntness, and always have some non-zero AOA. Although modern computational methods allow taking these factors into account, existing experimental data is insufficient for development and validation.

3.1 Conical Reentry Vehicles

Flight conditions for reentry vehicles involves dissociation and ionization, bluntness and ablation effects, poorly understood roughness effects, and complex wall-temperature distributions [11]. Asymmetric flows are of current interest, for boost-glide and maneuvering applications requiring lift, but most RV's have been nominally symmetric ballistic shapes [63]. Ground-test measurements of transition will not be able to simultaneously simulate all the characteristics of the high-enthalpy flight environment; thus, ground-based experiments must discover and document the transition mechanisms, in order to develop and validate computational models which are then extended to flight conditions [36]. For ground-test measurements of stability, a smooth-wall perfect-gas round cone with small bluntness is a reasonable first approximation. Measurements of the instability waves (or transition mechanisms) are needed under these conditions, for comparison to computation. A number of stability experiments have been carried out for this case. Although all contain significant flaws, a detailed reanalysis of this data was carried out for NATO RTO Working Group 10 (WG 10) [48]. Portions of this work are summarized here, with comparisons to computations reported in the literature, and to limited-accuracy e^N computations carried out by the author.

3.2 Overview of Instability Mechanisms on Circular Cones

For symmetric vehicles, three-dimensional effects may be small, and a cone at zero angle of attack may be a good first approximation. For smooth surfaces, first and second mode instabilities are then expected to dominate [17]. The first mode occurs at lower Mach numbers, is most unstable when oblique, and is damped by wall cooling. The second mode occurs at higher Mach numbers, is at higher frequencies, is most unstable when symmetric (at least in simple cases), and is amplified by wall cooling. All real vehicles are at least somewhat blunt. Bluntness brings in the effect of the entropy layer shed by the curved bow shock; this entropy layer is eventually swallowed by the boundary layer as it grows downstream [64]. Bluntness is often discussed in terms of the swallowing length, which is the distance downstream where the variations in

streamline entropy caused by passage through the curved bow shock are nearly completely swallowed by the boundary layer. Bluntness lowers the edge Mach number, which tends to favor the first mode instability.

The Reentry F flight test represents a somewhat simplified example, with a hypervelocity 5-deg. half-angle non-ablating beryllium frustum at nearly zero angle of attack [65]. The instabilities of this flow were computed by Malik, who showed that the 2nd-mode instability was dominant [66]. Malik found $N = 7.5$ for this case, suggesting that the 2nd mode could reasonably account for the observed transition location. Malik later reported additional computations related to Sherman's reentry experiments with 22-deg. half-angle beryllium cones [67, 68]. In Ref. [24], using different assumptions, Malik computed $N = 11.3$ for Sherman's data and $N = 9.6$ for the Reentry-F data, both based on dominant 2nd-mode instabilities. The near-agreement in N factor is encouraging, since the transition Reynolds numbers differ by an order of magnitude between the two flights. Malik also provided a possible explanation for the low transition Reynolds numbers observed by Sherman, which may have been caused by rapid wave growth due to the low edge Mach number and the very cold wall.

The simplest example of a lifting reentry vehicle is a cone at angle of attack. Angle of attack brings in two major new effects. The first effect is the thinning of the windward boundary layer and the thickening of the leeward boundary layer, due to the crossflow of low momentum fluid from windward to leeward. This thins and stabilizes the windward boundary layer, and thickens and destabilizes the leeward boundary layer. The effect is not simple, for Reynolds number, entropy-layer swallowing, and boundary layer thickness change along with the profiles. The second effect is the crossflow itself; the crossflow reaches a maximum about 2/3 of the way around the body from the wind to the lee rays, and is itself unstable to either stationary or traveling waves [18]. Roughness is more likely to have an effect in the thinner boundary layers on the windward side, but roughness is here treated only in passing.

3.3 Computations on Cones Using Approximate Methods

Several of the experimental flows were computed by the author using fairly elementary methods that are commonly available to nonspecialists. The inviscid axisymmetric flows were computed by Sandia National Labs and provided by Dr. Dave Kuntz. The `2IT` code was used to compute the inviscid

nosetip flow [69]. This code solves the unsteady Euler equations using a time-dependent, finite-difference technique, with the cylindrical flowfield mapped into a computational domain. The technique is shock-fitting in nature, with the characteristic compatibility relations invoked at the bow shock and impermeable surface boundaries. MacCormack's explicit scheme is used to integrate the governing equations, producing a solution technique which is second order in both time and space. The solution is converged in time to produce both a steady-state flowfield solution on the spherical nosetip and an initial data plane for the afterbody code.

The afterbody flowfield, surface pressure, and shock shape, were solved with the SANDIAC code [70], an extension of the GE-3IS-SCM/ACM code [71, 72, 73]. This code is also shock fitting, and solves the steady, two or three dimensional Euler and conservation of energy equations. A cylindrical based coordinate system transformed to a computational space is used to allow computations on an equally spaced grid. The difference equations are integrated by the Beam-Warming modified upwind MacCormack scheme [74] using the Van Leer flux vector splitting scheme [75]. Characteristic compatibility relations are also used to compute the surface pressure.

The shock shape and surface-pressure distribution were provided to the Harris finite-difference code [76]. This code is second-order accurate, and can include a first-order correction for variable entropy. In the first iteration, the boundary layer is computed as if the stagnation streamline wetted the entire body. Using conservation of mass, the code then traces streamlines upstream from where they enter the boundary layer to where they pass through the shock. The shock angle at this point is used to compute the entropy and total pressure on the streamline, downstream. In the second iteration, this variable entropy is used in a new edge condition, to recompute the boundary layer. Although it is well known that this will not give the correct boundary-layer profile in the outer region (Julius Harris, private communication, Sept. 1991 and Ref. [77]), this code is fairly easy to use and readily available. This code runs in a few seconds on a 400MHz Pentium II.

Unfortunately, the computations based on the first-order Harris code showed poor agreement with the Stetson blunt-cone experiments, as will be discussed in Section 5.2.3. Improved computations are needed, using viscous-shock-layer methods [78, 79], parabolized Navier-Stokes methods, second-order boundary-layer theory, thin-layer Navier-Stokes methods, or full Navier-Stokes methods [80].

The boundary-layer profiles from the Harris code were then supplied to the e^{MALIK} code for computation of instability waves [81, 82]. This code solves for compressible parallel-flow linear instability, including transverse curvature

effects. An automated system that links these codes was previously developed (e.g., Ref. [83]). The stability code can run several frequencies along the length of a cone in a few hours on the second processor of a dual-Pentium-II 400MHz PC. This speed is sufficient for design purposes, if a suitably validated code can be developed. See Ref. [84] for one recent effort towards developing a user-friendly stability-based transition-prediction code.

4 Sharp Cones at Zero Angle of Attack

4.1 Instability Measurements

Stability measurements have been carried out on sharp cones since the 1970's (earlier hypersonic measurements were on flat plates). Demetriades reported measurements on 4 and 5-deg. half-angle cones at Mach 8 in Tunnel B at AEDC [85, 86]. Hot wires were used to measure second-mode instabilities. Kendall also made hot-wire measurements of instabilities on a 4-deg. half-angle cone at Mach 8.5. Amplification rates were compared to theory and showed a dominance of the second mode [87]. Another effort was carried out by Stetson and Donaldson at Mach 8. Hot-wire measurements on a 7-deg. half-angle near-adiabatic sharp cone [88] were followed by measurements on a cooled cone [89] and by measurements at Mach 6 [90, 91]. A fourth major effort was carried out at NASA Langley in the Mach-6 quiet tunnel. Zero angle-of-attack sharp-cone instability measurements are reported by Lachowicz et al. [92] with cooled-cone measurements being reported by Blanchard et al. [93]. Finally, Russian stability measurements have recently been extended to Mach 6, although most of these have been performed with blunt cones [50]. Experiments of this type are extremely difficult, and all these examples fall short of code-validation quality. Two of the most complete studies will be discussed in detail here [48].

4.2 Instability on a Sharp Cone at Mach 8

4.2.1 General Information

Stetson et al. carried out calibrated measurements of instability wave growth on several conical models in AEDC Tunnel B at Mach 8, during the late 1970's and early 1980's [88, 64]. Detailed hot-wire measurements were carried out in this expensive production tunnel by J. Donaldson, under the direction of K. Stetson [94, 95]. The experiments were focused on the hypersonic second-mode instability, which is likely to be dominant on smooth convex nearly-symmetric

geometries with small crossflow. Although these are conventional-tunnel measurements with high ambient noise, the good-quality detailed measurements appear to deserve further computational comparisons. Detailed measurements of the disturbances in this tunnel are available [96].

The model was a 7-degree half-angle cone with a 40-inch (1.016-m) length and a sharp 0.0015-inch (38 micron) nose radius. The cone angle of attack was zero, to within the accuracy with which this could be set and measured. The model was in thermal equilibrium, but heat conduction within the model was not negligible.

Most of the measurements were carried out at a freestream Mach number of 7.95, with a total pressure of 225 psia (1.55 MPa) and a total temperature of 1310 R (728 K). Measurements were carried out with surface pressure taps (24) and thermocouples (32). Mean-flow profiles were obtained using pitot-pressure and total temperature probes. Instability-wave spectra were obtained using calibrated constant-current hot-wire anemometry. Hot-wire measurements were recorded at one-inch (2.54-cm) intervals between 10 and 37 inches (25.4 and 94.0 cm), using a single hot-wire with a single calibration. The measurements were obtained only along a single ray, and only at the height above the wall where the broadband amplitude is a maximum. Stetson has expressed concern that a single wire cannot measure any three-dimensional effects that may be present (pp. 14-15 of Ref. [64]).

Growth of first and second-mode instability waves was observed under cold-flow conditions. The second-mode instability was dominant. Second-harmonic amplification was observed downstream, a good indication of nonlinear effects. A comparison of the second-harmonic amplification rate to a nonlinear computation would be interesting.

Although Stetson [88] published a summary of these experiments, extensive tabulated data for the mean flow remained unpublished, along with extensive tabulations of the instability spectra for both uncalibrated and calibrated fluctuations. These data were provided courtesy of Roger Kimmel and have been entered into electronic form [48]; they are available from Kimmel or the author.

The amplification rates reported by Stetson et al. [88] were obtained by curve-fitting and differentiating the experimental spectral-amplitude data. Although most of the past comparisons to computation made use of these amplification rates, differentiation of experimental data is a notoriously uncertain process which can introduce substantial errors. It is recommended that future comparisons should instead be made by integrating the computed amplification rates and comparing amplitude ratios between computation and experiment. This more-accurate process is now possible, due to the availability of the tabulated spectral amplitudes.

4.2.2 Previous Computational Comparisons

Mack carried out the first set of detailed comparisons to this experiment [97, 98]. Three methods were used to obtain the mean-flow profiles: 1) transformed flat-plate profiles, 2) cone profiles from the axisymmetric boundary-layer equations, without the transverse curvature term, and 3) like (2), but with the transverse curvature term. The wall was assumed adiabatic. Preliminary computations including the effect of the experimental surface-temperature gradient are reported to show only minor effects. The stability was analyzed using parallel-flow linear instability theory. Locally planar flow is assumed in the stability analysis. Mack uses the Sutherland viscosity law down to 110.4K, and a linear law below this (see also p. 57 of Ref. [17], where this law is stated without justification; for justification see Ref. [99]).

The effect of total temperature was found to be significant. The effect of transverse curvature was small (7% for one amplification rate). At $R = 1730$, the measured frequency of the maximum amplification rate was less than 10% higher than the computation. However, the computed amplification rate is about 50% higher than the measured value. Here, $R = \sqrt{Re_{xe}}$, the square root of the usual length Reynolds number, $Re_{xe} = U_e x/\nu_e$. Fig. 19 in Ref. [88] shows that the experimental amplification-rate curve at this location is in general agreement with earlier measurements by Kendall [87] and Demetriades [100].

Fig. 5 in Ref. [98] shows that the computed maximum amplification rate is close to the measured value for $1200 < R < 1400$, but the measured value increasingly drops below the computed value for $R > 1400$. Fig. 21 in Ref. [64] shows that higher harmonics also become significant for $R > 1400$. Stetson [64] concludes that nonlinear effects become significant for $R > 1400$, making comparisons to a linear amplification rate inappropriate there. This is a very important point, for most later computations follow Mack in comparing to the experiment at $R \simeq 1732$. Fig. 18 in Ref. [97] shows an N-factor comparison that makes the same point – the experimental amplification rates are lower than the computed values, particularly above $R \simeq 1800$ where the experimental amplitudes actually decrease. Mack suggests that this is due to nonlinear effects or to the start of transition.

Mack also suggests that the experimental amplification rate may be lower because a pure 2D normal mode is not what is actually being measured. He points out that different frequencies may have their maximum response at different boundary-layer heights, so a Fourier analysis of the signal at the height where the broadband amplitude is a maximum does not necessarily determine the single-mode amplification rates.

Chang et al. [101] show one figure suggesting that a sharp-cone PNS solution can achieve better agreement at $R \simeq 1732$, but few details are given in the paper. Their linear-stability equations allow for shock motion. A similar comparison at $R \simeq 1730$ is shown in Fig. 4 of Ref. [102]; the computational growth rates are about 20% above the experimental values. Few details are again given.

Chang et al. [103] performed linear and nonlinear computations using PSE methods. The mean flow appears to be obtained using the Mangler transformation from the flat plate solution, but the details are sketchy. Chang et al. also find poor agreement between linear-instability theory and Stetson's amplification rates at $R \simeq 1730$. Nonparallel effects result in an increase in the computed growth rates, making the agreement worse. However, if appropriate nonlinear effects are taken into account, fairly good agreement can be obtained (Figs. 9 and 13 in Ref. [103]). Chang et al. suggest that nonlinear effects become dominant at $R \simeq 1600$. Various assumptions have to be made regarding the amplitude of the particular waves that are included in the nonlinear computation, so the nonlinear computation can only suggest an explanation for the experiment, it cannot be validated by the experiment. The linear-region data were not studied in detail, probably because Chang et al. did not have ready access to the detailed tabulated data.

A series of detailed computational comparisons were carried out by Dallmann's group at DLR, Göttingen, Germany. Simen et al. shows comparisons carried using a thin-layer Navier-Stokes code, combined with local linear instability theory [104, 105, 106]. Fairly good agreement is obtained for the downstream mean profiles, and for the second-mode growth rates. However, these comparisons were later repeated by Kufner, using the same code [107, Section 6.2]. Kufner did not obtain the same good agreement, even when using Simen's grid. According to Stefan Hein (private communications, October-December 2000) and Ref. [108], Kufner believed that Simen's good agreement was due to insufficient convergence, insufficient grid resolution, insufficient clustering of the grid near the shock, and a fortuitous value of the entropy-fix parameter that is needed to stabilize the solution. Kufner obtained fully converged grid-independent solutions that were independent of the entropy-fix parameter, over a certain range. These solutions resulted in amplification rates that were in general agreement with the other computations, and that disagree with the experimental data. Since Esfahanian also obtained fortuitous agreement when using Simen's grid (Stefan Hein, private communication, October 2000), it appears that Simen's good agreement was a misleading coincidence.

In summary, at the present time it appears that Stetson's sharp-cone experiments show waves that rise above the background noise for $R \simeq 1200$,

grow linearly only in the short region to $R \simeq 1400$, and become nonlinear downstream. Most detailed comparisons to linear instability have mistakenly been carried out downstream, where the growth is actually nonlinear, and comparisons to the $R \simeq 1730$ growth rates therefore show poor quantitative agreement. Now that the detailed tabulated data are available, new comparisons should be performed for the linear instability amplification (see Ref. [91] for one such effort).

4.2.3 Mean Flow Comparisons

Fig. 3 shows the wall temperature distributions measured on the sharp cone, at the time of various mean-profile measurement runs. The coordinate s is the arclength along the surface. The x locations in the legend are the axial locations of the respective mean-profile measurements, and T_w is the surface wall temperature. The forward portion of the model heats up with time, and the aft portion appears to cool slightly. While the nosetip is expected to approach adiabatic conditions during the run, the aft end of the model is cooler due to heat transfer to the water-cooled sting. The data do not agree with a simple analysis of the adiabatic wall temperature. The temperatures are the result of a complex heat balance in the thin-wall model, which incorporates a solid nosetip and a water-cooled sting support. Although Stetson et al. attempted to acquire data only after equilibrium was reached, after the model had been in the flow for more than 30 minutes (private communication, August 2003), the actual wall temperature distribution during hot-wire data acquisition is not presently known. The original records of the acquisition time of the wall-temperature records with respect to the hot-wire records may no longer be available.

Fig. 4 and 5 plot the sharp cone mean profiles, using the original tabulations. Both overshoot above the freestream values near the edge of the boundary layer. Such overshoots would be likely to have substantial effects on the instabilities, since the instability equations involve the second derivatives of the mean flow profile. While it is commonly accepted that the total temperature can overshoot near the boundary layer edge, the overshoot in the pitot profile is suspicious. Although Ref. [109] showed that for a Prandtl number of one the velocity can overshoot, this is reported only for favorable pressure gradients on heated walls. Stetson was always concerned about blockage effects due to the rather large probe system (private communication, April 2003).

Fig. 6 shows a preliminary comparison to a simple computation. The comparison is shown for Run 107, at $P_t = 225.3$ psia, $T_t = 1364.4$R, and $M_\infty = 7.95$. Here, P_t and T_t are the total pressure and temperature in the

stilling chamber, and M_∞ is the freestream Mach number in the test section. The computations were performed with 201 grid points in the wall-normal direction and 1000 stations in the streamwise direction; grids of this type are normally well resolved. The departure from self-similarity due to viscous interactions and curvature was not evaluated. The measured pitot profiles are compared to boundary layer computations based on the Harris finite-difference code [76] and the Taylor-Maccoll solution. The computational profiles were reduced to pitot pressure using the Rayleigh pitot formula above Mach 1, and the subsonic isentropic formula below Mach 1. The streamwise distance $x = 35.0$ inches, and the arc length distance $s = 35.26$ in. or 2.939 ft. The isothermal computation assumed a 1000R wall temperature, which is near the mean of the approximate measured wall temperature distribution. The adiabatic-wall computation results in wall temperatures $T_w \simeq 0.856T_t$, while the measured is $T_w \simeq 0.75T_t$.

The measurements show an overshoot in the pitot pressure which is not present in the computations. Such an overshoot has been observed before for blunt cones or at angle of attack [110], but the author is not aware of any reliable experimental data showing such an overshoot for a sharp cone at zero angle of attack. The obvious experimental causes might include small residual angles of attack or a bent cone tip. It was also thought possible that more sophisticated computational approaches may yield this overshoot. However, computations by Kufner using the thin-layer Navier-Stokes equations do not show this overshoot in the pitot profile (Fig. 7). These computations were carried out for the blunt-cone conditions of $T_t = 750$K, $T_\infty = 54.35$K, $M_\infty = 8.0$, $Re_\infty = 8.202 \times 10^6$/m, $\gamma = 1.4, R = 287.03$J/kg-K, and with a Sutherland constant of 110K. The Mack viscosity law is used [17, p. 57], resulting in a freestream Reynolds number that is 6% lower, as compared to the use of the Sutherland law even below 110K. The computational results were provided by Stefan Hein (private communication, April and October, 2000); see Ref. [111]. Neither the blunt cone nor the sharp cone (computed at the blunt-cone conditions, not the Stetson sharp-cone conditions) shows an overshoot in the pitot profile, although both show overshoots in the total-temperature profile (Fig. 8).

However, this pitot overshoot is similar to that observed by Kendall on a flat plate when insufficiently small pitot tubes were used. Measurements with smaller pitot tubes did not show an overshoot. The overshoot was then attributed by Kendall to probe interference [112]. A similar overshoot is observed in three references cited in Morkovin et al. [113]; Morkovin also explains the overshoot as probe interference. Since the overshoot decreases with downstream distance, as might be expected since the relative pitot-probe size

decreases with increasing boundary-layer thickness, it seems likely that probe interference is the cause. This problem then casts doubt on all the mean-flow profiles.

Accurate mean-flow computations at the Stetson sharp-cone conditions were not available to this author, who is unaware of any definitive comparisons. However, the lack of a pitot-profile overshoot for a sharp cone was confirmed in unpublished Navier-Stokes computations by Manning et al. (private communication, July 2000; cp. Ref. [114]). The pitot-profile data thus appear to be contaminated with probe interference. Since the total-temperature profile data were obtained at the same time with the same probe assembly, they may also be contaminated; however, this remains to be shown by a comparison to accurate computations.

4.2.4 Instability-Wave Comparisons

Spectra of the massflow fluctuations are shown in Fig. 9. The figure shows every fourth streamwise station, for improved clarity. The dominant feature is the second-mode instability, which peaks at just under 90kHz near the end of the cone at the $s = 37.288$-inch station. This peak is here first apparent at an arclength $s = 17.118$ in., where it occurs at about 120kHz. The amplitude increases and the frequency drops as the second-mode waves and boundary-layer thickness grow downstream. The large amplitudes at low frequencies below 20kHz are due to tunnel noise. The less obvious increases in amplitude near 50kHz are thought to be due to first-mode instabilities, although this is much less clear. Finally, the small peak in the $s = 29.208$ spectrum near 210kHz is thought to be a second harmonic of the now-nonlinear second-mode waves.

Since the measurements were made at the peak-rms-amplitude height in the boundary layer, and since the sharp cone profiles should be self-similar, all measurements should be at the same mean-flow condition. A single hot-wire was used for all these measurements. More detail is reported in Ref. [48], including the measurement heights. The spectra are normalized by the mean values at the probe height. Tabulated data are available from Roger Kimmel of AFRL or the author. Uncalibrated spectra from various freestream hot-wire measurements are also available in tabulated form.

In principle, the growth of these waves can be accurately and definitively determined using computational methods. In practice, such computations are not yet routinely accurate and straightforward. As an example, the integrated growth of these waves was computed using the e^{Malik} code and compared to Mack's results. Malik's internal similarity solver was used to obtain the mean-

flow profiles for the e^{Malik} code. The Mack data were digitized from Fig. 6 in Ref. [97], since the original tabulated data are lost (Les Mack, private communication, July 2000). Figure 10 shows the results, for $T_t = 1310$R, $Re_e = 1.42 \times 10^6$/ft., $M_e = 6.8$, $Pr = 0.72$, and an adiabatic wall. Here, Re_e and M_e are the unit Reynolds number and Mach number at the boundary-layer edge, Pr is the Prandtl number, and F is the usual nondimensional frequency. The grid included 141 points in the wall-normal direction. Significant differences exist; in particular, the present computations find no instability at the higher frequencies, where Mack does find instability, and the N-factor for $F = 1.4 \times 10^{-4}$ at $R \simeq 2000$ differs by about 30%.

The cause of the difference is difficult to determine; detailed analysis by a computational expert is clearly required. Highly accurate mean-flow profiles are needed so that accurate second derivatives can be used in the stability analysis. Possibilities for the discrepancies include differences in the numerical methods and the fluid property models, such as the heat-transfer coefficient, the viscosity coefficient, and the heat capacity. A different version of the e^{Malik} code was obtained from Roger Kimmel (private communication, July 2000); it gave results that differed substantially at high frequencies (e.g., from $N = 1.0$ to $N = 1.4$), when using the same input file and when executed on the same machine with the same compiler. The present version was earlier checked against Ref. [82]; see Ref. [115]. Stability computations are very sensitive to small errors, and it appears that even a well-established code must be repeatedly benchmarked. Further development is clearly needed to enable routine accurate computations of hypersonic laminar instability.

A set of computations was also carried out using the Taylor-Maccoll solution [116, Sec. 16.5], the Harris boundary-layer code, and the e^{Malik} code. Figure 11 shows another comparison to the Mack results, for $T_t = 1310$R, $P_t = 225$ psia, $Re_\infty = 1.0 \times 10^6$/ft., $M_\infty = 8.0$, $Pr = 0.72$, and an adiabatic wall. Here, the Harris code was modified to use the Mack-modified form of the Sutherland viscosity law. The first derivatives of the profiles are taken directly from the computations performed within the Harris code; the second derivatives are obtained by numerical differentiation using second-order centered differencing. The comparison for the higher frequencies is better than that obtained using the internal e^{Malik} solver, due to small changes in the boundary-layer profiles and their derivatives (not shown). A doubling of the wall-normal grid for the boundary-layer solution from 201 to 401 points changed the present N-factor results by less than 0.5%.

Figure 12 shows a final comparison between computations. All are carried out at $T_t = 1364.4$R, $P_t = 225.3$ psia, $M_\infty = 7.95$, and for an adiabatic wall. A single frequency is computed, and both the N-factor and the value of R is

shown vs. the streamwise distance s. For the first two sets, the profiles are obtained using the internal e^{Malik} similarity solver; for the last two, the profiles are obtained using the Taylor-Maccoll solution and the Harris boundary-layer code. The first pair of solutions differ in the value of the Prandtl number that is used. The first of the Harris-code solutions uses the Sutherland viscosity law, even below 110K; the second uses the Mack-modified Sutherland law. For the first 3 solutions, the value of R repeats almost exactly, as it should; for the last one, R differs somewhat due to the change in the freestream viscosity. For the two solutions using the internal similarity solver, the small change in Prandtl number changes the final N factor by some 12%. The larger of these two solutions is, in turn, about 10% below the Harris code solutions. The change in viscosity law (for the Harris code only) changes the N factor only slightly. Fairly good instability-wave amplification computations can be obtained fairly readily for these simple geometries, with reasonable agreement in code-to-code and code-to-experiment comparisons, but conclusively accurate results are not yet routinely available. Experimental data will be needed to validate the computations, even for the simple sharp cone, if only due to the uncertainties in the fluid properties at the low wind-tunnel freestream temperatures [99, 117, 118, 119].

The best method of comparing to the experimental data is to integrate the computed amplification factors and compare the amplitude ratio to the experimental value. Since the experimental data are linear only to about $R = 1400$, and since the signal-to-noise ratio becomes substantial only at about $R = 1150$, the comparison was carried out from $R \simeq 1150$ to $R \simeq 1350$, as shown in Figure 13. The experimental voltage spectra were used for this plot. The computation was carried out using the Harris boundary-layer code, for $P_t = 225.3$ psia, $T_t = 1364.4$R, $M_\infty = 7.95$, using the Sutherland viscosity law, and with a 1000R isothermal wall temperature. For the computation, amplitude ratios are referenced to the values at $s = 11.112$ in., while the reference location for the experiments is $s = 11.073$ in., which is sufficiently close for this initial comparison. The experimental amplitude growth in this region is small, less than a factor of 3, which limits the accuracy of any comparisons. The early nonlinearity is probably due to the relatively large amplitude at which the signal becomes larger than the noise of the conventional wind tunnel. Compare Ref. [120], where growth of a factor of 2 is measured at a far lower Reynolds number under controlled quiet conditions. The computed maximum amplitude ratio is 60% larger than the experimental value, and the most amplified frequency in the computation is about 10% lower. The experimental peak N factor is about 1.0, while the computational value is about 1.5.

Figure 14 shows that the difference is probably not due to the effect of wall

temperature distribution. Amplitude ratios are shown, as in Fig. 13, for the same flow conditions, again computed using the Harris boundary-layer code. The first set of amplitude ratios is obtained for a constant isothermal wall temperature of 1000R. The second set is for a linear variation of wall temperature from 1060R to 966R; this approximates the experimental distribution (Fig. 3). The reference location for both sets of amplitude ratios is $s = 11.112$ inches. The effect of the varying wall temperature is small.

4.2.5 Summary of Stetson Sharp-Cone Results

It is remarkable that accurate agreement between experiment and computation remains to be obtained for the growth of second-mode waves on a round sharp cone at zero angle of attack. This shows the difficulty of accurately measuring and computing hypersonic instability. The experimental mean-profile data is clearly contaminated by probe interference, and cannot be used as a reliable check on the mean-profile computations. This means that it cannot be used to check angle of attack, mean flow nonuniformity, or other experimental error sources. The early nonlinearity observed in the experiments also suggests that comparisons of linear amplification must be carried out either with controlled disturbances or with a quiet tunnel, or both.

The computational results shown here highlight the well-known sensitivity of instability computations to small errors in the numerics or the profiles. The difficulty no longer seems to be computer resources, but rather a robust and sufficiently accurate code. An accurate set of agreed-upon results should be readily available, for a mean flow and the instabilities, to allow benchmarking to be carried out. It is evident that this is needed even for an established code, when such a code is ported to a new location, user, or machine.

The poor agreement between the computation and experiment cannot be resolved until the computational and experimental methods are refined. The present experiments also suggest that nonlinear effects are a critical part of second-mode induced transition on sharp cones, since so much of the wave growth occurs nonlinearly. However, this remains to be confirmed by quiet-tunnel experiments.

4.3 Instability on a Sharp Flared Cone at Mach 6

Three instability experiments were carried out in the NASA Langley Mach-6 quiet tunnel before it was decommissioned [121]. Comparisons between experimental and computational N-factors are shown for all three experiments in Fig. 11 of Ref. [121]; good agreement was reported. Unfortunately, only one

of the three was able to obtain calibrated mean-flow profiles [122, 92, 123]. All measurements were made using natural fluctuations, without controlled disturbance generators. All experiments were carried out with constant-voltage anemometry (CVA), due to electromagnetic noise problems with more conventional anemometers. No systematic studies of CVA calibration techniques had been carried out at that time, so the calibrations are limited. The experiments were carried out on both sharp and blunt cones, but extensive data is available only for the sharp cone.

The model was a 50.8-cm sharp cone. The first 25.4 cm formed a straight cone with a 5-deg. half-angle. This was followed by a gentle flare with a 2.364-m radius of curvature. The profile shape is continuous; only the second derivative is discontinuous at the match point. The tip had a nominal radius of 2.5 microns. The cone angle of attack was nearly zero; however, most measurements were carried out at a yaw angle of approximately 0.1 deg. and a pitch angle of approximately 0.1 deg. [123, p. 20]. Appendix D of Ref. [123] reports additional measurements carried out after additional efforts were made to align the model at zero angle of attack.

The measurements were carried out at Mach 5.91, with a total pressure of 896 kPa and a total temperature of 450K. The freestream Reynolds number was 9.25×10^6/m (note the typographical error on p. 2497 of Ref. [92]).

Measurements were obtained with surface pressure taps (29) and thermocouples (51). Mean flow profiles were measured using hot wires and CVA. Fluctuating profiles were obtained using the same hot wires, but no calibrated fluctuations were reported. Thus, no calibrated eigenfunctions are available.

These data were also obtained under equilibrium-wall temperature conditions. That is, the measurements were obtained only after the model-wall thermocouples reached steady-state temperatures. This occurred approximately 15-20 minutes after initiation of Mach-6 flow, following a subsonic preheat. Unfortunately, as for the Stetson data, this is not the same as adiabatic-wall conditions, for Chokani (private communication) states that the heat-transfer within the model is not negligible. The effect on stability and transition of these relatively small changes in surface temperature remains to be determined.

Growth of first and second-mode instability waves was observed on the flared cone under cold-flow conditions, in a quiet tunnel [42]. An adverse pressure gradient exists on the rear half of the model. Second-mode amplification is observed. Görtler interactions are possible on the concave flare, although no experimental evidence is available.

Lachowicz et al. report agreement of 2-5% with linear-instabilty N-factor computations for the second-mode wave growth [92, Fig. 9]. However, the ra-

tio of CVA fluctuating voltages was taken as the ratio of wave amplitude. This assumption was used by Stetson and others for constant-current or constant-temperature anemometry, when the measurements were carried out with the hot wire at identical mean-flow conditions. However, the validity of this assumption for the Lachowicz CVA data is presently being reviewed.

If this assumption can be verified, and any errors caused by it can be quantified, this dataset may be the best instability-wave test case presently available. Although the aft end of the cone was outside of the fully quiet region, this is the only data obtained under quiet conditions. Static pressure data was obtained at 3 azimuthal positions to check angle of attack, although all boundary-layer measurements were again obtained on only one ray. The mean flow profiles are in fairly good agreement with existing computations.

Additional computations have now been carried out (Ref. [124] and [125]). However, the experimental data are not yet available in tabulated form; detailed comparisons may be carried out at a later date. New computations were reported in Refs. [114] and [52], but wave amplifications have not yet been compared.

4.4 Summary of Instability Data on Sharp Cones

For a sharp cone at zero angle of attack, experiments show clearly that the first and second-mode instabilities lead to transition. At Mach 8 wind tunnel conditions, the second-mode instability appears to dominate the transition process. The dominant frequencies agree well between computation and experiment, and amplification rates agree qualitatively.

However, much remains to be done, even for this simple case. Accurate agreement between computation and experiment remains to be achieved, even for linear instability amplification rates. The parametric dependence of the first and second-mode instabilities remains to be resolved, along with their interactions and dependence on freestream conditions. Nonlinear effects, wave interaction effects, and receptivity effects remain to be addressed, especially quantitatively.

4.5 Transition on Sharp Cones at Zero AOA

4.5.1 General Issues

Despite the apparent simplicity of this configuration, transition measurements in air at perfect-gas conditions are affected by cone half-angle, Mach number, tunnel size and noise, stagnation temperature, surface temperature distribu-

tion, surface roughness, and any blowing or ablation, as well as measurement technique. Sharp-cone smooth-wall instability growth does not scale with Mach number, Reynolds number, and T_w/T_t, even under perfect-gas conditions [126]. The mean boundary-layer profiles and their instability and transition depend on the absolute temperature; this is because the viscosity and heat-transfer coefficients depend on absolute temperature and do not scale. Angle-of-attack effects are difficult to rule out, except by systematic azimuthal comparisons that are all too rare.

Many measurements of transition location on cones have been reported, too many to catalog here; Ref. [127] lists 24 in 1967, of which 12 are at Mach 5 and above. Collected data are often plotted to show an increase of Re_T with M_e or M_∞ (e.g., Fig. 10 in Ref. [128] and Fig. 8 in Ref. [129]). Some support for this trend has been found in linear stability computations [130]. However, most of these measurements suffer from poor control of the factors not under study, allowing this purported increase with M_e to be disputed. Here, some of the more reliable approaches will be highlighted.

Stainback made measurements in several tunnels at M_∞ of 6, 8, and 22 on sharp cones at zero angle of attack. The cone half-angles were selected to provide a boundary-layer edge Mach number of 5 in all cases [131]. Transition was determined via heat-transfer measurements under cold-wall conditions. Although the edge Mach number is the same in all cases, the wall and edge temperatures differ with Mach number, so the boundary layer profiles are not identical. The 20-inch Mach-6 tunnel yields the largest transition Reynolds numbers, followed by the smaller Mach-6 tunnel, the Mach-8 tunnel, and the Mach-22 helium tunnel. Although these transition results scatter when plotted vs. unit Reynolds number, Stainback shows they appear to collapse to a single curve when plotted against tunnel noise level, despite the gas-property differences between air and helium.

Pate tabulates measurements on 5-deg. half-angle sharp cones under similar conditions in AEDC tunnels A (40-inch) and D (12-inch), to show the effect of tunnel noise [33]. The transition location was taken from the peak in measurements of surface pitot pressure, a method that should give a value near but not at the end of transition (see Section 2.5). The cone surface temperature does not seem to be stated, but is probably near adiabatic. The diameter of the 'sharp' nose was between 0.005 and 0.006 inches, and the surface finish was about 10 μin. rms. The results were extracted from Tables F-5 and F-6 of Ref. [32] and are shown in Fig. 15. The data with tunnel dewpoints above $-10°F$ were omitted, per Fig. 6a of Ref. [128], where Pate shows that higher dewpoints can affect transition measurements. Freestream unit Reynolds numbers range from 0.1 to 0.6 million per inch, and stagna-

tion temperatures vary between 500 and 650 Rankine. The dominant cause of scatter appears to be the increase in transition Reynolds number with unit Reynolds number. Some increase of transition Reynolds number with Mach number can be seen amid the scatter, but Pate correlated data for the end of transition with tunnel-noise parameters alone, independent of Mach number [132, 128, 31].

Pate's correlation can be put in the form of curve fits to the experimental data, as in Fig. X-11 of Ref. [33], regenerated here as Fig. 16, which reports data from various AEDC tunnels. Transition was again taken from the peak in measurements of surface pitot pressure. The figure shows a general experimental increase in transition Reynolds number with freestream Mach number; it also shows that this increase can be fairly accurately explained by the tunnel-noise-based correlation, which is in generally good agreement with the experimental data. For the present figure, Pate's correlation code was reentered from the listing in Ref. [33], and the correlation lines were regenerated (using data that is mostly contained in Ref. [33], especially Table 6). For this purpose it is important to note that AEDC Tunnels A and D operated with adiabatic walls, while Tunnels B, C, E, and F had water-cooled nozzles with nozzle-wall temperatures of approximately $540°R$. The Pate-correlation curves thus regenerated nearly duplicate the original figure, except for the Tunnel B and E cases, for which the regenerated lines are about 0.4×10^6 lower in Re_T, for unknown reasons. The correlation is evaluated at a unit Reynolds number of 2.4×10^6/ft., the same unit Reynolds number as the experimental data that is used. More data points are present in the original figure, and even more data should now be added to this figure, but the correlation program requires the circumference, length, and temperature of the nozzle wall, as well as the total temperature and pressure, and this kind of detailed data is usually not readily available. Since total temperature and other parameters are varied along with tunnel size, the tunnel noise and boundary-layer profiles are both affected, and tunnel-noise effects are identified but not isolated.

In these and similar papers, Pate showed that *tunnel-noise effects can be identified by testing the same model in different facilities at the same nominal conditions.* This approach provides an initial estimate of uncertainties due to tunnel noise effects. Although all conventional tunnels have noise levels much higher than flight, similar measurements in two very different tunnels provide noise-sensitivity data that might possibly improve estimates for transition in flight. For example, Pate used measurements in two different tunnels to show that when transition occurs immediately behind a large roughness element (*effective* roughness), the transition location is independent of tunnel noise [133]. This gives some confidence in extrapolating tunnel measurements of

effective roughness heights to flight. However, transition induced in part by smaller roughness elements remains dependent on tunnel noise, as Pate also showed [31].

Chen also made measurements of transition on a 5-deg. half-angle sharp cone at zero angle of attack, in the Mach 3.5 quiet tunnel at NASA Langley [134]. These measurements were also made using surface pitot tubes, and the tunnel has a 6 by 10 inch rectangular exit. The nose diameter is quoted at about 0.002 inches. Tabulated data supplied by Chen (private communication, Sept. 2000) included the Reynolds number based on the location of the peak in the surface pitot pressure, the same method reported by Pate. These data are reported under quiet conditions, with a laminar nozzle-wall boundary layer, and suction in the throat-region bleed slots. Data are also shown in Fig. 15 for a noisy condition with the throat suction shut off. The noisy data are somewhat below Pate's data in the tunnel A, but above the data in tunnel D. The quiet data are nearly a factor of 2 higher, as might be expected. Horvath et al. also report comparisons of transition measurements in both quiet and conventional tunnels, on a 5-deg. straight cone followed by a flare [52]. The N factor for the quiet tunnel data was about 7.8, about twice the value of 3.8 observed in the conventional tunnel.

High enthalpy effects are a major issue for transition on reentry vehicles. An e^N computation of these effects for two flight vehicles recently appeared in Ref. [24]. Ground tests are needed to help develop and validate mechanism-based models that include gas-chemistry effects [80]. However, such experiments are very difficult, for (1) high-enthalpy facilities are expensive and scarce, (2) there is no visible prospect of a low-noise high-enthalpy facility, and (3) measurements of the transition mechanisms under high-enthalpy conditions are very difficult and have not yet been attempted. Transition measurements on a nearly sharp cone under high-enthalpy conditions were carried out in the T5 facility during the last decade [135], in air, nitrogen, and carbon dioxide. Cones with a 5-deg. half-angle have been used, with recent experiments investigating a novel control scheme [136]. Transition Reynolds numbers based on edge conditions are an order of magnitude below flight, but when based on reference-enthalpy conditions they are comparable to flight [135]. The experiments are carried out in a noisy facility at Mach numbers of about 5, so the conditions differ markedly from high-enthalpy RV flights. Since changes in gas composition and enthalpy involve changes in the tunnel noise environment, measurements of transition alone are ambiguous. It would be interesting to compare the existing T5 measurements to Pate's correlation. Although measurements of instability would be difficult in these facilities, they should be possible using optical methods [137]. High-enthalpy measurements of stability

and transition using controlled perturbations remain a feasible but difficult topic for future research.

Refs. [138] and [139] have a very instructive discussion of transition measurements carried out at Ames and Langley. Initial disagreements in transition Reynolds number led to a detailed analysis and a second set of measurements, using various instrumentation. The thermocouple measurements on 5-deg. half-angle sharp cones are also included in Figure 15. The Langley data were obtained in the Mach-8 variable density tunnel. All the measurements shown were obtained using thin-wall calorimeter methods, apparently all at $T_w/T_t \simeq 0.4$. These data are for the end of transition, based on the intersection of lines fitted to the transitional and turbulent regions. All three datasets scatter, with the variation being primarily with unit Reynolds number. The Langley transition results rise from version A to version B of the tunnel, with the addition of flow conditioning elements to the settling chamber. The Ames data for the end of transition from version A of the tunnel are not available; these data are with helium bleed in the nozzle-wall boundary layer, and show reduced variation of transition onset with unit Reynolds number [31, 140]. The Ames data for the end of transition in the version B configuration also increase with unit Reynolds number. Version B of the Ames tunnel had an open-jet test section, air bleed, and a revised heater. The Ames data are at levels similar to the Tunnel A data at Mach 5 and the Langley data at Mach 8.

However, these data also show that even the Pate correlation for tunnel-noise effects may not be fully established yet. For example, Fig. 17 shows data for the end of transition on 5-deg. half-angle sharp cones at zero angle of attack, in the Ames and Langley tunnels [139, 138]. The data were taken from Table I of Ref. [138]. The solid square symbol that is circled appears to be a typographical error in the table. These two datasets for the end of transition seem nearly identical, although they were obtained in two tunnels of significantly different size. It remains to be seen whether the difference can be accounted for using Pate's correlation.

After all this detailed analysis, what remains to be seen in Fig. 15 is a high level of scatter; the scatter is comparable to the mean values. Much effort has been expended attempting to reduce such scatter by crossplotting with unit Reynolds number, and so on (e.g., Refs. [141, 142]). Many such correlations use only a small subset of the available data, and are thus open to question regarding the basis of their selectivity. In the author's judgement, the most effective work has been that of Pate, who correlated much of the data with tunnel noise parameters [132]. However, even Pate's work does not take into account variations with freestream and wall temperature [33,

p. 255], and involves various corrections to the original data. Although Pate states that the variations with temperature should be small, the data below show that wall temperature can sometimes have a large effect under controlled conditions. Fig. 15 is shown here to emphasize the high level of uncertainty associated with conventional tunnel measurements of the transition location alone. There are nearly always too many uncontrolled parameters in such experiments. Since tunnel noise is such a complex and poorly understood factor, it is in many ways the most important to control. Operating at fixed tunnel conditions may be the only way to control such noise effects.

4.5.2 Changes in Geometry Under Fixed Tunnel Noise

One way to minimize ambiguities due to tunnel noise effects is to measure transition with fixed tunnel conditions. One example of such measurements would be the measurement of transition on sharp cones with different half-angles and different edge Mach numbers. Of course, in this case the shock strength would still change with cone angle, and so the noise transmitted to the underlying boundary layer would also be expected to change. Deliberate sharp-cone measurements of this type were carried out by Stainback, as reported in Refs. [59, 143, 127, 144]. Similar measurements on plates are reported in Ref. [144].

Fig. 18 shows Stainback's cone measurements, replotted from Fig. 14a in Ref. [144]. The data were all obtained in the Mach-8 variable density tunnel at NASA Langley. The measurements were made with T_t ranging from 740K to 840K, using fusible paints on plastic models immediately after injection; this suggests that $T_w \simeq 300$K, although this is not clearly stated [143]. Transition is taken at the minimum in the heat-transfer rate (near onset). Four cone half-angles were used, as shown above the data for the local edge Mach number each generates. For each of the four pairs of freestream unit Reynolds number Re_∞, the tunnel conditions and thus the tunnel noise are nearly constant; each pair is assigned a different symbol in the legend. The cone half-angles also come in pairs, since for a given M_∞ and Re_∞ there are two cone half-angles that will produce equal values of unit Reynolds number at the boundary-layer edge, Re_e. Each of the four pairs of Re_∞ result in the same value of Re_e for the two pairs of cones, so each symbol corresponds to a given value of Re_e, as shown in the second column of the legend. The third column in the legend is the value of Re_∞ used to produce that Re_e for the 5 and 20.1-deg. half-angle cones. The fourth column is the value used to produce that Re_e for the 7.5 and 15.8-deg. cones. The values of Re_∞ in the third and fourth columns differ by some 10%, so there is a minimal variation in tunnel noise that might be expected to move

transition by about 10% [144]; this effect is thus thought to be small.

Fig. 18 shows no clear trend in Re_T with edge Mach number. It remains possible that this is due to cancelling effects of varying shock strength, T_e/T_w, receptivity, instability, and so on. Ref. [145] performed similar measurements near Mach 2 and reports a 20% decrease in $Re_{T,e}$ as the cone half-angle increases from 5 to 22.5 deg., with the tunnel conditions fixed. Measurements of cones with different half-angles in the Langley helium tunnel under fixed tunnel conditions yielded an increase in transition Reynolds number with edge Mach number [146, 147]. Using only transition measurements, it is very difficult to design a fully controlled experiment, as this example illustrates. Pate concludes that *'if a true Mach number effect on transition Reynolds number exists at supersonic and hypersonic speeds, it appears doubtful that the trend could be established by comparing transition data at different Mach numbers obtained in wind tunnels having turbulent boundary layers because of the influence of radiated aerodynamic noise [144].'*

4.5.3 Changes in Model Temperature Under Fixed Tunnel Noise

Another measurement under fixed tunnel noise would involve changing the model wall temperature with the tunnel conditions fixed. In general, the effect of wall temperature on transition scatters widely, presumably due to the other parameters, and possibly also due to frost formation on the model (see Refs. [148], [149], and [150]). The movement of transition with wall cooling is controversial; various reversals and re-reversals have been reported. However, many studies are misleading, for tunnel noise and roughness effects change when unit Reynolds number and stagnation temperature are varied, often under poorly specified conditions. It is now known that at low Mach numbers, below perhaps 3 or 5, uniform wall cooling should delay transition on smooth sharp cones at zero angle of attack, since it damps the first-mode instability waves, while at high Mach numbers wall cooling should accelerate transition, since it destabilizes the second-mode instability waves (e.g., Refs. [151, 152, 89, 85]). Since few detailed experiments have been accompanied by the necessary computations, it is not yet known whether most wall-cooling effects can be explained by the changes in the linear amplification of these modes, even for smooth sharp cones. Three systematic transition experiments carried out at fixed tunnel conditions are known to the author.

Van Driest et al. appear to have been the first to change wall temperature alone, at supersonic speeds from Mach 2 to 4 [153]. The measurements were made in the JPL 12-inch tunnel on a sharp round cone with a 5-deg. half-angle at zero angle of attack. The surface roughness was 10 μin. rms and

the nose radius is not stated. The effects of roughness and settling-chamber turbulence were examined. Round wires were placed on the model at 3 inches from the leading edge, and screens were added to the settling chamber. Van Driest et al. appear to have been unaware that settling chamber disturbances contribute minimally to tunnel noise for Mach numbers greater than about 2.5 [154]. Schlieren images were used to determine transition location, providing a location somewhat aft of the onset of transition [33, p. 165]; thermocouple data are also reported. The cone was internally cooled with liquid and gaseous nitrogen; typical wall temperatures are reported, and are not very uniform.

Fig. 19, replotted from Van Driest's Fig. 20, shows the results at $M_\infty = 2.81, Re_e = 0.67 \times 10^6$/inch, and $T_e = 228R$, at fixed tunnel conditions. When no trip is present, Re_T rises by a factor 3 as the wall temperature drops by 1/3. For the smallest 0.0005-in. dia. wire trip, the results are the same. However, sufficient roughness bypasses the cooling effect, reducing its magnitude or even eliminating it. When the trip diameter is increased to 0.001 in., the transition delay ends at about $Re_T \simeq 10 \times 10^6$, apparently as roughness begins to affect transition (note the single data point below $T_w/T_e \simeq 1.3$.) For a larger trip diameter of 0.002 in., the delay of transition due to wall cooling shows a clear maximum at about $Re_T \simeq 8 \times 10^6$, after which the thinning boundary layer interacting with the roughness and freestream noise cause transition to move increasingly forwards. Sufficient roughness thus causes a reversal effect, suggesting that roughness is one possible explanation for the anomalous reversal data. For the largest trip diameter, wall cooling has no effect on transition. Even when frost was detected, below about $T_w/T_e \simeq 1.8$, there was no reversal of the transition delay with increased cooling. Perhaps the roughness due to the frost was very small. The trip was located at $Re_x \simeq 2 \times 10^6$.

The results at the other Mach numbers are similar, although the plots are less comprehensive. At $M_\infty = 3.84, Re_T$ rose from about 4 million to about 8 million as T_w/T_e fell from 3.4 to 1.8.

Sanator et al. also varied wall temperature while holding tunnel conditions fixed, for sharp 5-deg. half-angle cones in the 36-inch wind tunnel at the Republic Aviation Corporation [155]. The nose radius and surface finish are not given in Ref. [155], but all measurements were made at $M_\infty = 10, T_t =$ 2000R, and a (freestream) unit Reynolds number of 2×10^6/ft. Transition was determined from heat flux gages on a thin-wall model. Although this tunnel is not well known, the results do appear to fit Pate's correlation [60, Fig. 76]. The cone was internally cooled using liquid nitrogen. The data are replotted in Fig. 20 (taken from Fig. 7b in Ref. [156]). Transition appears to be approximately independent of wall temperature. This is surprising, since at these high Mach numbers, one might expect transition to be dominated

by second-mode waves, which should grow faster under cold-wall conditions [89, 85]. However, the expected dominance of second-mode waves depends on the tunnel noise spectrum and the receptivity processes; second-mode waves do *not* dominate on flat plates in Tunnel B despite the high Mach number of 8 [35]. Without detailed measurements, it is impossible to know if transition was caused by first mode or second mode waves, or influenced by surface roughness or frost. It would be interesting to compare the results to an e^N computation.

Everhart and Hamilton made measurements on a 3.75-deg. half-angle sharp cone, also at $M_\infty = 10$ [156]. The nose diameter increased from 0.004 inches to 0.010 inches during the experiments. The surface was polished to 6 microinches, and the cone was internally cooled using gaseous nitrogen. The wall temperature is shown in Ref. [156], and is not particularly uniform. Transition was inferred from thermocouple measurements, all taken at $T_t = 1815$R. The model was initially cooled, and then the movement of transition was recorded as the model heated up under the continuous flow. Some of the results were obtained at constant tunnel conditions as shown in Fig. 20. There is very little effect of varying wall temperature, and the transition onset data is very similar to that of Sanator et al., which is taken at the same values of M_e and Re_e. The similarity is not surprising, since the 31-inch-square Mach-10 tunnel was used, and this nozzle size is similar to that of the 36-inch tunnel used by Sanator et al. The end of transition is substantially later than in Sanator et al.; the cause of this difference is unknown, but Everhart et al.'s data for the end of transition was also correlated by Pate [33, Table 6]. Again, without detailed measurements of the instability processes it is nearly impossible to explain why transition is not affected by wall temperature. It would again be interesting to compare the results to instability computations.

The rest of the sharp-cone data cited by Potter [148] is not measured at fixed tunnel conditions. For example, Mateer also made transition measurements on sharp 5-deg. half-angle cones with cooling [157]. However, Mateer kept cone wall temperature fixed, while varying tunnel pressure and temperature, so that tunnel noise varied along with T_w/T_t. This was an all-too-common practice which resulted in ambiguous data; it seems very likely that these uncontrolled transition parameters give rise to the high level of scatter shown by Potter.

5 Blunt Cones at Zero Angle of Attack

5.1 Instability Measurements

Stability measurements on blunt cones are even rarer than such measurements on sharp cones. Only two such datasets are known to the author: the first was obtained by Stetson [158], and the second was reported by Maslov et al. [159, 91, 50]. The Stetson data is discussed in detail here, as it is more readily available.

5.2 Instability on a Blunt Cone at Mach 8

5.2.1 General Information

In addition to the sharp cone measurements discussed in Section 4.2.1, Stetson et al. carried out additional calibrated measurements of instability wave growth on several blunt cone models in AEDC Tunnel B at Mach 8 [158, 64]. The apparatus was almost identical [94, 95]. This conventional wind tunnel is well characterized [96]. The blunt-cone experiments examined the effects of the entropy layer on the hypersonic second-mode instability.

The model was a 7-degree half-angle cone with a 40-inch (1.016-m) length and a 0.15-inch (3.81 mm) nose radius. The cone angle of attack was zero, to within the accuracy with which this could be set and measured. The model was in thermal equilibrium but heat conduction within the model was not negligible. Most of the measurements were carried out at a freestream Mach number of 7.99, with a total pressure of 580 psia (4.00 MPa) and a total temperature of 1350 R (750 K).

Measurements were obtained with surface pressure taps (24) and thermocouples (32). Mean profiles were measured using pitot-pressure and total temperature probes. Instability waves were measured using calibrated constant-current hot-wire anemometry. Hot-wire spectra were recorded at one-inch (2.54-cm) intervals between 10 and 31 inches (25.4 and 78.7 cm), with additional measurements at 33, 35, and 37 inches. Four hot-wires were used for these measurements, each calibrated separately. There is no data for transition onset on the blunt cone, according to Stetson; the small bluntness kept the boundary layer laminar at unit Reynolds numbers for which the hot wire survived well.

Growth of the first and second-mode instability waves was observed on a symmetric blunt cone under low-enthalpy conditions. The second-mode instability is dominant. Although amplification was only observed downstream of the nominal swallowing length, strong bluntness effects were apparent. Some

entropy-layer fluctuations were also apparent, although these could not be resolved clearly and no quantitative comparisons have been attempted. Second-harmonic amplification of the second-mode waves was observed downstream, a good indication of nonlinear effects. A comparison of the second-mode amplification rate to a nonlinear computation would be interesting.

5.2.2 Previous Computational Comparisons

Stetson's blunt-cone flows have been computed by numerous workers. The first paper that is known to the author is by Malik et al. [160], who used a Navier-Stokes code in the nose region, combined with a PNS code downstream, followed by linear instability theory. Most computations were carried out for the 0.15-inch nose radius that is described here. Malik et al. computed a peak amplification rate at $s/R_n = 175$ that was about 50% higher than the experimental value, although the frequency of peak amplification varies by only a few percent. Here, R_n is the nose radius. They speculate that the difference may be due to nonlinear effects, since a second harmonic is present there. A second comparison is shown further downstream at $s/R_n = 215$; the peak amplification rate agrees better but the shape of the curve is substantially different. A brief description of similar results is also shown in Ref. [102].

Herbert and Esfahanian et al. [161, 162] carried out a detailed comparison to the blunt-cone case. Fig. 10 in Ref. [162] shows that the actual measured wall temperatures on the cone are about 20% below adiabatic-wall values. Figs. 11 and 12 in Ref. [162] point out the lack of repeatability in the Stetson profile data, and a lack of agreement in the profile shapes. The critical importance of an accurate mean flow computation is emphasized. Fig. 15 in Ref. [161] shows computed values of the peak amplification rate at $s/R_n = 175$ that are about 70% above the experimental values, although the frequency of peak amplification agrees to within a few percent.

Kufner et al. [108, 77] carried out additional computations. Figure 2 in Ref. [108] summarizes the comparisons of all the authors; all the computations show a growth rate about 1.5 times the experimental value, at a frequency roughly 10% below the experimental value. However, these comparisons were carried out at a station 175 nose radii downstream of the tip. Figure 7b in Ref. [158] shows substantial amplification of second-harmonic frequencies at this station. Stetson believes that nonlinearity is substantial at this station, therefore a growth-rate comparison to linear theory has dubious validity. Many workers have selected this station for comparison to linear theory, following Malik et al. [160], and apparently through insufficient communication with Stetson et al. Fig. 4 in Ref. [77] shows a significant effect of the model for the second

viscosity of air; however, this effect does not come near to accounting for the discrepancy with experiment. Fig. 31 in Ref. [77] shows that computations based on a second-order boundary-layer method can give good agreement with computations based on the thin-layer Navier-Stokes equations. Ref. [111] reports later computations at the Stetson blunt-cone conditions, but does not provide additional comparisons. Ref. [163] reports preliminary comparisons to the entropy-layer instability reported by Stetson et al., but not to the first or second-mode instabilities.

Thus, existing computations of the instabilities on Stetson's blunt cone agree well with each other but only qualitatively with the experiments. New experimental measurements will probably be required to resolve the discrepancy.

5.2.3 Mean Flow Comparisons

Surface temperature distributions are shown in Fig. 21. These were collected at the time of various mean-flow profile runs. The x locations in the legend are those of the mean-flow profiles, and the dates and times at which the data were recorded were taken from the datasheets as shown. In the Run 101-105 series, the model appears to heat up during the 1 hour and 6 minutes spanning the runs. In the Run 74-76 series, smaller variations are present. Neither dataset agrees with a simple analysis of the adiabatic wall temperature, and the length of time the model remained in the flow from insertion until measurement is not known. Stetson stated (private communications, April and August 2003) that the model remained in the flow at least 30 minutes before hot-wire measurements were made, which should be long enough to equilibrate; the data in Fig. 21 may have been taken during this waiting period. No record now exists of how long the model was allowed to equilibrate before the hot-wire data was acquired (private communication, Roger Kimmel, June 2003). Stetson has repeatedly noted the difficulty of carrying out research measurements in an expensive production wind tunnel.

The mean flow was measured for this experiment, but existing comparisons have uncovered some difficulties. Fig. 5 in Ref. [161] shows that an adiabatic-wall computation overpredicts the wall temperature by roughly 20%. This is thought to be due to heat transfer to the water-cooled sting support. While the measurements were carried out after thermal equilibrium was achieved, heat transfer within the model apparently cannot be neglected.

Boundary-layer profiles were also measured using pitot and total-temperature probes, as shown in Figs. 22 and 23. The total temperature plots show runs 74-76 to have uniformly thinner profiles than runs 101-104, although these are

nominally repeat runs.

Unfortunately, the repeated runs reveal discrepancies of 10-15% under nominally the same conditions (see also Fig. 6 in Ref. [161]). The cause of this lack of repeatability remains uncertain. Stetson was always concerned that these profiles are likely to suffer from probe blockage; however, funds sufficient to build improved probes were not available (private communication, August 2003). Boundary-layer measurements were only obtained on one ray, so detection of residual three-dimensional effects is limited to surface pressure measurements on 3 taps at 90-deg. azimuthal intervals, at two streamwise stations. Although these generally match to within the experimental error, pressure is an insensitive measure of angle of attack.

It was not possible to repeat many runs, due to the high cost of operating at AEDC. However, Stetson believes that it will be extremely difficult to obtain higher quality data in a production facility. Since the facility is among the best of the conventional facilities, the primary limitation is cost; available funding has not permitted the usual kind of highly iterative experimental research. Furthermore, budget limitations currently prohibit further tests of this type.

Fig. 24 compares the experimental data to profiles computed using the thin-layer Navier-Stokes (TLNS) equations by Kufner et al. [77], and provided by S. Hein (private communication, April 2000). The conditions are as described with Fig. 7, where the same pitot profile is shown; an adiabatic wall is assumed. The two Stetson datasets are repeat runs, obtained at the same tunnel conditions. The Harris-code computations were obtained by the present author for $T_t = 1350$R, $P_t = 580$ psia, and $M_\infty = 8.00$.

Kufner's computation shows no overshoot in the pitot profile, while overshoots are observed in both experimental profiles. Probe interference is immediately suspected, as in the sharp-cone case. Although the Kufner computations give fair agreement for the boundary-layer thickness, the Harris-code computations show poor agreement for both the edge pitot pressure and the boundary-layer thickness. Recent computations using DNS methods show fairly good agreement with the outer part of the velocity profiles [164].

The limitations of the first-order boundary-layer theory are thought to cause the problems with the Harris-code results. The Harris code uses a variable `VELEDG` to define the edge of the boundary-layer as a fraction of the inviscid edge velocity. This parameter was changed to 99% from the usual value of 99.99% (which was used in order to get many grid points near the boundary-layer edge for the stability analysis). Fig. 25 shows the results for the same conditions as in Fig. 24, again at $s = 128.7R_N$. The edge pitot pressure decreases by 20%, causing the profiles to be even farther away from the experiment and the more-accurate Kufner computation. This effect must

be related to the way that the first-order boundary-layer approach obtains the edge conditions by tracing streamlines from the curved bow shock. The use of a first-order boundary-layer method for computation of the blunt-cone profile appears inadequate for stability purposes.

Fig. 26 compares total-temperature profiles from the same Kufner computation to the Stetson profiles from two repeat runs. The Stetson profiles were obtained at $s = 127.7R_N$, and the Kufner profile is from $s = 127.9R_N$. Here, the three profiles are qualitatively similar, as all contain similar overshoots near the boundary-layer edge. However, the quantitative agreement is poor. The poor agreement is particularly critical when one remembers that the stability computations are highly sensitive to the second derivatives of the mean-flow profiles. Since Stetson's total-temperature measurements were obtained at the same time as the pitot measurements, using a single rather large rake, both pitot and total-temperature measurements may be contaminated by probe interference. Also, the repeatability of the measurements is only about 15%. While the TLNS analysis may be accurate enough for stability purposes, the quality of the experimental data is insufficient to validate the computation.

5.2.4 Instability-Wave Comparisons

AEDC carried out spectral analyses of the hot-wire data and produced tables of amplitude vs. frequency at these streamwise stations. Tabulated data is available both for the uncalibrated voltage spectra *and* for calibrated spectra reported for total temperature and massflux. These printed tables were made available by Roger Kimmel, and have been entered into electronic form; additional details are reported in Ref. [48]. Figure 27 shows the massflow spectra, and Fig. 28 shows the total temperature spectra. The spectra are again normalized by the mean value at the hot-wire location, given by the streamwise arclength s and the probe height `ZA`, both in inches. The growth of the second-mode instabilities is again prominent. The signal-to-noise ratio appears larger for the total temperature spectra, which is not surprising since the constant-current hot wire was operated at low overheat. In Fig. 28, the second mode is first evident at $s = 28.244$ inches, with a peak just above 120 kHz. As the waves travel downstream, the boundary layer thickens, the frequency drops, and the amplitude increases, until at $s = 36.274$ in. the peak is at about 113 kHz. Low-frequency wind-tunnel noise is again evident. A second harmonic of the second-mode waves can be seen downstream of $s = 32.254$ in. near 230 kHz. This is evidence of nonlinear effects. First-mode instabilities are again difficult to identify if they are present.

Rosenboom et al. computed second-mode N-factors for this case [111], using an accurate thin-layer Navier-Stokes mean flow. The instabilities were computed using linear local and nonlocal methods. Hein provided the tabulated local-method N factors from Fig. 17 of Ref. [111] (private communication, August 2000). These data are replotted in Fig. 29, and compared to second-mode N factors computed by the present author using the Harris-code boundary-layer profiles and the e^{Malik} code. While the 110 and 120 kHz results are not too far apart, the N factors for the higher frequencies differ by a factor of more than 2. Both computations were carried out for $T_t = 1350$R or 750K, $M_\infty = 8.00$, and $R_N = 0.15$ in. or 3.81 mm. The present computation uses $P_t = 580$ psia and the Sutherland viscosity law, while Rosenboom et al. used $Re_\infty = 8.202 \times 10^6$/m, which is obtained from this same total pressure by using the Mack-modified form of the Sutherland law. If the normal Sutherland law is used, $Re_\infty = 8.76 \times 10^6$/m, which is only 7% higher and probably insufficient to explain the discrepancy. The substantial errors in the mean-flow profiles caused by the use of the first-order boundary-layer code result in very large errors in the highly-sensitive instability computation. If thee^N method was used to predict transition using Fig. 29 with $N = 4$, the arc-length locations of transition would disagree by a factor of about 2. First-order boundary-layer methods are inadequate for computation of blunt-cone instabilities, even for preliminary design purposes.

Rosenboom's e**N analysis shows transition moving monotonically downstream with increasing bluntness. This suggests that receptivity, roughness, or transient growth must come into play to explain the forward movement of transition that occurs at large bluntness.

Finally, the Kufner N-factors shown in Fig. 29 were used to compute amplification ratios, and compared to the Stetson amplification ratios for total temperature. The total temperature data was selected since the signal-to-noise ratio appears better. Run 56 at $s = 32.254$ in. was chosen as the terminal station for a linear comparison, since Fig. 28 shows that the (nonlinear) second harmonic becomes significant further downstream. Run 59 at $s = 29.231$ in. was chosen as the reference location, since this is the furthest upstream location for which the amplified frequencies rise clearly above the background noise. This again delineates a small linear-amplification region, as for the sharp cone, probably again due to signal-to-noise issues. The amplification ratios from Run 56 to Runs 58 and 59 were computed, and compared to values that were linearly interpolated from the Kufner data of Fig. 29. Fig. 30 shows the results. Both methods show a small amplification of about 1.4 or 1.5 to $S = 30.239$ in., and both show a larger amplification of 2.9 to 3.3 to $S = 32.254$. The most amplified frequencies differ by perhaps 10%

and the largest amplification factors differ by perhaps 10% also. Outside the range of computational amplification, the experimental amplification factors are generally not reliable, due to signal-to-noise problems. While the figure again shows general agreement, it is still clearly insufficient for reliable code validation. Better experimental data is needed.

5.2.5 Summary of Stetson Blunt-Cone Data

Profiles produced by a first-order boundary-layer method are clearly insufficient for stability analyses, although second-order boundary-layer techniques do appear to be sufficient. Good agreement between computation and experiment remains to be obtained. Since an accurate comparison of the mean flow profiles is not possible, due to probe interference, new experiments will almost certainly be needed to resolve the disagreement.

Entropy-layer disturbances were observed by Stetson. The frequencies of these disturbances have been explained by a new entropy-layer instability [163]. Ref. [164] reports recent computations of receptivity and linear instability for Stetson's blunt cone using DNS; however, quantitative comparisons are given-only for the mean-flow measurements.

Lyttle et al. [91] report computational comparisons to Stetson's blunt cone stability measurements. They also report new stability measurements in Russia at Mach 6, along with corresponding computations. This cooperative effort appears very promising.

5.2.6 Other Stability Measurements on Blunt Cones

Bountin et al. measured detailed wave growth on a blunt cone at zero AOA, at Mach 6 [50]. Second-mode instabilities that were measured on a sharp cone were damped when bluntness was added. A perturber was used to generate controlled first and second-mode disturbances. Additional measurements were recently obtained by the same group and are reported in Refs. [159, 91]. The second mode is again damped by bluntness, well downstream of where the entropy layer appears to be swallowed by the boundary layer. However, the second mode is still unstable, and is still most unstable when two-dimensional.

5.3 Summary of Stability Data on Blunt Cones

The boundary-layer profiles obtained during the Stetson cone experiments suffer from probe interference and are also repeatable only to 15%. The quality of these profiles is insufficient for code validation. On both the sharp and

blunt cones, the second-mode waves amplify by less than a factor of 4 within the linear region, after achieving a significant signal-to-noise ratio. This is insufficient for reliable code validation. Conventional tunnel experiments will require controlled perturbations to achieve substantial linear amplifications that would allow an accurate validation of linear computations. It is expected that a linear validation will usually be needed before a nonlinear computation can then be validated.

First-order boundary-layer methods are inadequate for computation of blunt-cone instabilities, even for preliminary design purposes. It is not yet clear whether viscous-shock-layer methods will provide results with sufficient accuracy for design purposes, or whether parabolized Navier-Stokes, thin-layer Navier-Stokes, second-order boundary-layer theory, or full Navier-Stokes will be required.

5.4 Transition on Blunt Cones at Zero AOA

Stetson also reported Mach-6 transition measurements on a blunt cone at zero AOA, scaling the reported data with the entropy-layer swallowing length [165]. The swallowing length is the distance downstream where the variations in streamline entropy caused by passage through the curved bow shock are nearly completely swallowed by the boundary layer. Stetson used approximate methods to compute the swallowing length and the local Reynolds numbers. Fig. 31 shows Stetson's results as obtained from his tabulated data (private communication, Dec. 2001; cp. Fig. 9 in Ref. [165]). Here, Re_{xT} is the Reynolds number based on local edge conditions and the arc-length to transition onset, while $(Re_{xT})_B$ is the value for blunt conditions, and $(Re_{xT})_S$ is the value for a sharp cone at the same tunnel conditions. These results were obtained on 8-deg. half-angle cones at $M_\infty = 5.9$ in the Air Force Flight Dynamics Lab tunnel at $T_0 \simeq 1100$R. Transition that occurs near the swallowing length is delayed compared to a sharp cone, and transition that occurs well forward of the swallowing length exhibits lower transition Reynolds numbers than for a sharp cone. The transition delay that occurs near the swallowing length is highly dependent on Mach number as well as bluntness. Ref. [166] reports additional detail, including the significant effect of placing the cone off the tunnel centerline.

The raw data corresponding to Fig. 31 are shown in Fig. 32. These previously unpublished data were furnished by Stetson from his notes, and were obtained in the high Reynolds number Mach 6 tunnel at the Air Force Flight Dynamics Lab in Dayton, at stagnation temperatures of about 1100R. Transition was determined from heat-transfer rate data obtained using a thin-

skin model. For repeated runs, the average is shown here. The model wall temperature was about 540R, except near the nose, since the measurements were made immediately following model injection. The nosetip was polished between each injection, although pits developed and remained after several runs. The 8-deg. half-angle cones had a 2.00-in. base radius and replaceable tips, and x_T is the arc length to the onset of transition, measured along the surface from the stagnation point. For fixed tunnel conditions, transition moves aft as the nose radius increases, up to a nose radii of 0.50 in. For a larger nose radius of 0.60 in., transition was not repeatable, and seemed to depend on the nosetip roughness (which itself was not repeatable due to grit impacts during the runs). The nosetip temperature had a substantial effect on the $R_n = 0.60$ in. runs (see the discussion in Section 5.4.1).

Ericsson correlated ground-test and flight data for transition on blunt cones [167]. He scaled the arclength with an inviscid entropy-wake length, adding a correlation and a comparison to the flight data. However, his Fig. 5 plots only a portion of the data he cites, and the strong statements common in this paper are not always well supported. Stetson [168] questions many of this paper's conclusions, including the use of inviscid correlating parameters for a viscous phenomenon. Correlations of this type can always be made to fit a selected set of data; however, their general applicability to a wide range of data is seldom addressed systematically (see Ref. [141] for one systematic treatment of various correlations).

5.4.1 Nosetip Roughness Effects on Frustum Transition

For the larger bluntnesses studied by Stetson [165], transition on the frustum became very sensitive to small roughness on the nosetip, in part due to the large unit Reynolds numbers necessary to achieve transition [169]. The nosetip pits during operation due to blasting by contaminating flowfield particulate, making repeatable experiments difficult. Transition becomes sensitive to the nosetip temperature as well as to the nosetip roughness, and the transitional region lengthens. Transition begins to move with time during a run, as the nosetip heats up.

Stetson isolated the effect as shown in Fig. 33. The measurements were made in the 12-inch Mach-6 blowdown tunnel at the Air Force Flight Dynamics Lab [165, 170]. The 8-deg. half-angle cone had a nose radius of 0.6 inches and a base radius of 2 inches. *'The cone contained two rays of thermocouples, located circumferentially 180 deg. apart. The nosetip was mounted such that one ray of thermocouples was downstream of the 'smooth' side of the nosetip and the other ray was downstream of the 'rough' side of the nosetip'* (Ken Stetson, private

communication, August 2003). The stagnation pressure was 1900 psia and the stagnation temperature was about 1100 Rankine, for a freestream Reynolds number of 26.6×10^6/ft. and a freestream static temperature of 137 Rankine. The freestream Mach number was 5.9 and the freestream velocity 3405 ft./sec. The nosetip was solid stainless steel, but contained no thermocouples. One side of the nosetip was polished smooth (although it still contained some pits that remained from previous runs), while the other side was grit-blasted to 45-50 μinch rms roughness. Transition was measured on the thin-skin cone using thermocouples. The results are compared to laminar and turbulent computations; the source of these computations is uncertain, although they probably derive from the GE or AEDC codes cited in Ref. [165].

Fig. 33 shows the measured heat-transfer rate at various times after the model reached the tunnel centerline following injection. The thermocouples along the ray centered on the smooth side show flow that remains laminar during the entire sequence. Initially, the thermocouples on the rough side show transition onset at $x \simeq 4$ inches; thus, roughening the nosetip has a dramatic effect. The same roughness on a 0.3-in. nose radius tip had no effect, so it is a combination of freestream conditions, model geometry, and nose roughness that produce the early frustum transition. As time goes on in the successive frames, the nosetip heats up, the nosetip roughness looks smaller to the thickening boundary layer, and the transitional heating falls, although the departure from laminar flow remains near $x \simeq 4$ inches at least through frame (c), after about 1 sec. on the centerline. Frames (e) and (f) show the heating on the rough side dropping completely to laminar levels by 2 sec. after arrival on centerline. The nosetip boundary layer has apparently thickened enough due to wall heating that the grit-blasted roughness is no longer sufficient to cause early frustum transition. A similar movement was observed by Muir and Trujillo [171]; see Ref. [172] for a detailed discussion of data that should be reanalyzed.

Stetson believes that the same effect contaminates the large-bluntness data of Muir and Trujillo (see Section 7.2). Since the effect was related to nosetip roughness, Stetson *'sought to demonstrate that some critical value of nosetip Reynolds number, combined with nosetip roughness, produced early transition on the frustum of a cone'* (private communication, July 2003). Stetson attempted to illustrate a trend by looking at a percentage of the PANT correlation for roughness-induced transition on nosetips [173, 174]. Fig. 34 replots the results from Fig. 10 of Ref. [165]. The vertical and horizontal axis coordinates are the usual PANT parameters. The Demetriades curve was digitized from Ref. [165]. The data points were provided in tabular form by Stetson (private communication, July 2003). The PANT curve is $Re_\theta[(T_e/T_w)(k/\theta)]^{0.7} = 215$,

from equation 6-1 in Ref. [174], where all values are evaluated at the sonic location on the nosetip. The Demetriades curve is an extension of PANT to smaller nose roughness.

Stetson (private communication, July 2003) explains the experiments as follows: *'Nosetip roughness was increased by grit-blasting solid 15% and 30% blunt nosetips. The entire nosetip then contained 45-50 microinch roughness. Upon completion of the experiments the process was repeated with a larger grit size, producing 90-100 microinch roughness. Each data point shown in Fig. 34 represents the result of a sequence of tests with varying conditions to find when the 'normal' frustum transition shifted to the 'early' frustum transition.'*

'For the 15% bluntness, the 45-50 microinch roughness had no effect on frustum transition. That is, the frustum transition data were similar to that obtained with a smooth nosetip. The maximum condition tested was at $P_t = 2000$ *psia. The threshold conditions for the nosetip to influence frustum transition required a higher pressure that was not obtainable. This led to the data point at* $Re_\theta = 86$ *and* $(k/\theta)(T_e/T_w) = 0.71$, *which is drawn with an upward arrow to indicate that the threshold would be at a higher pressure. Experiments with the larger 90-100 microinch roughness at* $P_t = 1400$ *psia gave results similar to those on the smooth nosetip. However, at* $P_t = 1600$ *psia early transition was observed on the frustum. This gave the data point at* $Re_\theta = 77$ *and* $(k/\theta)(T_e/T_w) = 1.26$.*'*

'For the 30% bluntness and the 45-50 microinch roughness, frustum transition at $P_t = 1600$ *psia was similar to the tests with the smooth nosetip. At* $P_t = 1700$ *psia, early transition was observed on the frustum. This gave the data point at* $Re_\theta = 113$ *and* $(k/\theta)(T_e/T_w) = 0.46$. *For the larger 90-100 microinch roughness, early transition was already observed at the lowest test pressure of* $P_t = 1400$ *psia. Thus, the threshold was at a lower pressure, leading to the data point at* $Re_\theta = 102$ *and* $(k/\theta)(T_e/T_w) = 0.83$, *with the downward arrow.' For another 30% bluntness nosetip with a 15 microinch roughness, tests resulted in* $Re_\theta = 119$ *and* $(k/\theta)(T_e/T_w) = 0.15$.*'*

Additional points were obtained by varying the nosetip temperature. *'The 30% bluntness tip was measured with the 45-50 microinch roughness but with the tip not being cooled between runs. The wall temperature was estimated to be about* $700°R$ *for this case. The tests for early frustum transition resulted in the data point at* $Re_\theta = 119$ *and* $(k/\theta)(T_e/T_w) = 0.37$. *For a similar test with a thin-skin 30% bluntness tip, the nosetip was hot, and early frustum transition was not observed at the maximum tunnel pressure. The threshold was therefore higher than* $Re_\theta = 122$ *and* $(k/\theta)(T_e/T_w) = 0.09$, *which is drawn with a upwards arrow. The computations of* θ *and* Re_θ *were carried out with several approximate methods that gave similar results. The easiest method was*

to scale the printed results from the GE code, using $\theta \sim \sqrt{Re_R}/\sqrt{P_t}$.

In Fig. 34, then, the region above the PANT/Demetriades correlation is where transition on the nosetip is expected. The region between 40% and 100% is the region where nosetip roughness is expected to cause early frustum transition, and the region below 40% is where nosetip roughness is expected not to influence frustum transition. Both these correlations are empirical, of course, and Stetson emphasizes that the 40% value is not significant, it is just a preliminary estimate based on very limited data. It only shows that frustum transition for these cases follows the same trend as would be expected from nosetip transition. The trend may be significant, the percentage value would be expected to differ for other conditions. An analytical curve similar to the Demetriades extension can be obtained by combining the 40% PANT line with a line at $Re_\theta = 115$; this simpler form might be just as good for initial efforts. Such use of a constant Re_θ value at low roughness heights would follow Batt's analysis [173].

These initial efforts by Stetson mainly serve to illustrate that nosetip roughness can cause early transition on the frustum, via a mechanism that at present has no theoretical explanation. The rough correlation shown in Fig. 34 provides an initial starting point for the future research that is clearly needed. It may be that transient-growth theory will be able to provide an explanation for this effect [175]. For more details on the Stetson experiments, see Ref. [176].

Similar experiments were reported by Zanchetta et al., who measured transition on a blunt cone at zero AOA in the gun tunnel at Imperial College at Mach 9 [177]. Intermittency was measured using an array of surface thin films. For a large bluntness with a Reynolds number of 1.08×10^6 based on nose radius and freestream conditions, the flow was visualized using liquid crystals. When the nosetip was polished, the flow remained laminar to $Re_s > 3 \times 10^7$. When 50 μm diameter roughness elements were placed on the nosetip, vortex streaks were observed downstream, and transition occured by $Re_s = 4 \times 10^6$. Few details are reported. It would be interesting to compare the Zanchetta results to Stetson's correlation.

6 Angle of Attack Effects on Sharp Cones

6.1 Instability Measurements

Stetson measured detailed boundary-layer profiles and laminar instability on a 7-deg. half-angle sharp cone at Mach 8 [178]. After two decades, this is still one of the most sophisticated experiments carried out on a hypersonic round

cone at AOA, although the data is very limited. Profiles were measured on the windward and leeward meridians. Instability-wave amplification was deduced from spectral measurements. The critical Reynolds number for the onset of instability increased on the windward ray and decreased on the leeward ray. First-mode amplification rates decreased on the windward ray, while second-mode amplification was not greatly affected by AOA. Windward-ray transition occured later than in any previous experiments.

Simen et al. made detailed computations for a sharp cone at AOA, at Stetson's conditions [105]. The thin-layer Navier-Stokes equations were used for the mean flow. Computed amplification rates on the leeward ray showed good agreement with Stetson's measurements.

Doggett et al. made stability measurements on a sharp flared cone at AOA in the Langley Mach-6 quiet tunnel [179]. This is the second existing set of hypersonic stability measurements on a cone at AOA, and the only set carried out under low noise conditions with RMS fluctuation levels that are comparable to flight [31]. The boundary-layer on the windward ray was more stable than at zero AOA, and the leeward ray was less stable. Second-mode instability was dominant at zero AOA but was stabilized on the windward ray at AOA. The very high frequency of the dominant instability on the leeward ray was thought to indicate the presence of an instability differing from the normal second mode. Quantitative comparison to computations is difficult since the hot-wire was not calibrated.

Boylan et al. made measurements of the mean shock-layer profiles on the leeward ray of a 4-deg. sharp cone at 2.94-deg AOA and Mach 9.82. The results were compared to a viscous-shock-layer computation, which showed limited agreement [180]. Although no instability measurements were made, the report is worthy of note due to the scarcity of profile measurements on hypersonic cones at angle of attack.

Hanifi et al. computed the stability of flow past a sharp cone at Mach 5, but based their mean-flow solutions on asymptotic approximations for small AOA [181]. They look at stability on the windward and leeward ray. For AOA of 1 deg. on a 10-deg. half-angle cone, the most unstable 2nd mode wave shifts from 2D to oblique, and the 1st-mode amplification rates change by 40%. Small AOA has a large effect on stability, mostly because the crossflow carries low-momentum fluid around the cone, and changes the boundary-layer profile.

Olsson made detailed measurements of instability on a 7-deg. round cone at AOA and Mach 3 [182]. Away from the sharp tip, similar profiles were observed along the windward and leeward rays. However, the uncalibrated hot-wire data were not reduced beyond plotting profiles. Ref. [183] reports

additional measurements on blunt cones including AOA, but again the report gives only raw profiles without analysis. Ref. [184] summarizes the work. At a 1-deg. AOA, the sharp-cone transition moves forward by more than 50% on the leeward ray. The sensitivity to AOA is about half that amount for a 10-mm nose radius.

Ladoon et al. measured amplification of repeatable instability-wave packets on a Mach-4 cone at AOA [120, 185]. However, the artificially-generated packets grew by factors of only 1.5-3 at the low Reynolds numbers available in the Purdue Mach-4 quiet Ludwieg tube.

Perraud et al. summarize Mach-7 experiments and computations on a 7-deg. half-angle sharp cone at 2-deg. AOA [186]. Transition location varied from 40% of the body length on the leeward ray to 76% on the windward ray. Halfway between, transition occured at 61%, and both crossflow and 2nd-mode instabilities had about the same N factor, with the first mode and crossflow modes becoming difficult to distinguish. Stability computations using e^N could predict the general trends, although quantitative agreement was poor, and N was only 1.2 in the small conventional wind tunnel that was used.

Adams reviewed flow visualization data on sharp cones at angle of attack [187]. These data show striations corresponding to crossflow vortices, which form some distance downstream of the nosetip, and disappear upon the onset of transition. For examples, see Refs. [188] and [189]; a magnified portion of Figure 21 from Ref. [189] is shown here in a grayscale version as Fig. 35. Fig. 35 was obtained using liquid crystals on a 10-deg. half-angle sharp cone at 15-deg. angle of attack. The Reynolds number based on freestream conditions and model length is 4.86×10^6, and the freestream Mach number is 8.0. A wave pattern is evident between about 30% and 60% of the model length; these waves are attributed to stationary crossflow vortices. Adams correlated the onset of vortex formation in Ref. [188] with the crossflow Reynolds number, computed using a 3D boundary-layer code. The angle of the vortices was also correlated using stability theory. This work is one of the very few in the existing literature which clearly show a relationship between experimental data and a theoretical transition mechanism.

6.2 Transition Measurements

DiCristina made measurements on an 8-deg. half-angle sharp cone at AOA and Mach 10 [190]. The bulk of the transition data was inferred from Schlieren photographs, so that it could be compared to photographs on a cold-ablating model. This optically-inferred transition point is near the end of transition, as described in some detail in the paper. For a 2-deg. AOA, transition on the

leeward ray moved forward by 20%, and was 60% forward at 4-deg. Transition can be very sensitive to small AOA, as has often been shown. However, here transition moved aft very little on the windward ray with AOA. The effect of dynamic motion was secondary, although ablating effects were as important as AOA.

Fischer measured transition on sharp and blunt cones at angle of attack in the 11-inch Langley tunnel at Mach 7 [191]. For the nonablating sharp cone, transition was obtained from thin-skin thermocouple measurements of heat transfer. Transition on the sharp non-ablating cone moved forward on the leeward ray and aft on the windward ray. For the blunt nonablating cone, transition occured only on the leeward ray, and was aft of the sharp cone case. Results are also reported for a cone with a low-temperature ablating frusta of paradichlorobenzene. This is one of several experiments that use low-temperature ablators in low-temperature tunnels to simulate ablation on reentry vehicles. The surface recession of the ablating cones was measured in order to determine massflow rates, after 30 sec. in the tunnel; these were the only measurements on the ablating cones. The ablating cone had a nonablating tip. Longitudinal vortices were observed in the ablated surface, especially at the higher unit Reynolds numbers where more ablation occurred. These were attributed to a Görtler-type instability aft of the rearward-facing step that formed behind the tip; the step was also larger at the higher Reynolds numbers. Ablation and the resulting step lowered the transition Reynolds number by 28 to 35 percent.

Fischer also measured transition on nearly-sharp 2.87-deg. half-angle cones at Mach 21 in the hypersonic helium tunnel at Langley [192]. Transition moved aft on the windward ray and forward on the leeward ray, except for AOA of less than 1 deg., where these trends were reversed. The results reported in Ref. [192] contradict earlier measurements in the same facility that used a pitot tube instead of heat-transfer measurements to detect transition. The complex curve of transition location vs. AOA that is shown in Fischer's Fig. 2 has never been explained.

Mateer measured transition on sharp cones at Mach 7.4 [193]. Reynolds numbers based on edge conditions were computed using the method of characteristics and a boundary layer analysis. For a 5-deg. half-angle cone, length transition Reynolds numbers based on edge conditions (Re_{xe}) increased with AOA on the windward ray, and decreased on the leeward ray. For a 15-deg. half-angle cone, Re_{xe} decreased with AOA on both the windward ray and the leeward ray. Windward-ray transition on several cones in several experiments were correlated using momentum-thickness Reynolds number divided by edge Mach number, plotted against a streamline-spreading parameter. More detail

is given in Ref. [157]. Although the title calls the cones 'sharp', the nose radius is not reported. Tabulated data shows that for the 15-deg. cone, transition on the windward ray actually moved forward as the AOA was increased. However, since unit Reynolds number was varied at the same time as AOA, tunnel noise effects corrupt the data, and would be very difficult to separate from AOA effects.

Kendall rolled a 4-deg. half-angle sharp cone at nominally zero AOA, and detected a 10% variation in transition Reynolds number, although the cone was visually free of defects, and no effects of tunnel nonuniformity were detected [194]. Transition is obviously very sensitive to small asymmetry, although a 10-deg. half-angle cone was much more symmetric.

Stetson made transition measurements on both sharp and blunt cones at AOA [195], as described in Section 7.2. Figure 36, similar to Fig. 3 in Ref. [195], shows data from 6 sources, in different facilities, with different cone angles and freestream Mach numbers. The horizontal axis is the angle of attack normalized with the cone half-angle. The vertical axis is the arclength to transition onset, normalized by the value for a sharp cone at zero angle of attack at (nearly) the same unit Reynolds number. The transition-onset locations were all taken from heat-transfer measurements. The data labeled 'McCauley' were digitized from Fig. 6 in Ref. [196], and were apparently taken at $Re_\infty = 5.2 \times 10^6$/m. The 'Holden' data were digitized from Fig. 12 in Ref. [197], and were taken at $Re_\infty = 10 \times 10^6$/m. The 'Muir' data are from Fig. 18 in Ref. [171]; the leeward data at $Re_\infty \simeq 9.2 \times 10^6$/m, and the windward at $Re_\infty \simeq 3.2 \times 10^7$/m. The two different unit Reynolds numbers were used in order to keep transition on the instrumented section of the model; it is not certain if no other datasets also varied unit Reynolds number. Such a variation does of course also vary tunnel noise, at the same time; noise effects are discussed in Ref. [31]. The data labeled 'Stetson 1981' were digitized from Fig. 3 of Ref. [195], and were taken at $Re_\infty = 3.2 \times 10^7$/m. The data labeled 'Stetson and Rushton' were digitized from Fig. 7 of Ref. [198], and were taken at $Re_\infty = 4.9 - 15.4 \times 10^6$/m. There is a 4% error in the anchor point at zero angle of attack, which is due to the limited accuracy of the original figure. The data labeled 'Krogmann' were digitized from Fig. 7 of Ref. [199], and were taken at $Re_\infty = 1.78 \times 10^7$/m (see also Ref. [200]).

In all cases, transition moves aft on the windward ray, and forward on the leeward ray. However, the large scatter in the figure shows the limitations of a simple non-dimensionalization, which cannot account for all of the variables that differ between the datasets. To the author's knowledge, these data have never been explained, although various attempts have been made to correlate subsets of the data. Unit Reynolds number, noise, freestream Mach num-

ber, and cone angle are all parameters for this complex problem. Although the crossflow instability is obviously critical away from the windward and leeward rays, flow on those rays is probably affected only indirectly by crossflow, through changes in the boundary layer profiles. One would thus expect that transition on the windward and leeward rays is caused by the first-mode or second-mode instabilities, but further research is clearly needed.

7 Angle of Attack Effects on Blunt Cones

7.1 Instability Measurements

No measurements of instability on blunt cones at angle of attack are known to the author. Measurements of this type are clearly needed, in coordination with detailed computations.

7.2 Transition Measurements

Fischer made measurements of transition on the windward and leeward rays of ablating and nonablating 10-deg. half-angle cones at zero and nonzero AOA [191]. For the sharp cone, transition moved forward on the lee side and aft on the windward side. Transition only occured on the lee side of the blunt cones when at angle of attack, due to limitations on the unit Reynolds number in the tunnel.

Stainback made measurements on the windward and leeward rays of a blunt cone with roughness at AOA [143]. The roughness was all downstream of the nosetip. Transition exhibited the usual unit Reynolds number effect, and moved forward on the leeward ray and aft on the windward ray.

Muir and Trujillo measured transition on the windward and leeward rays of sharp and blunt cones at AOA, at Mach 6 [171]. Tabulated data from Ref. [171] is replotted here in Fig. 37, in Stetson's coordinates. The horizontal axis is the angle of attack normalized with the cone half-angle. The vertical axis is the arclength to transition onset, normalized by the value for a sharp cone at zero angle of attack at (nearly) the same unit Reynolds number, both as determined from heat-transfer measurements on a thin-skin model in the same tunnel. This normalization for the vertical axis is an attempt at scaling out the tunnel noise effects. The open symbols are the Muir et al. data, connected by hand-drawn lines to aid the eye. All datasets shown were obtained at $M_\infty = 6$, on 8-deg. half-angle cones, in tunnels with pebble-bed heaters. The Muir et al. data was obtained in Tunnel 8 at the Naval Ordnance Lab on a cone with

a 2.5-inch base radius.

At zero AOA, transition moves aft as bluntness rises from zero, and then moves forward again at large bluntness. For very large bluntness, transition moved aft during the run as the model heated up. This effect may well be due to nosetip temperature increases and the resulting reduction in roughness effects (see Section 5.4.1; see Refs. [172] and [201] for more details). For small bluntness, transition is leeside forward and windside aft, but at large bluntness, AOA effects reverse, and transition is windside forward and leeside aft. The initial nosetip surface roughness is reported as 16 microinches rms, but no after-run nosetip roughness was reported. NOL Tunnel 8, the facility used, was well-known for blasting models with particles from the pebble-bed heater (e.g., Dan Reda, private communication, 2002). Such blasting effects would be similar to those observed by Stetson, as the Flight Dynamics Tunnel also had a pebble-bed heater [165]. Muir stated (private communication, 2002) that they never considered the effect of tunnel-induced roughness on the nosetip, although repeated runs are present in the detailed tabulated data, and repeatability is fairly good.

Martellucci et al. also measured transition on the windward and leeward rays of sharp and blunt cones at AOA, at Mach 8 [202, 203, 204]. A reversal of AOA effects from leeside-forward to windside-forward was also observed, as the nose bluntness increased from 1% to 2%. Nose radius (bluntness) is quoted as a percentage of the base radius, following the original paper, but the most appropriate means of scaling nose radii for transition purposes remains to be determined. A plot similar to Fig. 37 can be made using Tables IV-VI in Ref. [202], wherein the *end* of transition is tabulated as inferred from heat-transfer measurements on a 7.2-deg. thin-skin cone at Mach 8 in Tunnel B at AEDC. The base radius is 5.5 inches. The tunnel stagnation temperature was about $1360°R$, and the measurements were made shortly after model injection, at a surface temperature of about $540°R$. The results are shown in Fig. 38, where the vertical axis is the arc length to the end of transition normalized by the value for a sharp cone at zero AOA at the same unit Reynolds number, and the horizontal axis is the AOA normalized by the half angle. The freestream unit Reynolds numbers are given in the legend; selected data for two unit Reynolds numbers are shown. Transition is delayed by increasing nose bluntness, with the degree of delay markedly larger at the higher unit Reynolds number. For the sharp cone, transition is delayed on the windward ray and moves forward on the lee ray, as expected. The variation with angle of attack is affected by unit Reynolds number, particularly on the lee ray. For the blunt cones, angle of attack always moves transition forwards, both on the leeward and windward rays. For the 1% bluntness cone, transition is further forward on

the lee ray, whereas on the 2% bluntness cone, transition is further forward on the windward ray. For the 2% bluntness case, unit Reynolds number again affects the quantitative results.

Sakell measured transition on the windward and leeward rays of sharp and blunt 10-deg half-angle cones at AOA, at Mach 6 [205]. For the sharp cones, transition moved forward on the leeside ray and aft on the windward ray. As bluntness increased, transition moved aft at zero AOA. However, transition then became very sensitive to tunnel pressure, moving forward by 90% of the body length when stagnation pressure was increased by 10% (p. 9). For large bluntness, high unit Reynolds numbers were needed to obtain transition on the model, and AOA effects reversed to windside forward and leeside aft. For the 0.5-inch nose-radius cone, Fig. 65 in Ref. [205] shows transition reversing from leeside forward to windside forward as the tunnel stagnation pressure increased from 900 to 1400 psia. Clearly, there is a shift in mechanism, which Sakell was not able to explain. It seems likely that this was again due to the roughness effect identified by Stetson [165]. Sakell reports no measurements of nosetip roughness, and (private communication, 2002) did not consider nosetip roughness generated by tunnel particulate.

Stetson measured transition on sharp and blunt cones at angle of attack in a Mach-6 tunnel [195], as is also shown in Fig. 37. The Stetson data were obtained on a cone with a 2-inch base radius, so the $R_N/R_B = 0.10$ Stetson data was obtained with the same 0.20-inch nose radius as the $R_N/R_B = 0.08$ Muir data. On a sharp cone, the movement of transition with angle of attack depends on tunnel and Mach number (and noise levels [31]). However, transition always moves aft on the windward ray and forward on the leeward ray. On the windward ray of the blunt cone, transition first moves aft with AOA, and then forward with larger AOA. Transition always moves forward with AOA on the leeward ray. On a 2%-blunt-nosetip 8-deg half-angle cone (not shown here), an AOA of 1 deg. moved transition forward by 50% on the leeward ray. The Muir et al. data at 8% bluntness is similar to the Stetson data at 10% bluntness, although there are quantitative differences, particularly on the windward ray.

Ref. [169] provides details on the sensitivity to nosetip roughness at large bluntness; due to tunnel-particulate sandblasting, the data becomes unrepeatable, at zero or nonzero AOA. It is curious that the nonrepeatability observed by Stetson was not observed by Muir et al., despite the similarity of the models and tunnels. Stetson did not obtain repeatable data at large bluntness where transition might have been windside forward, as in the 32% bluntness case of Muir et al. Stetson polished his nosetips between every tunnel run, whereas Muir did not; this may possibly account for the discrepancy.

Holden measured transition on sharp and blunt cones at AOA at Mach 11 and 13 [197]. The data were reanalyzed in Ref. [206], and possibly combined with later data. For small-bluntness cones, transition moved forward on the leeward ray and aft on the windward ray. However, for the largest bluntness, this pattern reversed, and transition moved forward on both the windward and leeward rays (differing from Muir and Trujillo). Limited measurements also explore the marked effect of nosetip gouges on frustum transition. Steps and gaps in the frustum surface had a lesser effect on transition.

Thyson et al. put roughness trips and blowing trips just aft of the nose of a hypersonic blunt cone at AOA [207]. The trips cause transition to occur first on the windward side, since the boundary layer is thinner there. Thus, a shift from a smooth-wall stability-based mechanism to a roughness-induced one would tend to shift transition from leeside forward to windside forward.

For blunt and sharp 5-deg. half-angle cones at Mach 6, Bailey showed that transition can move center-of-pressure by about 4% for angles of attack of one or two degrees [208]. Boudreau also measured transition on a very blunt cone at zero and nonzero angle of attack [209], but few data are reported, and the roughness of the blowing model may have affected the no-blowing meausurements.

Martellucci later reported additional measurements of transition on a blunt cone at angle of attack, obtained using infrared thermography techniques [210]. The measurements were carried out on a 7-deg. half-angle cone with a 12.3-inch base diameter at Mach 8 in Tunnel B. The 4% bluntness model yielded transition that moved forward on the lee ray with angle of attack. On the windward ray, transition moved slightly aft for angles of attack of about 0.5 deg., and then moved forward for larger angles. Although several nosetip radii were tested, the reported data is not sufficient to add these data to Fig. 37.

Nowak et al. made measurements on a 12.5-deg. half-angle cone at zero and non-zero angle of attack, in the 8-foot High Temperature Tunnel at NASA Langley [211]. Three nosetips were tested: one with a nearly-sharp 0.02-inch radius, one with 1-inch radius, and one with a 3-inch radius. The two sharper nosetips had ogive nosetip frusta, and the primary 12.5-deg. frusta had a 3-foot base diameter. The experiments were carried out at a total temperature of $3300^{\circ}R$ in air that was heated by combusting methane, producing a freestream gas with properties different from air, including a lower effective specific-heat ratio. Transition was inferred from heat-transfer measurements. Most measurements were carried out at a unit Reynolds number of 1.4×10^6/ft. For all three nosetips, transition was furthest aft at zero angle of attack, and moved forward on both the windward and leeward rays. For the larger nose radii, windward-ray transition was generally further forward than leeward-ray

transition. Data for the nosetip roughness is not reported.

Johnson and Candler et al. computed the effect of chemistry on the stability of blunt cones at angle of attack [212]. Sharp and blunt cones are computed at 4 km/s and a 20 km altitude. Full nonequilibrium chemistry is included, but the linear stability analysis is presently limited to parallel flow without curvature terms. Bluntness stabilized the flow.

8 Summary of Stability and Transition on Circular Cones

1. Hypersonic transition on sharp cones at zero angle of attack is probably caused by growth of the second-mode instability, for smooth non-ablating cones at sufficient Mach number. Quantitative validation of the stability computations remains to be achieved.

2. Transition on sharp cones at zero angle of attack can be correlated with tunnel-noise parameters, independent of Mach number. Thus, measurements of transition alone do not provide a reliable means of estimating transition location in flight.

3. Hypersonic transition on smooth nonablating blunt cones at zero angle of attack is probably caused by growth of the second-mode instability, for sufficiently small bluntness and sufficiently high Mach number.

4. Transition on both sharp and blunt cones is very sensitive to small angle of attack, especially for slender cones with smaller nose radii. This is presumably due to crossflow, which carries low-momentum fluid from the windward to the leeward sides, affecting the streamwise instabilities and introducing the crossflow instability.

5. Both sharp and blunt cones appear to exhibit the crossflow instability at angle of attack. Flow visualization shows clear evidence of these nearly-streamwise vortices, just like in low-speed measurements on swept wings. This suggests that the vortices can be induced under controlled conditions using very small roughness elements, as in Saric's work [213]. It also suggests that careful computations using the nonlinear parabolized stability equations could reproduce the experimentally measured amplification, and enable a physics-based prediction method.

6. For blunt cones at angle of attack, there is good evidence for a change from an apparently smooth-wall mechanism for small nose radii to a

nosetip-roughness-related mechanism for larger nose radii. This change in mechanism would explain the reversal from leeward-forward transition at small nose radii to windward-forward transition at large radii. Careful measurements with small roughness on the nosetip should explain this phenomenom, which may be related to the transient-growth instability (e.g., Ref. [214]).

7. Mechanism-based approaches to hypersonic transition are only beginning to be developed. For two-dimensional and axisymmetric flows, stability-based computations are now feasible but not yet routine. Validation of these quasi-2D methods is only beginning, even for smooth non-ablating walls without blowing. Study of roughness, ablation, and blowing is in its infancy. For three-dimensional flows, mechanism-based methods appear feasible, but have yet to be developed and validated.

8. Rapidly decreasing computational costs make mechanism-based approaches more feasible every year. The limiting factor is no longer the computer hardware, but rather the lack of user-friendly, reliable, and validated codes. Experimental work is needed in order to develop and validate these codes. The primary limitation on the experimental work has been the high cost of the difficult, detailed, and iterative experiments that are required. Quiet tunnel development and mechanism-based high-enthalpy experiments are also pacing items. Direct numerical simulations are also needed, particularly in cases where the relevant experiments are too difficult or expensive.

9. Experimental studies should be carried out in close coordination with computations. This is becoming less difficult, as codes for accurate computation of the mean-flow and linear instability become more accessible.

9 Transition on Scramjet Forebodies

9.1 Hypersonic Airbreathing Vehicles

Boundary-layer transition is critical to the development of large airbreathing hypersonic vehicles [1, 215]. The 1992 Defense Science Board report on the National Aerospace Plane Program found that *'Perhaps the highest technical risk in the program is the ability to quantify the characteristics of the scramjet and its flowpath integration into the airplane. Not far behind in technical risk is the uncertainty associated with boundary layer transition. It is essential to*

understand the boundary layer behavior at hypersonic speeds in order to ensure thermal survival of the airplane structure as designed, as well as to accurately predict the propulsion system performance and airplane drag.' [2].

A 1988 review by the Defense Science Board found that ... *estimates* [of the point of transition] *range from 20% to 80% along the body ... The assumption made for the point of transition can affect the vehicle gross takeoff weight by a factor of two or more.* [216, p. 9] Fig. 39, replotted from Fig. 12 in Ref. [217], illustrates this point for a single-stage-to-orbit NASP design. A fully laminar boundary layer reduces drag by about 6% compared to the baseline target, while a fully turbulent layer increases drag by 8%. For the baseline, with substantial laminar flow on the forebody, *'the reduced drag and lower heating over the forebody can result in a 60-70% increase in payload over the all turbulent condition.'* [217, p. 5] Wilhite et al. in an earlier paper showed a 27% increase in gross takeoff weight for a different all-turbulent design, as compared to a nominal transition criterion [218]. While future designs are unlikely to return to the single-state-to-orbit concept of NASP, any large airbreathing stage with a long cruising period is likely to experience similar effects [219]. The forebody boundary layer should be laminar and attached, to reduce skin friction and heating on the forebody, and provide the largest massflow to the cowl inlet [217]. However, the boundary layer must remain attached, and this is more difficult to achieve with a laminar layer [220, Sect. 5.7].

9.2 Scramjet-Forebody Geometries

Since airbreathing hypersonic vehicles have not yet flown successfully, considerable uncertainty remains regarding the forebody geometries that might be used. One candidate would be axisymmetric geometries such as that of the Russian Kholod vehicle [221, 222]. Another set of likely candidates would be geometries similar to the Hyper-X or X-43A [223]. A similar but generic geometry called the 'Hyper2000' was obtained from the Hyper-X Program Office at NASA Langley, through Charles McClinton.

Figure 40 shows a detail of the side view of the Hyper2000 forebody. The forebody is flat over the middle of the vehicle. The Hyper-X and the Hyper2000 have two compression corners, of 5.5 and 3 degrees, following an initial wedge with an included angle of 2.5 degrees. The chines (to the sides of the flat part of the lower surface) and the upper surface are very important to establishing the 3D pressure distribution, and any crossflow.

9.3 Properties of the Flowfield on the Hyper-X or Hyper2000

Scott Berry from NASA Langley has published aerothermodynamic measurements on the Hyper-X forebody [224, 223]. Taken as a whole, the data suggest the following picture. Upstream of the first corner, the boundary-layer flow is nearly streamwise, with little spanwise crossflow. The laminar boundary layer entering the first corner forms a separation bubble. The bubble affects the flow near the surface, as does the change in spanwise pressure gradient presumably associated with the increased wedge angle downstream of the corner. Crossflow is induced in the boundary layer downstream of the first corner, with *the amount of crossflow that occurs being dependent on the properties of the boundary layer entering the first ramp, downstream of the first corner.* The second corner does not seem to cause any dramatic changes. Since the Mach-6 oilflow seems generally similar to the Mach-10 data, these appear to be generic effects.

These data suggest that the following instability mechanisms should be considered.

1. First or second mode instability in the cold-wall flow at Mach 6 upstream of the first corner. The dominant streamwise mode would depend in part on the nose bluntness and wall temperature [90]. Reshotko points out that the bluntness effect may extend much farther downstream in nearly two-dimensional flow, as compared to conical flow; this would tend to make the first mode more important ([15]; also, private communication, March 2003).

2. Shear-layer instabilities in the separated flow at the corner(s).

3. Crossflow instability in the ramp flow.

Görtler instability near the compression corner is also a possibility [225]. Balakumar et al. [225] made computations of the flow past a 5.5-deg. compression corner, simulating the first corner of the Hyper-X. Balakumar et al. primarily focused on the second-mode instability, which does not amplify markedly in the corner. However, the Görtler number was also computed near the corner, using the curvature of the streamlines, and found to exceed 800, over a short distance. Following this work and that of Ref. [226] for streamwise-vortex instabilities in low-speed separation bubbles, a Görtler-like instability should also be considered.

Several questions are immediately evident:

1. Can streamwise vortices from the leading edge, any trips, or from shear-layer instabilities, couple into the crossflow instability downstream of the corner, to form a dominant mechanism? This seems particularly likely, since for reattaching shear layers above the separation bubbles that can occur in compression corners, vorticity from the leading edge is known to be a trigger.

2. Can second mode waves generated upstream of the first corner couple into the shear layer instabilities to form the dominant transition mechanism?

3. Do first mode waves have large amplitude upstream of the corner, and how do they interact?

Berry's data also shed light on the difference between Mach 6 and Mach 10, and on some of the tripping questions that will remain issues for the smaller-scale missile designs. Tripping at Mach 10 was much more difficult, as would be expected [133, 227]. Larger trips are required, and transition begins downstream of the trips anyway. Trips that are too large tend to cause streamwise vorticity that convects right into the combustor inlet. At Mach 6, relatively small trips caused transition to occur downstream of the first corner. Larger trips could move transition to the roughness element.

Only one high Reynolds number quiet-flow test of a scramjet forebody is reported in the open literature, and the information presented there is very limited [228]. The model was a NASP-like geometry and was tested in the Langley Mach 3.5 quiet tunnel. It had a 0.012-inch radius nose on a 3.6-degree wedge forebody, followed by unspecified discrete compression ramps. Measurements in the region past the first corner showed length transition Reynolds numbers of about 6 million for quiet conditions, and about half that under noisy conditions [228]. Forward of the first corner, on the centerline, transition did not occur under quiet-flow conditions. Transition did occur forward of the first corner off the centerline.

The other quiet-flow test of a scramjet forebody was carried out at low Reynolds number and Mach 4 [222]. Transition was induced by adding fairly large roughness elements, and it was shown that both tunnel noise and roughness height affect transition location.

The streamwise-vortex instability on the Hyper-2000 was addressed in Ref. [229], where controlled roughness elements were placed on the leading edge in order to generate repeatable streamwise streaks. Temperature-sensitive paints were used to measure the growth of the streaks at the wall (a technique which may give misleading results in the separated flows near the corners).

The streamwise vorticity was observed to amplify dramatically in the region between the compression corners. However, the leading edge used in these experiments was not nearly as uniform as it should be, and the accuracy of the temperature paints technique left much to be desired. Much research is still needed.

9.4 Review of Laminar Compression Corners and Their Effects on Transition

The Hyper-X geometry contains a flow feature which is rarely studied in connection with transition. This section therefore reviews compression corners and boundary layer transition.

The compression corner is a classical example of shock/boundary-layer interaction [230, 231, 232, 233, 234, 235]. A shock is generated at the corner and interacts with the incoming boundary layer. Many practical cases involve turbulent incoming boundary layers, so many reviews consider primarily the turbulent case [234]. Stollery reviews the laminar case in two pages [235]. He points out a repeated issue, that *'No real interaction can be genuinely two-dimensional.'* Separation is more likely as the turning angle is increased. Incipient separation for a laminar layer is correlated to

$$M_\infty \alpha_i \simeq 80 \bar{\chi}^{1/2},$$

where

$$\bar{\chi} = M_\infty^3 \left(C/Re_L\right)^{1/2},$$

α_i, the compression angle at incipient separation, is measured in degrees, Re_L is the length Reynolds number of the laminar boundary layer approaching the corner, and C is taken as unity. Stollery also points out that *'The detailed patterns described here are crucially dependent on two phenomena which will powerfully influence the whole flow field, namely transition and separation.'*

Delery points out that most 'laminar' interactions are actually transitional, since transition commonly occurs in the shear layer above the separation bubble, which is very sensitive to small disturbances [230]. Since nearly all known studies were carried out in noisy conventional tunnels, substantially different results might be observed in a quiet tunnel. Streamwise vortices are commonly observed in heat-transfer measurements at reattachment; these are presumably generated by an unknown instability in the shear layer [230, 236].

De Luca et al. studied these streamwise vortices in detail, using IR imaging, using corner angles of 10-deg. and larger, at Mach 7. De Luca shows that their location can be connected to small flaws in the leading edge [237]. De

Luca's work is reminiscent of Saric's work with the triggering of stationary crossflow vortices by small roughness [213], and suggests that careful experiments with small roughness elements should be able to work out the vortex-growth mechanisms. The small roughness elements could be simulated with small streamwise vorticity in computations, for comparison. Vermeulen et al. made similar measurements of streamwise striations in a compression corner, at Mach 6 [238].

Tobak examines the generation of streamwise vortices on a flat plate at angle of attack using linear theory [239]. Fig. 6 in Ref. [239] shows a oil-flow image of the vortex developing behind a leading edge flaw at $M_\infty = 7.4$. The oil flow image suggests a local separation line underneath a vortex swept back from the flaw, along with local crossflow in the region near the vortex. Tobak sketches the flowfield and presents a linear analysis. The size of the leading edge flaw is not specified.

Stollery outlines free-interaction theory, which gives fairly good agreement for the mean properties [235]. Sophisticated triple-deck theory is presented by Cassel et al., but the results were not compared to experiment or theory [240]. Cassel et al. claim to have discovered a new form of instability in the separating boundary layer, but this claim remains to be confirmed by computation or experiment [241]. Inger presents free-interaction theory for prediction of incipient separation, but no flowfield details are presented [242].

Grasso presents 2D computations of a laminar compression corner [243]. Upstream of the corner, laminar computations give fairly good agreement when a fine grid is used. However, agreement is poor downstream, perhaps because transition occurs in the experimental shear layer.

Rudy et al. compute a Mach 14 compression corner using four methods [244]. For laminar incoming flow, with small corner angles that cause little or no separation, 2D computations provide good agreement with surface pressure and heat transfer. For the largest corner angle, the separated region is roughly 50% of L, and a 3D computation must be performed to obtain good agreement. The good agreement obtained in this 1991 work suggest that stability computations are a reasonable next step. This work also suggests that 2D computations are a reasonable place to start.

A number of experimental studies have measured some of the flow details, although nearly all contain only surface measurements. Chpoun et al. measure the surface pressure and heat transfer in a laminar 2D compression corner [245, 246]. At larger angles, the flow reattaches turbulent. For a 10-degree corner at Mach 5 and $Re_L \simeq 1 \times 10^6$, the flow reattaches laminar.

Simeonides et al. performed both computations and experiments for 2D compression corners, at Mach 6 and 14 [247, 248]. Schlieren images were ob-

tained and surface pressure and temperature were measured. Good agreement is obtained, but not of a quality sufficient for stability analysis.

Heffner et al. use an axisymmetric geometry for their measurements, to avoid end-effect difficulties [249]. For a 10-degree corner at Mach 5, transition moves from just downstream of the reattachment point, at $Re_L \simeq 0.65 \times 10^6$, to the location of the reattachment point, at $Re_L \simeq 1.0 \times 10^6$.

Lu et al. measure transition using corners of 10 and 20 degrees, at Mach 8 and $Re_L = 2.27 \times 10^6$. They attempt to determine the effect of the corners on transition [250]. Although they predicted separation for a 5-7 degree corner, it did not occur. Unfortunately, their shock-tunnel surface pressure measurements did not discriminate well between tunnel noise and turbulent fluctuations.

The author is aware of three experiments in which flowfield details were measured [251, 252, 253]. Lewis et al. made broadband hot-wire measurements in a 2D 10.25-deg. corner at $M_\infty \simeq 6$, with a laminar incoming boundary layer at $Re_L = 0.068 - 1.0 \times 10^6$ [251]. At $Re_L = 0.15 \times 10^6$, the flow was laminar through reattachment. Hot wire measurements were performed in the separated shear layer, and the RMS fluctuations were obtained. In the corner region, these were sharply peaked in the wall-normal direction. At low Reynolds number, the peak increases slowly in the aft direction, with the location moving towards the wall. At higher Reynolds number, the peak is more broad and the maxima is less well defined, indicating transitional flow. The uncalibrated fluctuation profiles are shown in Ref. [254].

Kosinov et al. made hot-wire measurements at Mach 2 on a 5-deg. half-angle cone-flare with a 5-deg. compression corner [252]. Separation occured in the corner. The fluctuations in the corner were measured, and controlled perturbations were introduced at 20kHz using a glow perturber set up as a harmonic point source. Oblique first-mode waves were observed to grow at all angles. Low frequency oscillations were observed in the separated region (up to 10kHz), but few details are provided. Kosinov (private communication, March 1999) stated that the length was 150 mm from the nose to the corner, resulting in $Re_L \simeq 1.0 \times 10^6$. Laminar separation occured about 6-7 mm upstream of the corner. In the wall-normal direction, there were two maxima in the fluctuation amplitudes, one at $y/\delta = 0.2 - 0.3$, and one at $y/\delta = 0.5 - 0.6$. The details have not yet been written up for publication due to budget limitations.

Maslov et al. performed the most systematic measurements of transition in the corner, with funding from Aerospatiale [253]. The model was a 7-deg. half-angle cone with a 10-deg. corner at the flare. The measurements were made at $M_\infty = 6$, with $L = 120$ mm, and $Re_L \simeq 1.4 \times 10^6$. Flowfield measurements were made with hot wires and pitot probes, and surface measurements of the

static pressure, heat flux and temperature were obtained. A glow perturber was operated at 40kHz as a harmonic point source. Laminar flow was observed through reattachment, with turbulent flow downstream. *'Low-frequency disturbances (less than 20 kHz) in the separation region increase slowly (by about 1.5 times). Disturbances in the medium-frequency region are neutral. High frequency pulsations (greater than 80kHz) increase strongly (about by a factor of 5).'* The fluctuation amplitudes peak near the boundary layer edge; this is true upstream, within, and downstream of the separation zone. Maslov was not yet able to introduce the high frequencies in a controlled way. For controlled disturbances generated at 40kHz with the harmonic point source, the first mode was observed at high wave angles, and the 2nd mode at small wave angles. The conventional tunnel is noisy, so the hot-wire spectra have lots of low frequency noise.

The author is aware of only two sets of flight measurements in which a compression corner was present. These were made on the flare of a flared cone-cylinder. In the first, it unfortunately appears from the surface heat-transfer data that the boundary layer was turbulent before it arrived at the corner [255]. In the second, transition may occur on the flare at high Mach numbers, but angle-of-attack effects are present, and 3D computations would be required to determine if transition occurs [256].

Finally, the corner separation raises the issue of transition in free shear layers. This topic was reviewed by Demetriades [257], who provides various correlations. Liang and Reshotko worked out a stability analysis for a shear layer between streams at Mach 3 and Mach 8, and compared to other data by Demetriades [258]. King et al. studied transition in a free-shear layer above a cavity, in the Langley quiet tunnel at Mach 3.5 [259]. They showed that quiet flow had almost no effect on the shear-layer transition, presumably because of noise transmitted upstream from the shear-layer reattachment, through the subsonic cavity. It seems possible that end effects or the impinging nozzle shock could also be the explanation. The effect of tunnel noise on the transition mechanisms associated with compression-corner flow remains to be determined.

In summary, various correlations exist for incipient separation in the corner and for the heat transfer and pressure distribution. Three sets of measurements exist for the flowfield properties in the laminar separating corner. A number of computations have also been performed. It appears that work on the transition mechanisms observed in compression-corner flows is a good topic for further research.

10 Summary

Blunt cones at angle of attack remain a configuration of interest to the user community, yet the mechanisms of transition on these shapes remain uncertain. The existing literature suggests that streamwise instability, roughness, and crossflow can all be important. Measurements of the mechanisms of transition will be required to sort out the dominant effects under different conditions. Reliable computations of the traveling and stationary instabilities are now possible but not yet routine. Mechanism-based prediction methods need to be developed and validated.

Airbreathing cruise vehicles are also critically dependent on transition, although the dominant mechanisms remain largely unstudied. Streamwise and crossflow instabilities are all candidates for dominance, depending on the geometry selected and the conditions flown. New streamwise-vortex instabilities may be discovered near the separation bubbles in the compression corners.

Despite the many decades of work on hypersonic instability and transition, both these problems remain rich with practically important scientific problems that are more than sufficient to challenge a new generation of researchers. It is hoped that the present review can aid in making the existing literature accessible to this new generation. In addition, it is hoped that this review can help to identify the many problems that have *not* been solved over the past 50 years, and thus remain as suitable topics for future research.

11 Acknowledgements

The author's research has been funded by AFOSR, Sandia National Laboratory, NASA Langley, TRW (now Northrop-Grumman), and NASA Johnson. The author has benefited from the advice of many technical leaders over the past two decades. Particularly helpful in the preparation of this paper have been Dr. James Kendall, retired from JPL, Dr. Dave Kuntz, of Sandia National Lab, Ken Stetson and Roger Kimmel from the Air Force Research Laboratory, Scott Berry from NASA Langley, and Stefan Hein from the DLR in Göttingen, Germany. Discussions with the members of NATO RTO WG-10 have also been helpful; these members include Daniel Arnal of ONERA, Toulouse, France, Eli Reshotko of Case Western University, Cleveland, Ohio, Graham Candler of the Univ. of Minnesota, USA, Roger Kimmel of AFRL, and Anatoly Maslov of ITAM, Novosibirsk, Russia.

References

[1] John J. Bertin and Russell M. Cummings. Fifty years of hypersonics: where we've been, where we're going. *Progress in Aerospace Sciences*, 39:511–536, 2003.

[2] Defense Science Board. Report of the defense science board task force on national aero-space plane program, November 1992. DTIC citation AD-A274530.

[3] Tony C. Lin, Wallis R. Grabowsky, and Kevin E. Yelmgren. The search for optimum configurations for re-entry vehicles. *J. of Spacecraft and Rockets*, 21(2):142–149, March-April 1984.

[4] S. A. Bouslog, M. Y. An, L.N. Hartmann, and S. M. Derry. Review of boundary layer transition flight data on the space shuttle orbiter. Paper 91-0741, AIAA, January 1991.

[5] K.E. Wurster. An assessment of the impact of transition on advanced winged entry vehicle thermal protection system mass. Paper 81-1090, AIAA, June 1981.

[6] H. Legner, A. Gelb, D. Rosen, and G. Caledonia. High velocity interceptor investigations. Technical Report PSI-1239/TR-1573, Physical Sciences Inc., September 1998. DTIC citation AD-A357979.

[7] H.A. Korejwo and M.S. Holden. Ground test facilities for aerothermal and aero-optical evaluation of hypersonic interceptors. Paper 92-1074, AIAA, February 1992.

[8] Daniel C. Reda. Boundary-layer transition experiments on sharp, slender cones in supersonic free flight. *AIAA Journal*, 17(8):803–810, August 1979.

[9] Daniel C. Reda. Boundary-layer transition experiments on sharp, slender cones in supersonic free flight. Technical Report NSWC/WOL TR 77-59, Naval Surface Weapons Center, September 1977. DTIC citation AD-A054591.

[10] H.H. Hamilton II, D.R. Millman, and R.B. Greendyke. Finite-difference solution for laminar or turbulent boundary layer flow over axisymmetric bodies with ideal gas, CF4, or equilibrium air chemistry. Technical Paper 3271, NASA, December 1992.

[11] Steven P. Schneider. Flight data for boundary-layer transition at hypersonic and supersonic speeds. *Journal of Spacecraft and Rockets*, 36(1):8–20, 1999.

[12] Christopher J. Roy and Frederick G. Blottner. Assessment of one- and two-equation turbulence models for hypersonic transitional flows. Paper 2000-0132, AIAA, January 2000.

[13] A. Martellucci, S. Weinberg, and A. Page. Maneuvering aerothermal technology (MAT) data bibliography (Task 2). Technical Report TR-82-15, BMO, March 1981. DTIC citation AD-A118876.

[14] D. M. Bushnell. Notes on initial disturbance fields for the transition problem. In M. Y. Hussaini and R.G. Voigt, editors, *Instability and Transition, Volume I*, pages 217–232, Berlin, 1990. Springer-Verlag. Materials of the workshop held May 15 – June 9,1989 in Hampton, Virginia.

[15] Eli Reshotko. Boundary layer instability, transition, and control. Paper 94-0001, AIAA, January 1994. The 1994 Dryden Lecture in Research.

[16] William S. Saric. Görtler vortices. *Annual Review of Fluid Mechanics*, 26:379–409, 1994.

[17] L. M. Mack. Boundary layer linear stability theory. In *Report 709, Special Course on Stability and Transition of Laminar Flow*, pages 1–81. AGARD, March 1984.

[18] W.S. Saric, H.L. Reed, and E.B. White. Stability and transition of three-dimensional boundary layers. *Annual Review of Fluid Mechanics*, 35:413–440, 2003.

[19] D. Arnal and G. Casalis. Laminar-turbulent transition prediction in three-dimensional flows. *Progress in Aerospace Sciences*, 36:173–191, 2000.

[20] Dietmar Rempfer. Low-dimensional modeling and numerical simulation of transition in simple shear flows. *Annual Reviews of Fluid Mechanics*, 35:229–266, 2003.

[21] R. Narasimha. The laminar-turbulent transition zone in the turbulent boundary layer. *Progress in Aerospace Science*, 22:29–80, 1985.

[22] P.S. Klebanoff and Z.W. Diehl. Some features of artificially thickened fully developed turbulent boundary layers with zero pressure gradient. Technical Note 2475, NACA, 1950.

[23] Helen L. Reed, William S. Saric, and Daniel Arnal. Linear stability theory applied to boundary layers. *Annual Reviews of Fluid Mechanics*, 28:389–428, 1997.

[24] Mujeeb R. Malik. Hypersonic flight transition data analysis using parabolized stability equations with chemistry effects. *Journal of Spacecraft and Rockets*, 40(3):332–344, May-June 2003.

[25] T.S. Haynes and H.L. Reed. Simulation of swept-wing vortices using nonlinear parabolized stability equations. *Journal of Fluid Mechanics*, 405:325–349, 2000.

[26] H. Reed, R. Kimmel, D. Arnal, and S. Schneider. Drag prediction and transition in hypersonic flow. In *Sustained Hypersonic Flight*. AGARD, April 1997. Paper C15 in CP-600, vol. 3. Also appears as AIAA Paper 97-1818, June 1997.

[27] L. Kleiser and T. Zang. Numerical simulation of transition in wall-bounded shear flows. *Annual Reviews of Fluid Mechanics*, 23:495–537, 1991.

[28] Thorwald Herbert. On the stability of 3D boundary layers. Paper 97-1961, AIAA, June 1997.

[29] Th. Herbert. Parabolized stability equations. In *AGARD Report 793, Special Course on* Progress in Transition Modelling, pages 4/1 – 4/34, 1994.

[30] I.E. Beckwith and C.G. Miller III. Aerothermodynamics and transition in high-speed wind tunnels at NASA Langley. *Annual Review of Fluid Mechanics*, 22:419–439, 1990.

[31] Steven P. Schneider. Effects of high-speed tunnel noise on laminar-turbulent transition. *Journal of Spacecraft and Rockets*, 38(3):323–333, May–June 2001.

[32] S.R. Pate and C.J. Schueler. Radiated aerodynamic noise effects on boundary-layer transition in supersonic and hypersonic wind tunnels. *AIAA Journal*, 7(3):450–457, March 1969.

[33] S. R. Pate. Dominance of radiated aerodynamic noise on boundary-layer transition in supersonic/hypersonic wind tunnels. Technical Report AEDC-TR-77-107, Arnold Engineering Development Center, Arnold Air Force Station, Tennessee, March 1978.

[34] F.-J. Chen, M.R. Malik, and I.E. Beckwith. Boundary-layer transition on a cone and flat plate at Mach 3.5. *AIAA Journal*, 27(6):687–693, 1989.

[35] K.F. Stetson, Roger Kimmel, E.R. Thompson, J.C. Donaldson, and L.G. Siler. A comparison of planar and conical boundary layer stability at a Mach number of 8. Paper 91-1639, AIAA, June 1991.

[36] Kenneth F. Stetson. Hypersonic transition testing in wind tunnels. In M. Y. Hussaini and R.G. Voigt, editors, *Instability and Transition, Volume I*, pages 91–97, Berlin, 1990. Springer-Verlag.

[37] Kenneth F. Stetson. Hypersonic boundary-layer transition. In J.J. Bertin, J. Periaux, and J. Ballman, editors, *Advances in Hypersonics: Defining the Hypersonic Environment*, pages 324–417. Birkhauser, Boston, 1992.

[38] S. P. Wilkinson, S. G. Anders, and F.-J. Chen. Status of Langley quiet flow facility developments. Paper 94-2498, AIAA, June 1994.

[39] J. M. Kendall, Jr. Supersonic boundary layer stability experiments. In W.D. McCauley, editor, *Boundary Layer Transition Study Group Meeting, Volume II: Session on Boundary Layer Stability*. Aerospace Corporation, 1967. Air Force Report No. BSD-TR-67-213, Vol II.

[40] I. Beckwith, T. Creel, F. Chen, and J. Kendall. Freestream noise and transition measurements on a cone in a Mach-3.5 pilot low-disturbance tunnel. Technical Paper 2180, NASA, 1983.

[41] F.J. Chen, S.P. Wilkinson, and I.E. Beckwith. Görtler instability and hypersonic quiet nozzle design. *J. of Spacecraft and Rockets*, 30(2):170–175, March-April 1993.

[42] Alan E. Blanchard, Jason T. Lachowicz, and Stephen P. Wilkinson. NASA Langley Mach 6 quiet wind-tunnel performance. *AIAA Journal*, 35(1):23–28, January 1997.

[43] Steven P. Schneider, Craig Skoch, Shann Rufer, and Erick Swanson. Hypersonic transition research in the Boeing/AFOSR Mach-6 quiet tunnel. Paper 2003-3450, AIAA, June 2003.

[44] Y.S. Kachanov and A. Michalke. Three-dimensional instability of flat-plate boundary layers: theory and experiment. *European J. of Mechanics B/Fluids*, 13(4):401–422, 1994.

[45] H.L. Reed, T.S. Haynes, and W.S. Saric. CFD validation issues in transition modelling. *AIAA Journal*, 36(5):742–751, May 1998.

[46] D. P. Aeschliman and W. L. Oberkampf. Experimental methodology for computational fluid dynamics code validation. *AIAA Journal*, 36(5):733–741, May 1998.

[47] Christopher J. Roy, Mary A. McWherter Payne, and William Oberkampf. Verification and validation for laminar hypersonic flowfields, part 2, validation. *AIAA Journal*, 41(10):1944–1954, October 2003.

[48] Steven P. Schneider. Hypersonic laminar instability on round cones near zero angle of attack. Paper 2001-0206, AIAA, January 2001.

[49] Eli Reshotko. A program for transition research. *AIAA Journal*, 13(3):261–265, March 1975.

[50] D.A. Bountin, A.N. Shiplyuk, and A.A. Sidorenko. Experimental investigations of disturbance development in the hypersonic boundary layer on a conical model. In H. Fasel and W. Saric, editors, *Laminar-Turbulent Transition. Proceedings of the IUTAM Symposium, Sedona, 1999*, pages 475–480, Berlin, 2000. Springer-Verlag.

[51] R.L. Kimmel. Experimental transition zone lengths in pressure gradient in hypersonic flow. In L.D. Kral and T.A. Zang, editors, *FED – Vol. 151, Transitional and Turbulent Compressible Flows*, pages 117–127. ASME, 1993.

[52] Thomas J. Horvath, Scott A. Berry, Brian R. Hollis, Chau-Lyan Chang, and Bart A. Singer. Boundary layer transition on slender cones in conventional and low disturbance Mach 6 wind tunnels. Paper 2002-2743, AIAA, June 2003.

[53] Robert Betchov and William O. Criminale, Jr. *Stability of Parallel Flows*. Academic Press, New York, 1967.

[54] P.G. Drazin and W.H. Reid. *Hydrodynamic Stability*. Cambridge University Press, Cambridge, 1981.

[55] Peter J. Schmid and Dan S. Henningson. *Stability and Transition in Shear Flows*. Springer, New York, 2001.

[56] Ronald F. Probstein and C.C. Lin. A study of the transition to turbulence of the laminar boundary layer at supersonic speeds. Preprint 596, Institute of the Aeronautical Sciences, January 1956.

[57] Thomas H. Bowden and John J. Bertin. Boundary-layer transition for cones in supersonic flow – a literature review. Aerospace Engineering Research Report 68004, University of Texas at Austin, 1968.

[58] M.V. Morkovin. Panoramic view of changes in vorticity distribution in transition instabilities and turbulence. In D.C. Reda, H.L. Reed, and R. Kobayashi, editors, *FED - Vol. 114, Boundary Layer Stability and Transition to Turbulence*. ASME, 1991.

[59] Mark V. Morkovin. Critical evaluation of transition from laminar to turbulent shear layers with emphasis on hypersonically traveling bodies. Technical Report AFFDL-TR-68-149, Air Force Flight Dynamics Laboratory, 1969. DTIC citation AD-686178.

[60] Samuel R. Pate. Effects of wind tunnel disturbances on boundary-layer transition with emphasis on radiated noise: A review. Paper 80-0431, AIAA, March 1980. Paper was distributed in person at the conference, and missed the usual archiving. Now available from AIAA through the Linda Hall Library, Kansas City, Missouri, or from DTIC as citation AD-A384962.

[61] Frank M. White. *Viscous Fluid Flow*. McGraw-Hill, second edition, 1991.

[62] John J. Bertin. *Hypersonic Aerothermodynamics*. AIAA, Washington, DC, 1994.

[63] Tony C. Lin. Development of the U.S. Air Force intercontinental ballistic missile weapon systems. *J. of Spacecraft and Rockets*, 40(4):491–509, July-August 2003.

[64] K. Stetson and R. Kimmel. On hypersonic boundary-layer stability. Paper 92-0737, AIAA, January 1992.

[65] R.L. Wright and E.V. Zoby. Flight boundary layer transition measurements on a slender cone at Mach 20. Paper 77-719, AIAA, June 1977.

[66] Mujeeb R. Malik. Stability theory for chemically reacting flows. In D. Arnal and R. Michel, editors, *Laminar-Turbulent Transition*, pages 251–260, Berlin, 1990. Springer-Verlag. Proceedings of the IUTAM Symposium, Toulouse, France, September, 1989.

[67] M.M. Sherman and T. Nakamura. Flight test measurements of boundary layer transition on a nonablating 22-deg. cone. *J. Spacecraft and Rockets*, 7(2):137–142, February 1970.

[68] M. R. Malik. Hypersonic boundary-layer receptivity and stability. In H. Fasel and W. Saric, editors, *Laminar-Turbulent Transition. Proceedings of the IUTAM Symposium, Sedona, 1999*, pages 409–414, Berlin, 2000. Springer-Verlag.

[69] J. Daywitt, D. Brant, and F. Bosworth. Computational technique for three-dimensional inviscid flow fields about reentry vehicles. Technical report, General Electric Company, Philadelphia, Pennsylvania, April 1978.

[70] R.W. Noack and A.R. Lopez. Inviscid flow field analysis of complex reentry vehicles: Volume I, description of numerical methods, Volume II, users manual. Technical Report SAND87-0776, Sandia National Laboratories, Albuquerque, New Mexico, October-November 1988.

[71] J. E. Daywitt, D. Brant, and F. Bosworth. Computational technique for three-dimensional inviscid flow fields about reentry vehicles. Technical Report TR-79-5, SAMSO, April 1978.

[72] J. E. Daywitt, M. Wade, D. J. Szostowski, and S. Yalisove. Split-coefficient matrix form of the GE-RSD three-dimensional inviscid supersonic flow field code (3IS/SCM). Technical Report 82SDR2029, General Electric Company, Philadelphia, Pennsylvania, April 1982.

[73] J. E. Daywitt, D. J. Szostowski, and D. A. Anderson. A split-coefficient/locally monotonic scheme for multishocked supersonic flow. *AIAA Journal*, 21(6):871–880, June 1983.

[74] R. F. Warming and R. M. Beam. Upwind second-order difference schemes and applications in aerodynamic flows. *AIAA Journal*, 14:1241–1249, September 1976.

[75] B. Van Leer. Flux vector splitting for the Euler equations. *Lecture Notes in Physics*, 170:507–512, 1982.

[76] J.E. Harris and D.K. Blanchard. Computer program for solving laminar, transitional, or turbulent compressible boundary-layer equations for two-dimensional and axisymmetric flow. Technical Report NASA-TM-83207, NASA, February 1982.

[77] E. Kufner, U. Dallmann, and J. Stilla. Instability of hypersonic flow past blunt cones – effects of mean flow variations. Paper 93-2983, AIAA, July 1993.

[78] R.N. Gupta, K.P. Lee, E.V. Zoby, J.N. Moss, and R.A. Thompson. Hypersonic viscous shock-layer solutions over long slender bodies – Part I: high Reynolds number flows. *J. Spacecraft*, 27(2):175–184, March-April 1990.

[79] Kam-Pui Lee and Roop N. Gupta. Viscous-shock-layer analysis of hypersonic flows over long slender vehicles. Contractor Report CR-189614, NASA, March 1992.

[80] Heath B. Johnson, Trevor G. Seipp, and Graham V. Candler. Numerical study of hypersonic reacting boundary layer transition on cones. *Physics of Fluids*, 10(10):2676–2685, October 1998.

[81] Mujeeb R. Malik. e**Malik: A new spatial stability analysis program for transition prediction using the e**N method. Technical Report HTC-8902, High Technology Corporation, March 1989. See also HTC-9203, which is almost identical.

[82] M.R. Malik. Numerical methods for hypersonic boundary layer stability. *Journal of Computational Physics*, 86:376–413, 1990.

[83] Steven P. Schneider. Design of a Mach-6 quiet-flow wind-tunnel nozzle using the e**N method for transition estimation. Paper 98-0547, AIAA, January 1998.

[84] Chau-Lyan Chang. The Langley stability and transition analysis code (LASTRAC): LST, linear and nonlinear PSE for 2-D, axisymmetric, and infinite swept wing boundary layers. Paper 2003-0974, AIAA, January 2003.

[85] Anthony Demetriades. New experiments on hypersonic boundary layer stability including wall temperature effects. *Proc. Heat Transfer and Fluid Mech. Institute*, pages 39–54, 1978.

[86] A. Demetriades. Hypersonic viscous flow over a slender cone, part III: laminar instability and transition. Paper 74-535, AIAA, June 1974.

[87] J. Kendall. Wind tunnel experiments relating to supersonic and hypersonic boundary-layer transition. *AIAA Journal*, 13:290–299, 1975.

[88] K.F. Stetson, E.R. Thompson, J.C. Donaldson, and L.G. Siler. Laminar boundary layer stability experiments on a cone at Mach 8, part 1: Sharp cone. Paper 83-1761, AIAA, June 1983.

[89] K.F. Stetson, E.R. Thompson, J.C. Donaldson, and L.G. Siler. Laminar boundary layer stability experiments on a cone at Mach 8, part 5: Tests with a cooled model. Paper 89-1895, AIAA, June 1989.

[90] K. F. Stetson and R. L. Kimmel. Example of second-mode instability dominance at a Mach number of 5.2. *AIAA Journal*, 30(12):2974–2976, December 1992.

[91] Ian J. Lyttle, Helen L. Reed, Alexander N. Shiplyuk, Anatoly A. Maslov, Dmitry A. Buntin, Eugene V. Burov, and Steven P. Schneider. Numerical-experimental comparisons of second-mode behavior for blunted cones. Paper 2004-0097, AIAA, January 2004.

[92] J.T. Lachowicz, N. Chokani, and S. P. Wilkinson. Boundary-layer stability measurements in a hypersonic quiet tunnel. *AIAA Journal*, 34(12):2496–2500, December 1996.

[93] Alan E. Blanchard and Gregory V. Selby. An experimental investigation of wall-cooling effects on hypersonic boundary-layer stability in a quiet wind tunnel. Technical Report NASA-CR-198287, NASA, February 1996.

[94] L.G. Siler and J.C. Donaldson. Boundary layer measurements on slender blunt cones at free-stream Mach number 8. Technical Report AEDC-TSR-79-V71, AEDC, December 1979.

[95] D.B. Carver, L.G. Siler, and J.C. Donaldson. Boundary layer measurements on slender blunt cones at Mach number 8 – Part II. Technical Report AEDC-TSR-80-V36, AEDC, July 1980.

[96] J. Donaldson and S. Coulter. A review of free-stream flow fluctuation and steady-state flow quality measurements in the AEDC/VKF supersonic tunnel A and hypersonic tunnel B. Paper 95-6137, AIAA, April 1995.

[97] L. M. Mack. Boundary-layer stability analysis for sharp cones at zero angle-of-attack. Technical Report AFWAL-TR-86-3022, Air Force Wright Aeronautical Laboratories, August 1986.

[98] L. M. Mack. Stability of axisymmetric boundary layers on sharp cones at hypersonic Mach numbers. Paper 87-1413, AIAA, June 1987.

[99] Anthony Fiore. Viscosity of air. *J. of Spacecraft and Rockets*, 3(5):756–758, May 1966.

[100] A. Demetriades. Laminar boundary layer stability measurements at Mach 7 including wall temperature effects. Technical Report AFOSR-TR-77-1311, AFOSR, November 1977.

[101] C.-L. Chang, M. R. Malik, and M.Y. Hussaini. Effects of shock on the stability of hypersonic boundary layers. Paper 90-1448, AIAA, June 1990.

[102] M. Malik, T. Zang, and D. Bushnell. Boundary layer transition in hypersonic flows. Paper 90-5232, AIAA, October 1990.

[103] C.-L. Chang and M. R. Malik. Non-parallel stability of compressible boundary layers. Paper 93-2912, AIAA, July 1993.

[104] Martin Simen and Uwe Dallmann. On the instability of hypersonic flow past a pointed cone – comparison of theoretical and experimental results at Mach 8. Technical Report DLR-Forschungsbericht DLR-FB-92-02, Deutsche Forschungsanstalt für Luft- und Raumfahrt, Göttingen, Germany, August 1991. In English.

[105] Martin Simen and Uwe Dallmann. On the instability of hypersonic flow past a pointed cone – comparison of theoretical and experimental results at Mach 8. In *Theoretical and experimental methods in hypersonic flows*. AGARD, May 1992. Paper 31 in CP-514.

[106] M. Simen and U. Dallmann. Nonlocal vs. local instability of compressible flows including body metric, flow divergence, and 3D-wave propagation. Paper 93-2982, AIAA, July 1993.

[107] Ewald Kufner. Numerische Untersuchungen der Strömungsinstabilitäten an spitzen und stumpfen Kegeln bei hypersonischen Machzahlen. Technical Report DLR-Forschungsbericht 95-11, Deutsche Forschungsanstalt für Luft- und Raumfahrt, Göttingen, Germany, February 1995. In German.

[108] E. Kufner and U. Dallmann. Entropy- and boundary layer instability of hypersonic cone flows – effects of mean flow variations. In R. Kobayashi, editor, *Laminar-Turbulent Transition*, pages 197–204, Berlin, 1995. Springer-Verlag. Proceedings of the IUTAM Symposium held in Sendai, Japan, September 1994.

[109] C.B. Cohen and I.E. Beckwith. Similar solutions for the compressible laminar boundary layer with heat transfer and pressure gradient. Technical Report 1293, NACA, 1956.

[110] Joseph W. Cleary. Effects of angle of attack and nose bluntness on the hypersonic flow past cones. Paper 66-414, AIAA, June 1966.

[111] I. Rosenboom, S. Hein, and U. Dallmann. Influence of nose bluntness on boundary-layer instabilities in hypersonic cone flows. Paper 99-3591, AIAA, June 1999.

[112] James M. Kendall, Jr. An experimental investigation of leading-edge shock-wave–boundary-layer interaction at Mach 5.8. *J. Aero. Sci.*, 24:47–56, January 1957.

[113] M. V. Morkovin and W.S. Bradfield. Probe interference in measurements in supersonic laminar boundary layers. *Journal of the Aeronautical Sciences*, 21(11):785–787, November 1954.

[114] M.L. Manning and N. Chokani. PSE analysis of a quiet tunnel hypersonic boundary layer flow. Paper 2000-2652, AIAA, June 2000.

[115] Steven P. Schneider. Development of quiet-flow supersonic wind tunnels for laminar-turbulent transition research. Contractor Report CR-197286, NASA, January 1995.

[116] M.J. Zucrow and J.D. Hoffman. *Gas Dynamics, Volume II: Multidimensional Flow*. Robert Krieger, Malabar, Florida, 1985.

[117] B. Latto and M.W. Saunders. Absolute viscosity of air down to cryogenic temperatures and up to high pressures. *Journal of Mechanical Engineering Sciences*, 15(4):266–270, August 1973.

[118] Daniel R. Grieser and William H. Goldthwaite. Experimental determination of the viscosity of air in the gaseous state at low temperatures and pressures. Technical Documentary Report AEDC-TDR-63-143, Arnold Engineering Development Center, June 1963.

[119] Y.S. Touloukian, S.C. Saxena, and P. Hestermans. *Viscosity*. IFI/Plenum, 1975. Thermophysical Properties of Matter: Volume 11.

[120] Dale W. Ladoon and Steven P. Schneider. Measurements of controlled wave packets at Mach 4 on a cone at angle of attack. Paper 98-0436, AIAA, January 1998.

[121] Stephen P. Wilkinson. A review of hypersonic boundary layer stability experiments in a quiet Mach 6 wind tunnel. Paper 97-1819, AIAA, June 1997.

[122] J.T. Lachowicz, N. Chokani, and S.P. Wilkinson. Hypersonic boundary layer stability over a flared cone in a quiet tunnel. Paper 96-0782, AIAA, January 1996.

[123] J.T. Lachowicz and N. Chokani. Hypersonic boundary layer stability experiments in a quiet wind tunnel with bluntness effects. Technical Report CR-198272, NASA, January 1996. Identical to Lachowicz's PhD thesis.

[124] P. Balakumar and M.R. Malik. Effect of adverse pressure gradient and wall cooling on instability of hypersonic boundary layers. Technical Report HTC-9404, High Technology Corporation, March 1994.

[125] C. D. Pruett and C.-L. Chang. Direct numerical simulation of hypersonic boundary-layer flow on a flared cone. *Theoret. Comput. Fluid Dynamics*, 11(1):49–67, March 1998.

[126] Roger L. Kimmel and Jonathan Poggie. Effect of total temperature on boundary-layer stability at Mach 6. *AIAA Journal*, 38(9):1754–1755, September 2000.

[127] P. Calvin Stainback. Some effects of roughness and variable entropy on transition at a Mach number of 8. Paper 67-132, AIAA, January 1967.

[128] S.R. Pate. Measurements and correlations of transition Reynolds numbers on sharp slender cones at high speeds. *AIAA Journal*, 9(6):1082–1090, June 1971.

[129] L.E. Ericsson. Effect of nose bluntness and cone angle on slender-vehicle transition. *AIAA Journal*, 26:1168–1174, October 1988.

[130] L. M. Mack. Linear stability theory and the problem of supersonic boundary-layer transition. *AIAA Journal*, 13(3):278–289, 1975.

[131] P.C. Stainback, M.C. Fischer, and R.D. Wagner. Effects of wind-tunnel disturbances on hypersonic boundary-layer transition. Paper 72-181, AIAA, January 1972.

[132] S.R. Pate. Comparison of NASA helium tunnel transition data with noise-transition correlation. *AIAA Journal*, 12(11):1615, Nov. 1974.

[133] S.R. Pate. Supersonic boundary-layer transition: effects of roughness and freestream disturbances. *AIAA Journal*, 9(5):797–803, May 1971.

[134] F.J. Chen. Boundary-layer transition extent measurements on a cone and flat plate at Mach 3.5. Paper 93-0342, AIAA, January 1993.

[135] P.H. Adam and H. G. Hornung. Enthalpy effects on hypervelocity boundary-layer transition: ground test and flight data. *J. of Spacecraft and Rockets*, 34(5):614–619, Sept.-Oct. 1997.

[136] A. Rasheed, H. G. Hornung, A.V. Federov, and N.D. Malmuth. Experiments on passive hypervelocity boundary-layer control using an ultrasonically absorptive surface. *AIAA J.*, 40(3):481–489, March 2002.

[137] Terry R. Salyer, Steven H. Collicott, and Steven P. Schneider. Feedback stabilized laser differential interferometry for supersonic blunt body receptivity experiments. Paper 2000-0416, AIAA, January 2000.

[138] P. C. Stainback, R.D. Wagner, F.K. Owen, and C.C. Horstman. Experimental studies of hypersonic boundary-layer transition and effects of wind-tunnel disturbances. Technical Report NASA TN-D-7453, NASA, March 1974.

[139] F.K. Owen, C.C. Horstman, P. C. Stainback, and R.D. Wagner. Comparison of wind tunnel transition and freestream disturbance measurements. *AIAA Journal*, 13(3):266–269, March 1975.

[140] G. G. Mateer and H.K. Larson. Unusual boundary-layer transition results on cones in hypersonic flow. *AIAA Journal*, 7(4):660–664, April 1969.

[141] Ivan E. Beckwith and Mitchel H. Bertram. A survey of NASA Langley studies on high-speed transition and the quiet tunnel. Technical Report TM-X-2566, NASA, July 1972. Citation 72N26239 in NASA Recon.

[142] K. K. Muramoto. Algebraic correlations for high-speed transition prediction on sharp and blunt cones. Paper 99-0405, AIAA, January 1999.

[143] P. Calvin Stainback. Effect of unit Reynolds number, nose bluntness, angle of attack, and roughness on transition on a 5-deg. half-angle cone at Mach 8. Technical Report NASA TN-D-4961, NASA, January 1969.

[144] S. R. Pate and C. J. Schueler. An investigation of radiated aerodynamic noise effects on boundary-layer transition in supersonic and hypersonic wind tunnels. Paper 68-375, AIAA, April 1968.

[145] K. R. Czarnecki and Mary W. Jackson. Effects of nose angle and Mach number on transition on cones at supersonic speeds. Technical Note 4388, NACA, September 1958.

[146] D.V. Maddalon and A. Henderson, Jr. Boundary-layer transition at hypersonic Mach numbers. Paper 67-130, AIAA, January 1967.

[147] D.V. Maddalon and A. Henderson, Jr. Boundary-layer transition on sharp cones at hypersonic Mach numbers. *AIAA Journal*, 6(3):424–431, March 1968.

[148] J. Leith Potter. Review of the influence of cooled walls on boundary-layer transition. *AIAA Journal*, 18(8):1010–1012, August 1980.

[149] V.I. Lysenko and A. Maslov. Transition reversal and one of its causes. *AIAA Journal*, 19(6):705–708, June 1981.

[150] K. F. Stetson and R. L. Kimmel. Surface temperature effects on boundary-layer transition. *AIAA Journal*, 30(11):2782–2783, November 1992.

[151] V.I. Lysenko and A. Maslov. The effect of cooling on supersonic boundary-layer instability. *J. Fluid Mech.*, 147:39–52, 1984.

[152] Leslie M. Mack. Effect of cooling on boundary-layer stability at Mach number 3. In D.E. Ashpis, T.B. Gatski, and R. Hirsh, editors, *Instabilities and turbulence in engineering flows*, pages 175–188. Kluwer Academic Publishers, Boston, 1993.

[153] E.R. Van Driest and J. Christopher Boison. Experiments on boundary-layer transition at supersonic speeds. *Journal of the Aeronautical Sciences*, 24:885–899, December 1957.

[154] John Laufer. Aerodynamic noise in supersonic wind tunnels. *Journal of Aerospace Sciences*, 28(9):685–692, September 1961.

[155] R.J. Sanator, J.P. DeCarlo, and D.T. Torrillo. Hypersonic boundary-layer transition data for a cold-wall slender cone. *AIAA Journal*, 3(4):758–760, 1965.

[156] Philip E. Everhart and H. Harris Hamilton. Experimental investigation of boundary-layer transition on a cooled 7.5-deg. total-angle cone at Mach 10. Technical Note TN-D-4188, NASA, October 1967.

[157] George G. Mateer. Effects of wall cooling and angle of attack on boundary-layer transition on sharp cones at Mach 7.4. Technical Report NASA TN-D-6908, NASA, August 1972.

[158] K.F. Stetson, E.R. Thompson, J.C. Donaldson, and L.G. Siler. Laminar boundary layer stability experiments on a cone at Mach 8, part 2: Blunt cone. Paper 84-0006, AIAA, January 1984.

[159] A.A. Maslov. Experimental study of stability and transition of hypersonic boundary layer around blunted cone. Technical report, Institute of Theoretical and Applied Mechanics, Russian Academy of Sciences, Siberian Branch, Novosibirsk, Russia, December 2001. Final Technical Report, International Science and Technology Center Grant 1863-2000. Funded by the European Office of Aerospace Research and Development, U.S.A.F. Defense Technical Information Center citation AD-A408241.

[160] M.R. Malik, R.E. Spall, and C.-L. Chang. Effect of nose bluntness on boundary layer stability and transition. Paper 90-0112, AIAA, January 1990.

[161] T. Herbert and V. Esfahanian. Stability of hypersonic flow over a blunt body. In *Theoretical and Experimental Methods in Hypersonic Flows*, May 1992. Paper 28 in AGARD CP-514.

[162] V. Esfahanian, Th. Herbert, and O.R. Burggraf. Computation of laminar flow over a long slender axisymmetric blunted cone in hypersonic flow. Paper 92-0756, AIAA, January 1992.

[163] G. Dietz and S. Hein. Entropy-layer instabilities over a blunted flat plate in supersonic flow. *Physics of Fluids*, 11(1):7–9, January 1999.

[164] Xiaolin Zhong and Yanbao Ma. Receptivity and linear stability of Stetson's Mach 8 blunt cone stability experiments. Paper 2002-2849, AIAA, June 2002.

[165] K.F. Stetson. Nosetip bluntness effects on cone frustum boundary layer transition in hypersonic flow. Paper 83-1763, AIAA, July 1983.

[166] K.F. Stetson. Effects of bluntness and angle of attack on boundary layer transition on cones and biconic configurations. Paper 79-0269, AIAA, January 1979.

[167] L.E. Ericsson. Effect of nose bluntness and cone angle on slender-vehicle transition. *AIAA Journal*, 26(10):1168–1174, 1988.

[168] Kenneth F. Stetson. Comments on 'effect of nose bluntness and cone angle on slender-vehicle transition'. *AIAA Journal*, 28(7):1336–1337, July 1990.

[169] K.F. Stetson. Hypersonic boundary layer transition experiments. AFWAL-TR 80-3062, Air Force Wright Aeronautical Laboratories, October 1980.

[170] K. F. Stetson. Unsteady transition location. *AIAA Journal*, 27(8):1135–1137, August 1989.

[171] J. F. Muir and A. A. Trujillo. Experimental investigation of the effects of nose bluntness, freestream Reynolds number, and angle of attack on cone boundary layer transition at a Mach number of 6. Paper 72-216, AIAA, January 1972.

[172] James F. Muir and Amado A. Trujillo. Effects of nose bluntness and freestream unit Reynolds number on slender cone transition at hypersonic speeds. Technical Report SC-DC-71-4492, Sandia Laboratories, December 1971.

[173] R. G. Batt and H.H. Legner. A review of roughness-induced nosetip transition. *AIAA Journal*, 21(1):7–22, January 1983.

[174] M.R. Wool. Interim report, passive nosetip technology (PANT) program, volume X, Summary of experimental and analytical results (for the period May 1973 to December 1974). Technical Report TR-74-86-Vol-X, SAMSO, January 1975. Citation AD-A020708 in DTIC.

[175] Eli Reshotko and Anatoli Tumin. The role of transient growth in roughness-induced transition. Paper 2002-2850, AIAA, June 2002.

[176] K.F. Stetson. Effect of nosetip bluntness on boundary layer transition on the frustum of a slender cone. AFWAL-TM 82-202-FIMG, Air Force Wright Aeronautical Laboratories, December 1982.

[177] M.A. Zanchetta and R. Hillier. Blunt cone transition at hypersonic speeds: the transition reversal regime. In R. Henkes and J. van Ingen, editors, *Transitional Boundary Layers in Aeronautics*, pages 433–440, Amsterdam, 1996. North-Holland.

[178] K.F. Stetson, E.R. Thompson, J.C. Donaldson, and L.G. Siler. Laminar boundary layer stability experiments on a cone at Mach 8, part 3: Sharp cone at angle of attack. Paper 85-0492, AIAA, 1985.

[179] Glen P. Doggett, Ndaona Chokani, and Stephen P. Wilkinson. Effect of angle of attack on hypersonic boundary-layer stability. *AIAA Journal*, 35(3):464–470, March 1997.

[180] D.E. Boylan, W.T. Strike, and F.L. Shope. A direct comparison of analytical and experimental surface and flow-field data on a 4-deg. cone at incidence in a hypersonic stream with laminar boundary layers. Technical Report AEDC-TR-76-84, AEDC, August 1976. DTIC citation AD-A029367, NASA citation 77N18080.

[181] A. Hanifi and A. Dahlkild. Stability characteristics of 3-D boundary layer on a yawed cone. In R. Kobayashi, editor, *Laminar-Turbulent Transition*, pages 381–388, Berlin, 1995. Springer-Verlag. Proceedings of the IUTAM Symposium held in Sendai, Japan, September 1994.

[182] Jorgen Olsson. Transition measurements on a sharp cone at angle of attack. Technical Report FFA-TN 1996-16, FFA, the Aeronautical Research Institute of Sweden, 1996.

[183] Jorgen Olsson. Transition measurements on blunt cones at angle of attack. Technical Report FFA-TN 1996-17, FFA, the Aeronautical Research Institute of Sweden, 1996.

[184] Jorgen Olsson. Summary of experimental cone transition research. Technical Report FFA-TN 1996-18, FFA, the Aeronautical Research Institute of Sweden, 1996.

[185] Dale W. Ladoon. *Wave packets generated by a surface glow discharge on a cone at Mach 4*. PhD thesis, School of Aeronautics and Astronautics, Purdue University, December 1998.

[186] J. Perraud, D. Arnal, L. Dussillols, and F. Thivet. Studies of laminar-turbulent transition in hypersonic boundary layers at ONERA. In *European Symposium on Aerothermodynamics for Space Vehicles, Third*, pages 309–316, November 1998.

[187] John C. Adams, Jr. Three-dimensional laminar boundary-layer analysis of upwash patterns and entrained vortex formation on sharp cones at angle of attack. Technical Report AEDC-TR-71-215, Arnold Engineering Development Center, December 1971.

[188] John B. McDevitt and Jack A. Mellenthin. Upwash patterns on ablating and nonablating cones at hypersonic speeds. Technical Note TN-D-5346, NASA, July 1969.

[189] William L. Oberkampf, Daniel P. Aeschliman, Roger E. Tate, and John F. Henfling. Experimental aerodynamics research on a hypersonic vehicle. Technical Report SAND92-1411, Sandia National Laboratories, Albuquerque, New Mexico, April 1993.

[190] V. DiCristina. Three-dimensional laminar boundary-layer transition on a sharp 8-deg. cone at Mach 10. *AIAA Journal*, 8(5):852–856, May 1970.

[191] Michael C. Fischer. An experimental investigation of boundary-layer transition on a 10-deg. half-angle cone at Mach 6.9. Technical Report NASA TN-D-5766, NASA, April 1970.

[192] Micheal C. Fischer and David H. Rudy. Effect of angle of attack on boundary-layer transition at Mach 21. *AIAA Journal*, 9(6):1203–1205, June 1971.

[193] George G. Mateer. The effect of angle of attack on boundary-layer transition on cones. *AIAA Journal*, 10(8):1127–1128, August 1972.

[194] J. Kendall. Wind tunnel experiments relating to supersonic and hypersonic boundary-layer transition. Paper 74-133, AIAA, Jan. 1974.

[195] K. F. Stetson. Mach 6 experiments of transition on a cone at angle of attack. *J. of Spacecraft*, 19(5):397–403, September-October 1982.

[196] W.D. McCauley, A.R. Saydah, and J.F. Bueche. Effect of spherical roughness on hypersonic boundary-layer transition. *AIAA Journal*, 4(12):2142–2148, December 1966.

[197] M. S. Holden. Experimental studies of the effects of asymmetric transition on the aerothermal characteristics of hypersonic blunted slender cones. Paper 85-0325, AIAA, January 1985.

[198] K. F. Stetson and G. H. Rushton. Shock tunnel investigation of boundary-layer transition at Mach 5.5. *AIAA Journal*, 5(5):899–906, May 1967.

[199] P. Krogmann. An experimental study of boundary layer transition on a slender cone at Mach 5. In *Laminar-Turbulent Transition*, October 1977. AGARD CP-224, Paper 26.

[200] P. Krogmann. An experimental investigation of laminar and transitional heat transfer to a sharp slender cone at mach 5, including effects of angle of attack and circumferential heat transfer. Paper 90-0628, AIAA, July 1974.

[201] James F. Muir and Amado A. Trujillo. Effects of nose bluntness and freestream unit Reynolds number on slender cone transition at hypersonic speeds. In W. D. McCauley, editor, *Proceedings of the Boundary Layer Transition Workshop, Volume III*, 1971. Paper 2 in the proceedings. Aerospace Corp. Report TOR-0172(S2816-16)-5, NASA citation 91N71710.

[202] A. Martellucci, R.S. Neff, and W.H. True III. An experimental investigation of boundary layer transition on a cone at angle of attack. Technical Report TR-69-383, SAMSO, September 1969. DTIC citation AD864331.

[203] A. Martellucci and R.S. Neff. The influence of asymmetric transition on re-entry vehicle motion. Paper 70-987, AIAA, August 1970.

[204] A. Martellucci and R.S. Neff. The influence of asymmetric transition on re-entry vehicle characteristics. *J. of Spacecraft and Rockets*, 8(5):476–482, May 1971.

[205] Leonidas E. Sakell. *An experimental investigation of boundary layer transition over three axially symmetric bodies at Mach 6.* PhD thesis, New York University, School of Engineering and Science, New York, New York, May 1972. Available from Univ. Microfilms, Order No. 73-9083.

[206] M. Holden, D. Bower, and K. Chadwick. Measurements of boundary layer transition on cones at angle of attack for Mach numbers from 11 to 13. Paper 95-2294, AIAA, June 1995.

[207] N. Thyson, A. Todisco, and B. Reeves. Active and passive tripping of frustum transition at Mach numbers of 8 and 10. Paper 78-1128, AIAA, July 1978.

[208] A. B. Bailey. Effect of boundary-layer transition on center-of-pressure of conical bodies. *AIAA Journal*, 19(8):1082–1083, August 1981.

[209] A.H. Boudreau. Transition measurements via heat-transfer instrumentation on a 0.5 bluntness 9.75-deg. cone at Mach 7 with and without mass addition. Paper 85-1004, AIAA, June 1985.

[210] A. Martellucci and F. Makowski. Performance technology program (PTP-S II): Vol. V, infrared mapping of boundary layer transition on a slender cone. Technical Report TR-81-2, BMO, April 1980. DTIC citation AD-A108847.

[211] Robert J. Nowak, Cindy W. Albertson, and L. Roane Hunt. Aerothermal tests of a 12.5-deg. cone at Mach 6.7 for various Reynolds numbers, angles of attack, and nose shapes. Technical Paper 2345, NASA, 1985.

[212] H.B. Johnson, G.V. Candler, and M.L. Hudson. Numerical study of hypersonic boundary layer transition on a blunt body. Paper 97-0554, AIAA, January 1997.

[213] R.H. Radeztsky, M.S. Reibert, and W.S. Saric. Effect of isolated micron-sized roughness on transition in swept-wing flows. *AIAA J.*, 37(11):1370–1377, November 1999.

[214] Eli Reshotko and Anatoli Tumin. The blunt body paradox – a case for transient growth. In H. Fasel and W. Saric, editors, *Laminar-Turbulent Transition. Proceedings of the IUTAM Symposium, Sedona, 1999*, pages 403–408, Berlin, 2000. Springer-Verlag.

[215] M.K. Lockwood, D.H. Petley, J.G. Martin, and J.L. Hunt. Airbreathing hypersonic vehicle design and analysis methods and interactions. *Progress in Aerospace Sciences*, 35:1–32, 1999.

[216] Defense Science Board. Report of the Defense Science Board task force on the National Aerospace Plane (NASP), September 1988. DTIC citation AD-A201124.

[217] A. Whitehead, Jr. NASP aerodynamics. Paper 89-5013, AIAA, July 1989.

[218] Alan Wilhite, Richard Powell, Stephen Scotti, Charles McClinton, S.Z. Pinckney, C.I. Cruz, L.R. Jackson, and J.L. Hunt. Concepts leading to the National Aero-Space Plane program. Paper 90-0294, AIAA, January 1990.

[219] AGARD, editor. *Sustained Hypersonic Flight*. AGARD, April 1997. CP-600, vol. 3.

[220] W.H. Heiser and D.T. Pratt. *Hypersonic Airbreathing Propulsion*. AIAA, Washington, DC, 1994.

[221] C. McClinton, A. Roudakov, V. Semenov, and V. Kopenhenov. Comparative flow path analysis and design assessment of an axisymmetric hydrogen fueled scramjet flight test engine at a Mach number of 6.5. Paper 96-4571, AIAA, November 1996.

[222] Takeshi Ito, Laura A. Randall, and Steven P. Schneider. Effect of noise on roughness-induced boundary-layer transition for scramjet inlet. *J. Spacecraft and Rockets*, 38(5):692–698, September-October 2001.

[223] Scott Berry, Aaron Auslender, Arthur D. Dilley, and John Calleja. Hypersonic boundary-layer trip development for Hyper-X. *Journal of Spacecraft and Rockets*, 38(6):853–864, Nov.-Dec. 2001.

[224] Scott Berry, Aaron Auslender, Arthur D. Dilley, and John Calleja. Hypersonic boundary-layer trip development for Hyper-X. Paper 2000-4012, AIAA, August 2000.

[225] P. Balakumar, H. Zhao, and H. Atkins. Stability of hypersonic boundary-layers over a compression corner. Paper 2002-2848, AIAA, June 2002.

[226] O. Marxen, U. Rist, and S. Wagner. The effect of spanwise-modulated disturbances on transition in a 2D separated boundary layer. Paper 2003-0789, AIAA, January 2003.

[227] Jack D. Whitfield and F.A. Iannuzzi. Experiments on roughness effects on cone boundary-layer transition up to Mach 16. *AIAA Journal*, 7(3):465–470, March 1969.

[228] T. Elias and E. Eiswirth. Stability studies of planar transition in supersonic flows. Paper 90-5233, AIAA, October 1990.

[229] Shin Matsumura, Steven P. Schneider, and Scott A. Berry. Streamwise-vortex instability and transition on a generic scramjet forebody. Paper 2003-3592, AIAA, June 2003.

[230] Jean M. Delery and A. G. Panaras. Shock-wave/boundary-layer interactions in high-Mach-number flows. In *Hypersonic Experimental and Computational Capability, Improvement and Validation*, pages 2–1 to 2–61. AGARD, May 1996. AR-319 v. I.

[231] W.L. Hankey, Jr and M.S. Holden. Two-dimensional shock wave-boundary layer interactions in high speed flows. AGARDograph 203, AGARD, 1975.

[232] Doyle Knight and Gerard Degrez. Shock-wave/boundary-layer interactions in high-Mach-number flows: A critical survey of current numerical prediction capabilities. In *Hypersonic Experimental and Computational Capability, Improvement and Validation*, pages 1–1 to 1–35. AGARD, December 1998. AR-319 v. II.

[233] Robert Korkegi. Survey of viscous interactions associated with high Mach number flight. *AIAA Journal*, 9(5):771–784, May 1971.

[234] Gary S. Settles and Lori J. Dodson. Supersonic and hypersonic shock/boundary layer interaction database. *AIAA Journal*, 32:1377–1383, July 1994.

[235] J.L. Stollery. Some viscous interactions affecting the design of hypersonic intakes and nozzles. In J.J. Bertin, J. Periaux, and J. Ballman, editors, *Advances in Hypersonics: Defining the Hypersonic Environment*, pages 418–437. Birkhauser, Boston, 1992.

[236] Jean Ginoux. Streamwise vortices in reattaching high-speed flows: a suggested approach. *AIAA Journal*, 9(4):759–760, April 1971.

[237] Luigi de Luca, Gennaro Cardone, Dominique Chevalerie, and Alain Fonteneau. Viscous interaction phenomena in hypersonic wedge flow. *AIAA Journal*, 33(12):2293–2299, December 1995.

[238] J.P. Vermeulen and G. Simeonides. Parametric studies of shock wave/boundary layer interactions over 2D compression corners at Mach 6. Technical Note 181, Von Karman Institute for Fluid Dynamics, September 1992.

[239] Murray Tobak. On local inflexional instability in boundary-layer flows. *Zeitschrift für angewandte Mathematik und Physik (ZAMP)*, 24:330–354, 1973.

[240] K.W. Cassel, A.I. Ruban, and J.D.A. Walker. Separation and instability in the hypersonic boundary layer on a cold wall. Paper 95-2272, AIAA, June 1995.

[241] K.W. Cassel, A.I. Ruban, and J.D.A. Walker. An instability in supersonic boundary-layer flow over a compression ramp. *Journal of Fluid Mechanics*, 300:265–285, 1995.

[242] G. R. Inger. Similitude properties of high-speed laminar and turbulent boundary-layer incipient separation. *AIAA Journal*, 15(5):619–623, May 1977.

[243] F. Grasso, G. Leone, and J.M. Delery. Validation procedure for the analysis of shock-wave/boundary-layer interaction problems. *AIAA Journal*, 32(9):1820–1827, September 1994.

[244] D. H. Rudy, J. L. Thomas, Ajay Kumar, and P. Gnoffo. Computation of laminar hypersonic compression-corner flows. *AIAA Journal*, 29(7):1108–1113, July 1991.

[245] A. Chpoun. Hypersonic flow in a compression corner in 2D and 3D configurations. Paper 89-1876, AIAA, June 1989.

[246] A. Chpoun. Hypersonic flow in a compression corner in 2D configuration. In D. Arnal and R. Michel, editors, *Laminar-Turbulent Transition*, pages 533–543. Springer-Verlag, Berlin, 1990. Proceedings of the IUTAM Symposium, Toulouse, 1989.

[247] G. Simeonides and W. Haase. Experimental and computational investigations of hypersonic flow about compression ramps. *Journal of Fluid Mechanics*, 283:17–42, 1995.

[248] G. Simeonides, W. Haase, and M. Manna. Experimental, analytical, and computational methods applied to hypersonic compression ramp flows. *AIAA Journal*, 32(2):301–310, February 1994.

[249] K.S. Heffner, A. Chpoun, and J.C. Lengrand. Experimental study of transitional axisymmetric shock-boundary layer interactions at Mach 5. Paper 93-3131, AIAA, July 1993.

[250] Frank K. Lu and Kenneth A. Pistone. Preliminary surface pressure measurements of transitional, hypersonic shock boundary layer interactions. Paper 96-4541, AIAA, November 1996.

[251] John E. Lewis, Toshi Kubota, and Lester Lees. Experimental investigation of supersonic laminar, two-dimensional boundary-layer separation in a compression corner with and without cooling. *AIAA Journal*, 6(1):7–14, January 1968.

[252] A.D. Kosinov and S.G. Shevelkov. Experimental investigation of separation and stability of supersonic laminar boundary layers. In *Separated Flows and Jets*, pages 741–745, Berlin, 1990. Springer-Verlag. Proceedings of an IUTAM meeting.

[253] A.A. Maslov, A.N. Shipyluk, A.A. Sidorenko, and Ph. Tran. Study related to hypersonic boundary layer stability on a cone with a flare. Preprint 2-97, Institute of Theoretical and Applied Mechanics, Russian Academy of Sciences, Siberian Branch, Novosibirsk, Russia, 1997.

[254] John E. Lewis. *Experimental investigation of supersonic laminar, two-dimensional boundary layer separation in a compression corner with and without cooling.* PhD thesis, California Institute of Technology, 1967. Available from University Microfilms at dissertation number 67-8457.

[255] Charles B. Rumsey and Dorothy B. Lee. Measurements of aerodynamic heat transfer on a 15-deg cone-cylinder-flare configuration in free flight at Mach numbers up to 4.7. Technical Note TN-D-824, NASA, May 1961. Citation 62N71398 in NASA Recon. Supersedes NACA RM L57J10, 1958.

[256] Dorothy B. Lee, Charles B. Rumsey, and Aleck C. Bond. Heat transfer measured in free flight on a slightly blunted 25-deg. cone-cylinder-flare configuration at Mach numbers up to 9.89. RM L58G21, NACA, Sept. 1958. Citation 63N20529 in NASA RECON.

[257] A. Demetriades. Transition in high-speed shear layers. In M. Y. Hussaini and R.G. Voigt, editors, *Instability and Transition, Volume I*, pages 52–67, Berlin, 1990. Springer-Verlag.

[258] F.-P. Liang, Eli Reshotko, and A. Demetriades. A stability study of the developing mixing layer formed by two supersonic laminar streams. *Physics of Fluids*, 8(12):3253–3263, December 1996.

[259] Rudolph A. King, Theodore R. Creel Jr., and Dennis M. Bushnell. Experimental transition investigation of a free-shear layer above a cavity at Mach 3.5. *J. Propulsion*, 7(4):626–634, 1991.

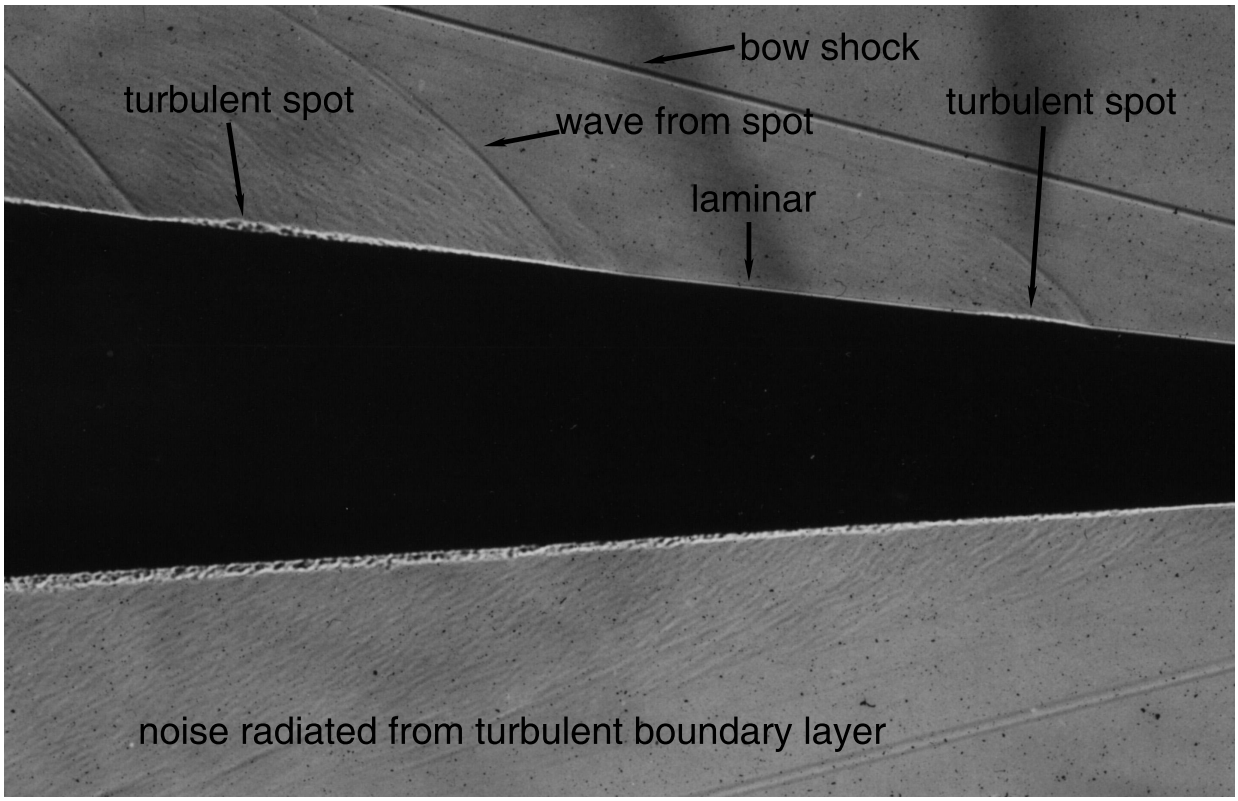

Figure 1: Shadowgraph of Transition on a Sharp Cone at Mach 4.31

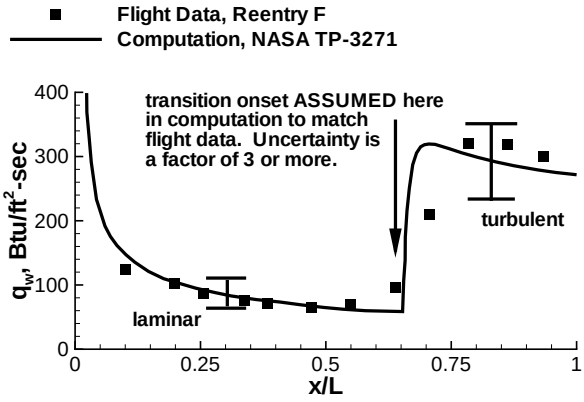

Figure 2: Heating-Rate Distribution Along Cone for Reentry F

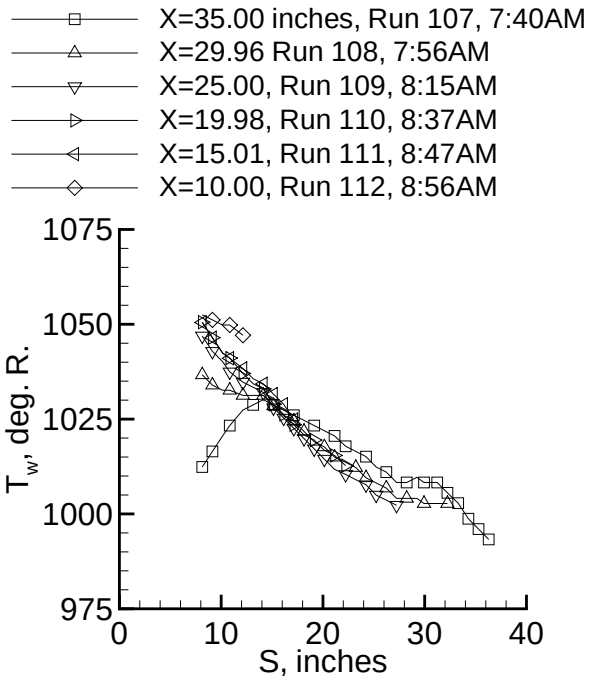

Figure 3: Wall Temperatures for Stetson Sharp Cone

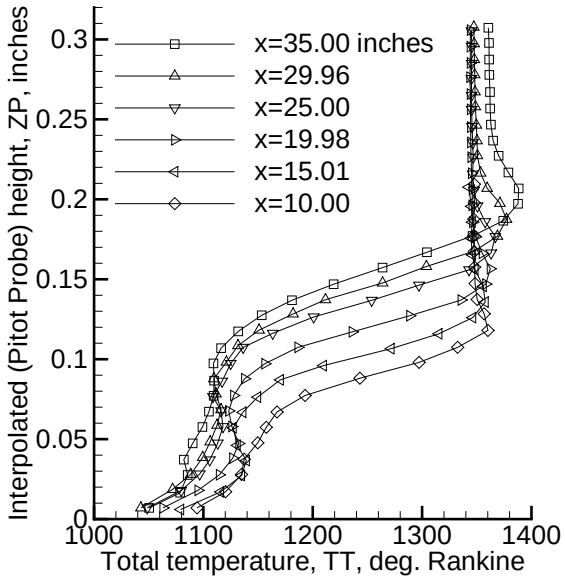

Figure 4: Mean Total Temp. Profiles for Stetson Sharp Cone

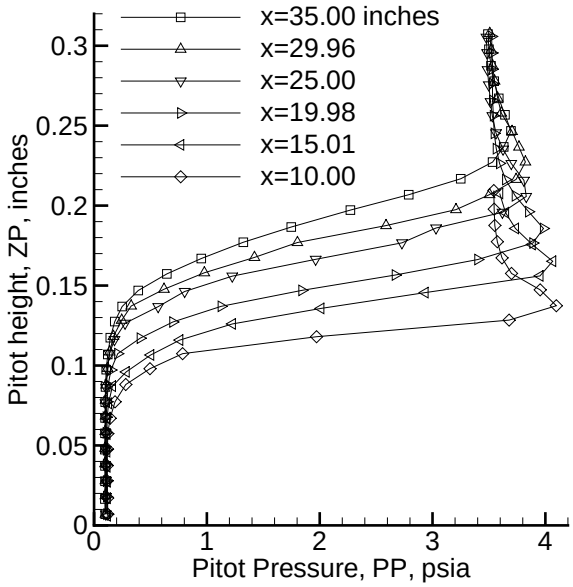

Figure 5: Mean Pitot Profiles for Stetson Sharp Cone

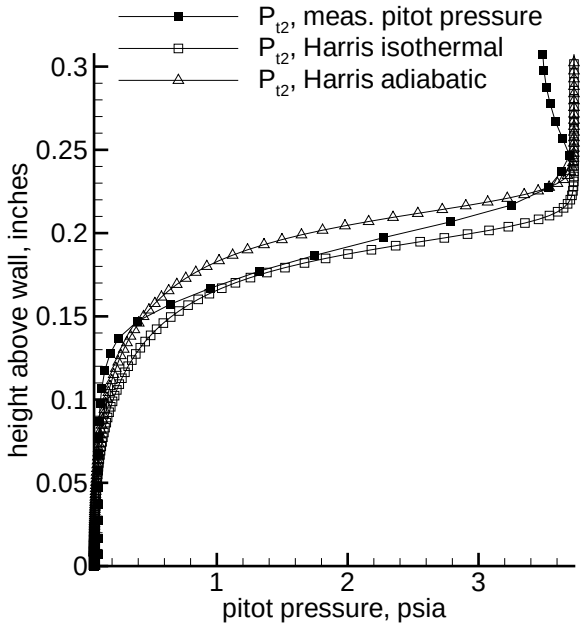

Figure 6: Pitot Profile Comparison for Stetson Sharp Cone

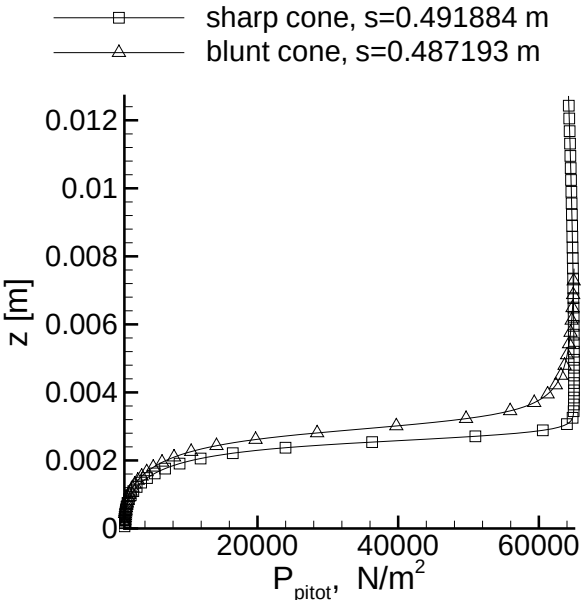

Figure 7: TLNS Pitot Profiles for Stetson Sharp and Blunt Cones at Blunt-Cone Flow Conditions, from Kufner via Hein

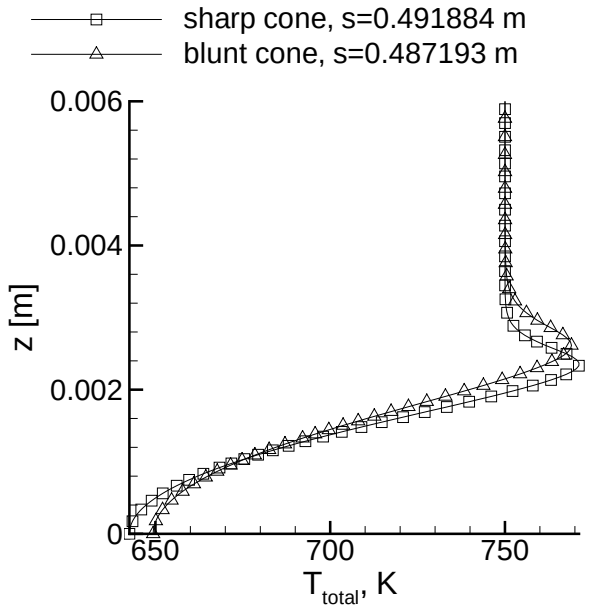

Figure 8: TLNS Total Temperature Profiles for Stetson Sharp and Blunt Cones at Blunt-Cone Flow Conditions, from Kufner via Hein

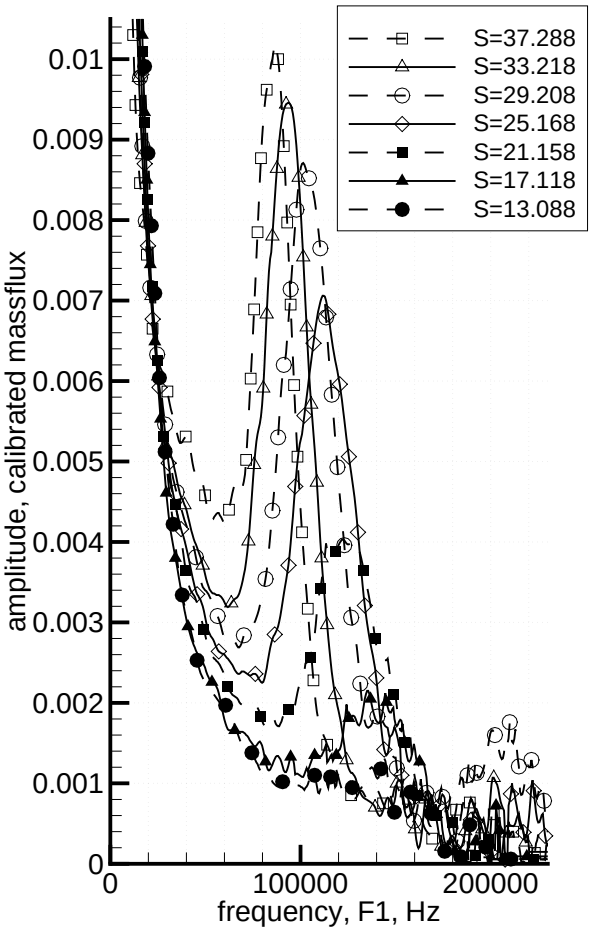

Figure 9: Massflux Spectra for Stetson Sharp Cone

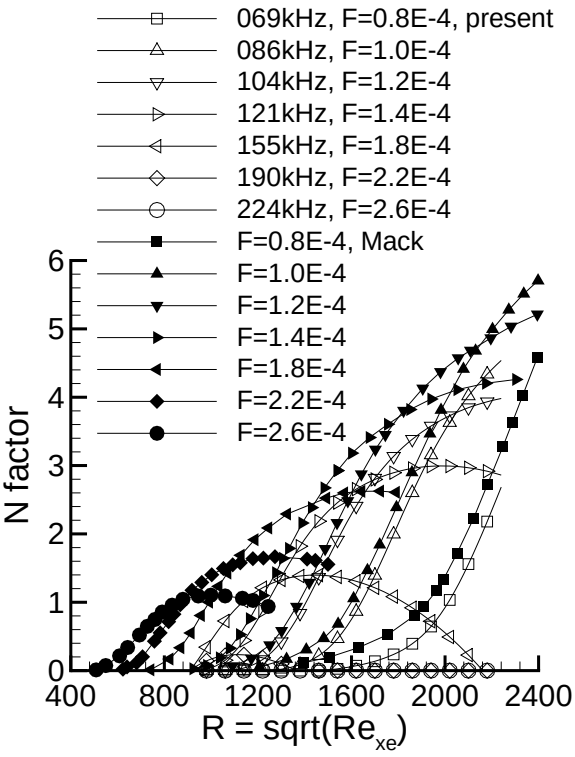

Figure 10: N-factor Computations for Stetson Sharp Cone; Profiles from Internal e**Malik Solver

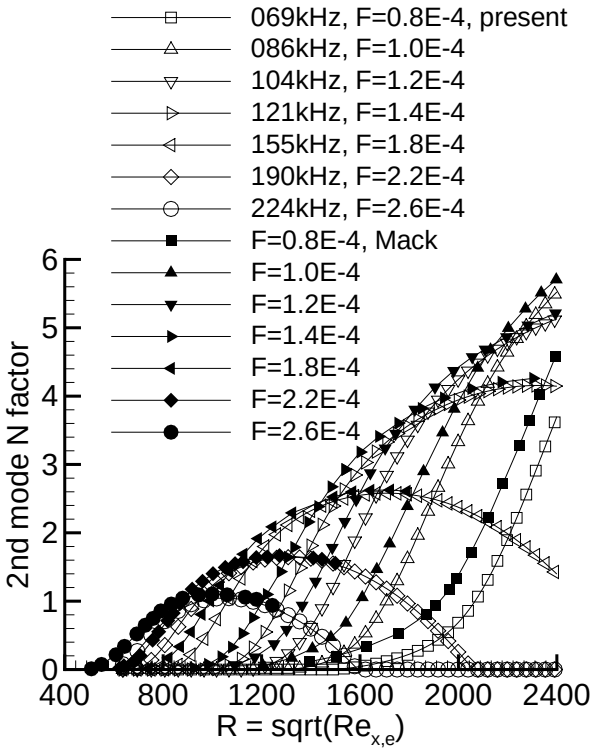

Figure 11: N-factor Computations for Stetson Sharp Cone; Profiles from Harris Boundary-Layer Code

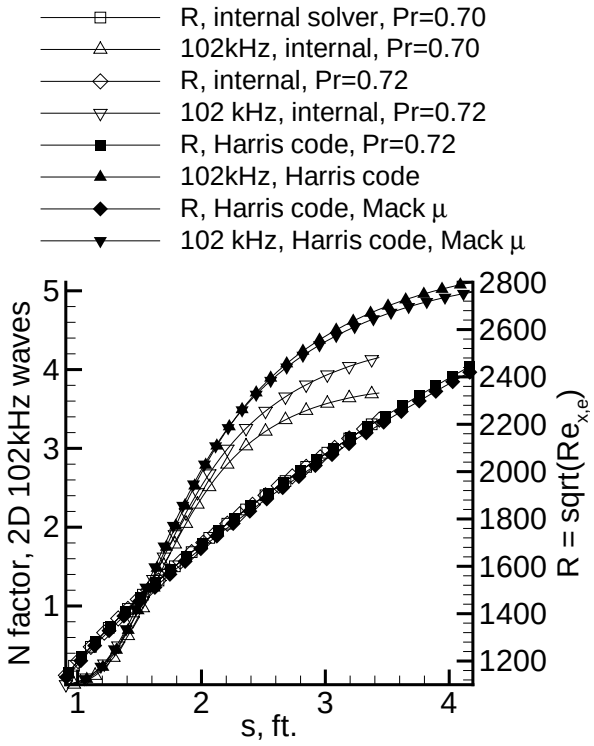

Figure 12: N-factor Computations for Stetson Sharp Cone; Four Methods for One Frequency

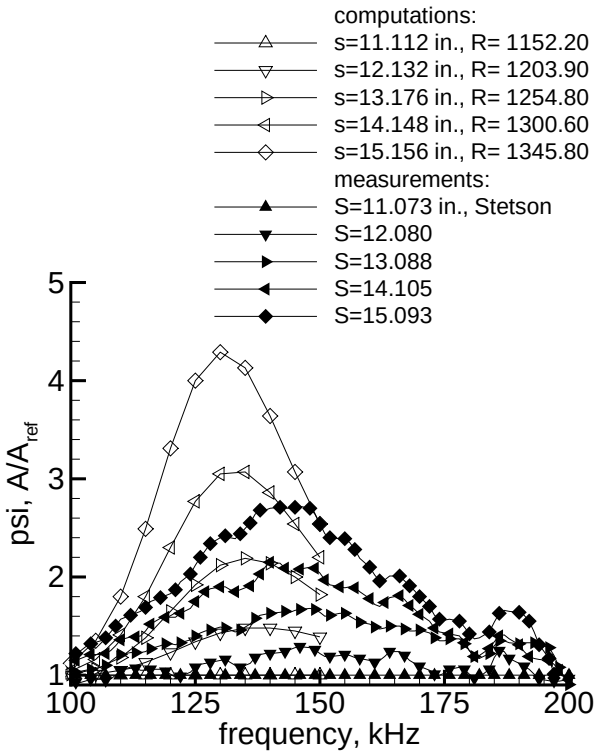

Figure 13: Amplitude-Ratio Comparisons for Stetson Sharp Cone

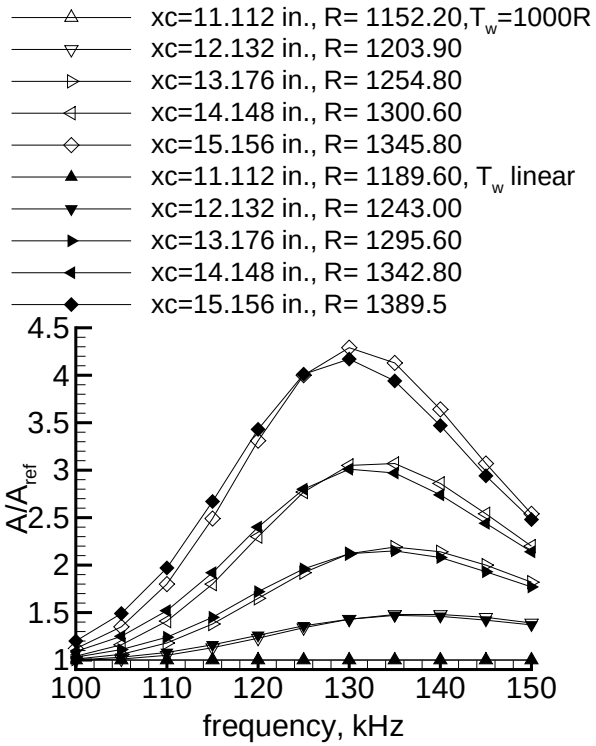

Figure 14: Amplitude-Ratio Comparisons for Stetson Sharp Cone: Two Wall Temperature Distributions

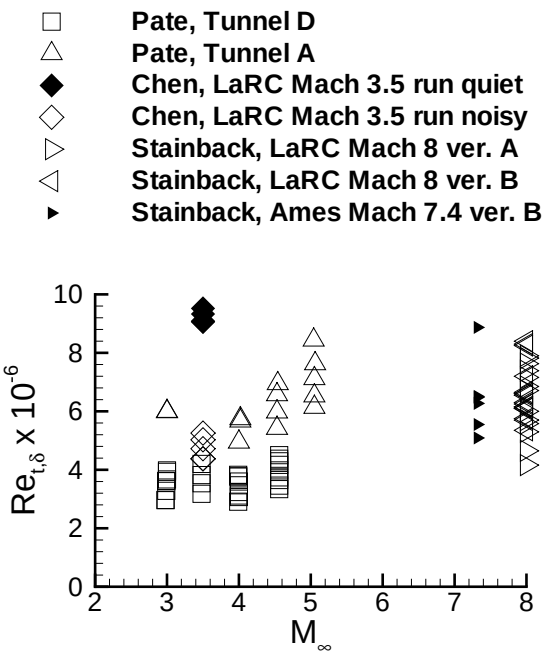

Figure 15: Selected Transition Data for Sharp Cones

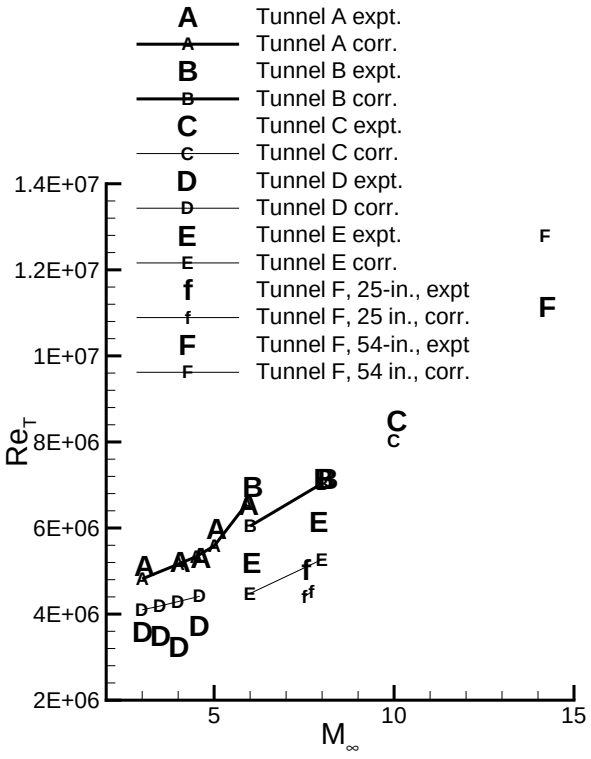

Figure 16: Pate Correlation for Sharp Cones vs. Mach Number

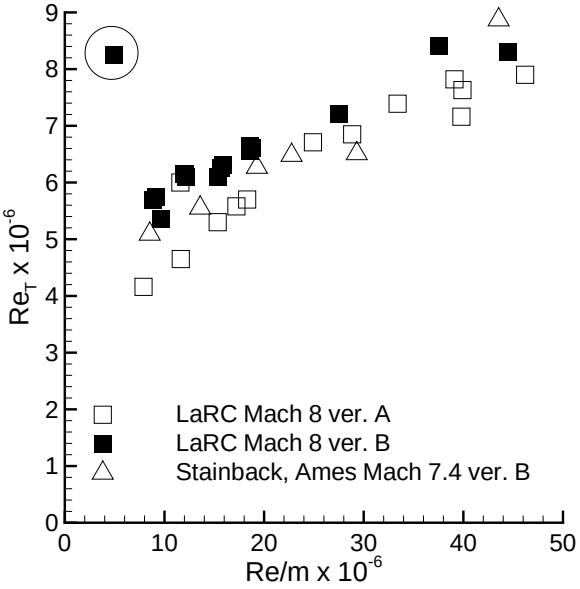

Figure 17: Unit Reynolds Number Effect on End of Transition for Sharp Cones

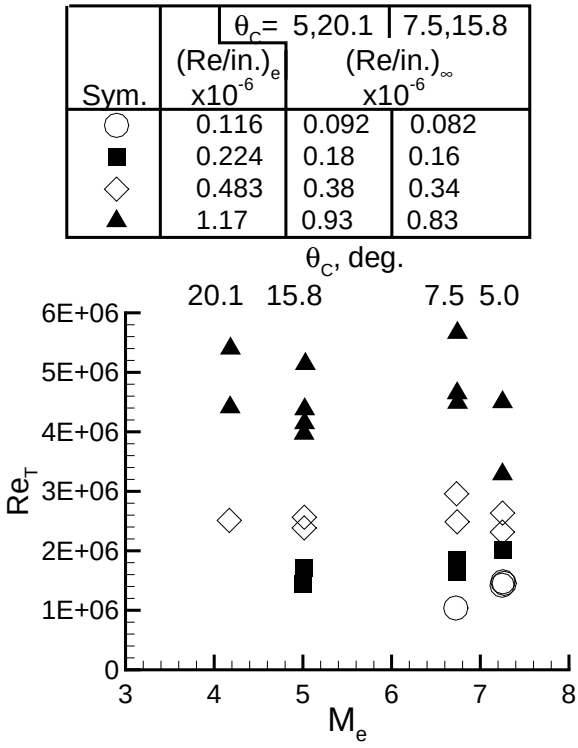

Figure 18: Transition on Cones at Fixed Tunnel Conditions and $M_\infty = 8$

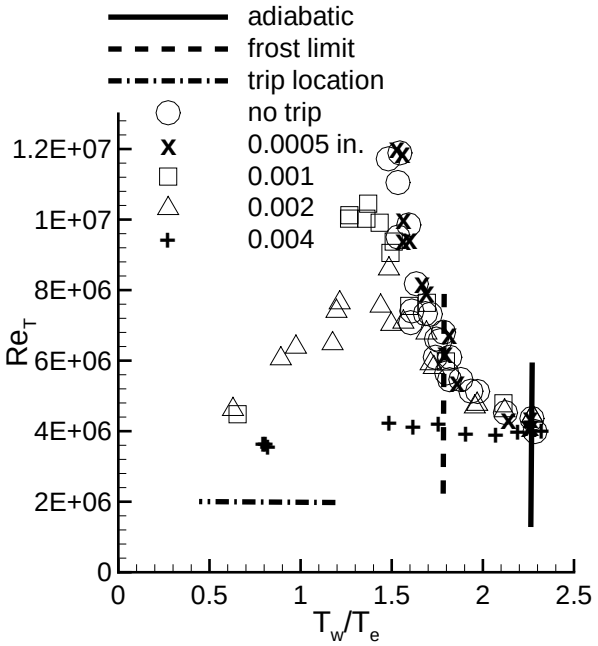

Figure 19: Effect of Wall Cooling and Roughness for Sharp Cones at $M_\infty = 2.81$

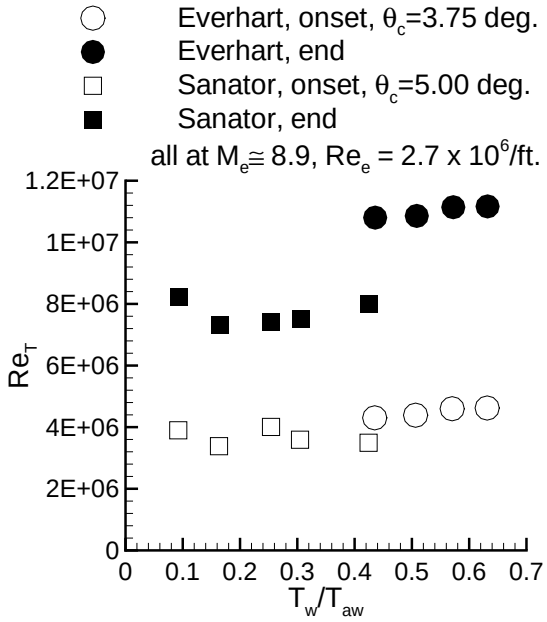

Figure 20: Effect of Wall Cooling for Sharp Cones at $M_\infty = 10$

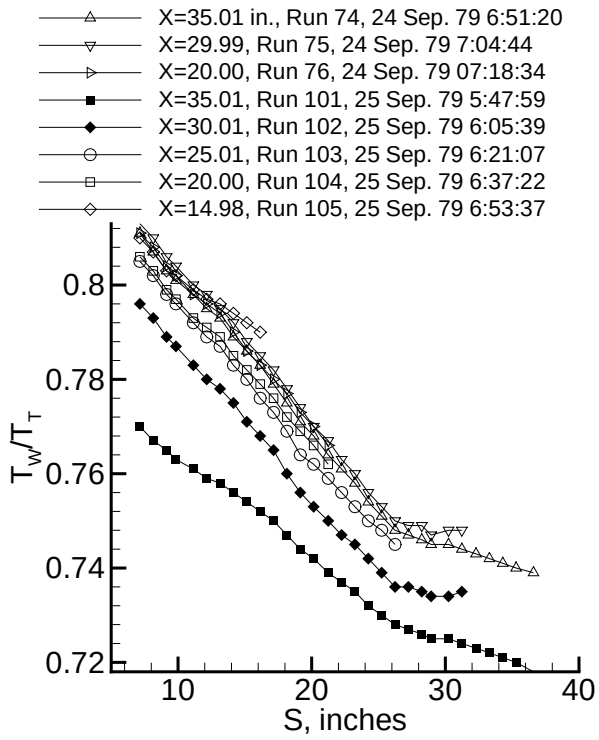

Figure 21: Wall Temperature Distributions for the Stetson Blunt Cone

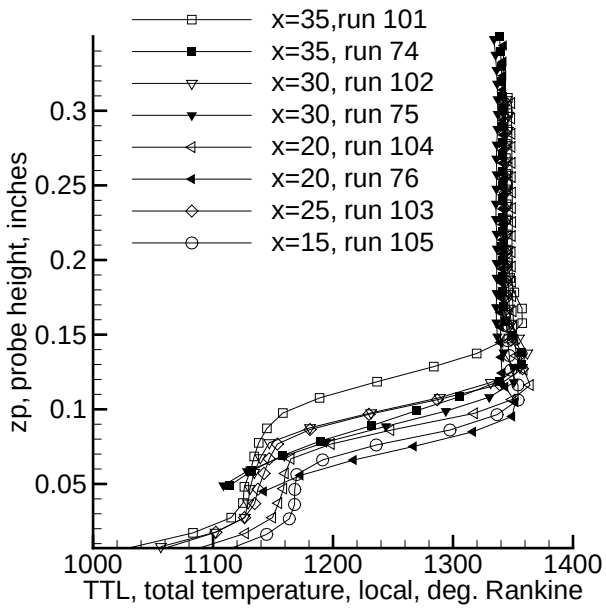

Figure 22: Mean Total Temp. Profiles for Stetson Blunt Cone

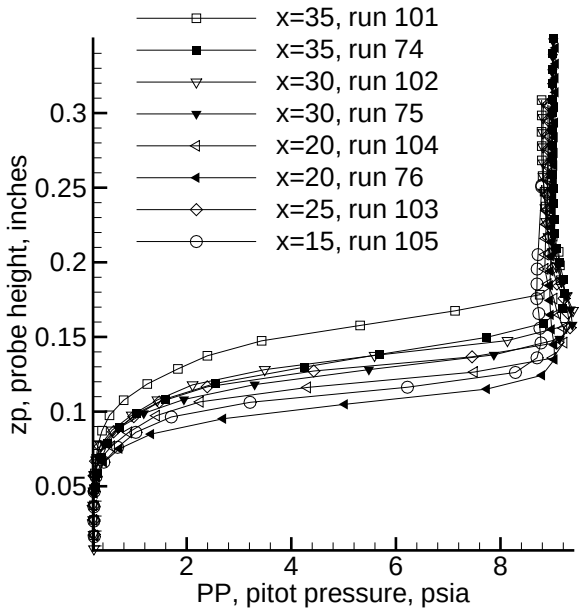

Figure 23: Mean Pitot Profiles for Stetson Blunt Cone

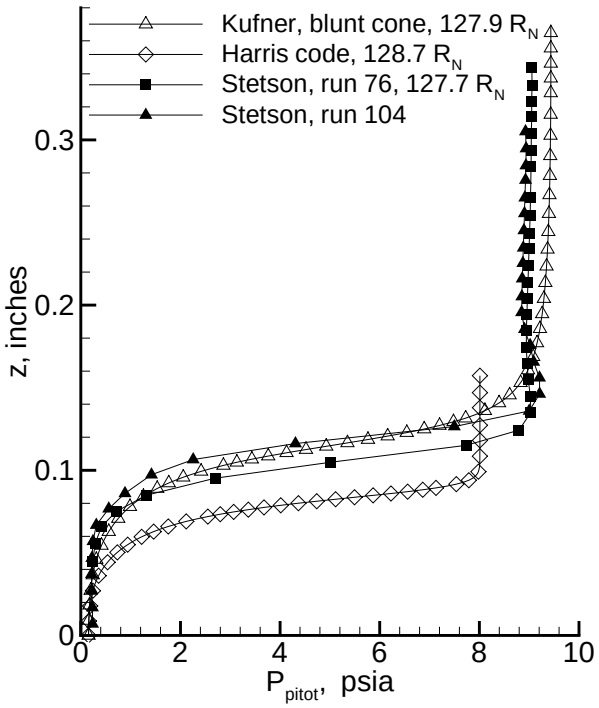

Figure 24: Comparison of Pitot Profiles for Stetson Blunt Cone

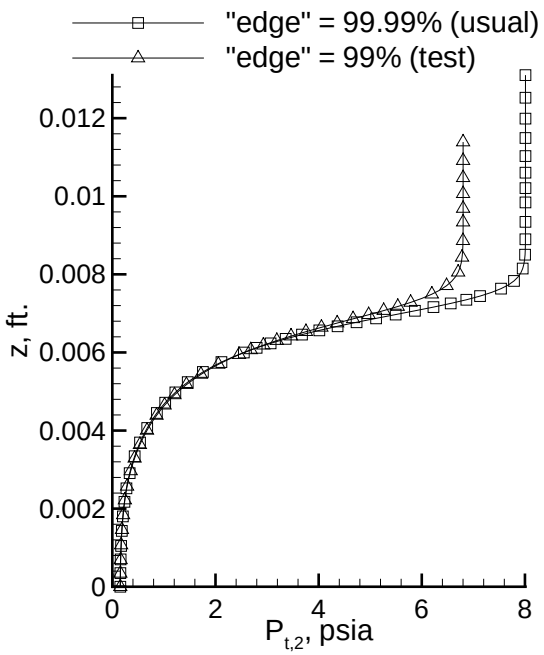

Figure 25: Effect of Boundary-Layer Edge Parameter on Harris-Code Profile

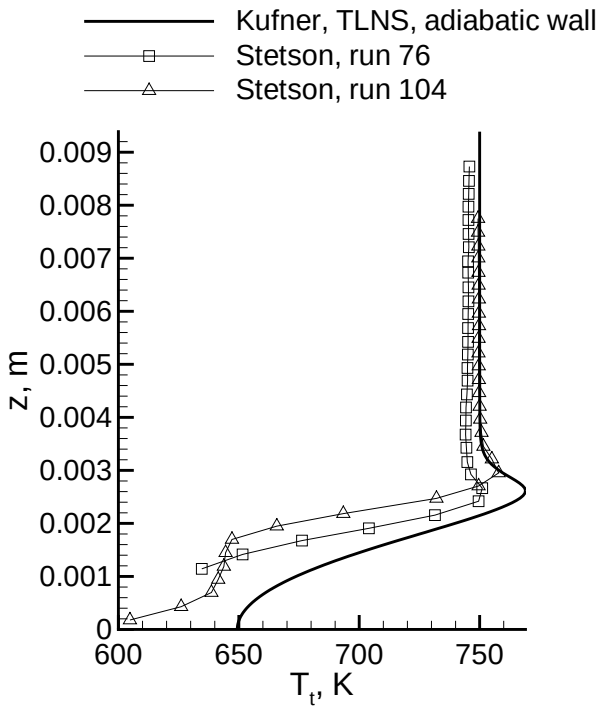

Figure 26: Comparison of Total-Temperature Profiles for Stetson Blunt Cone

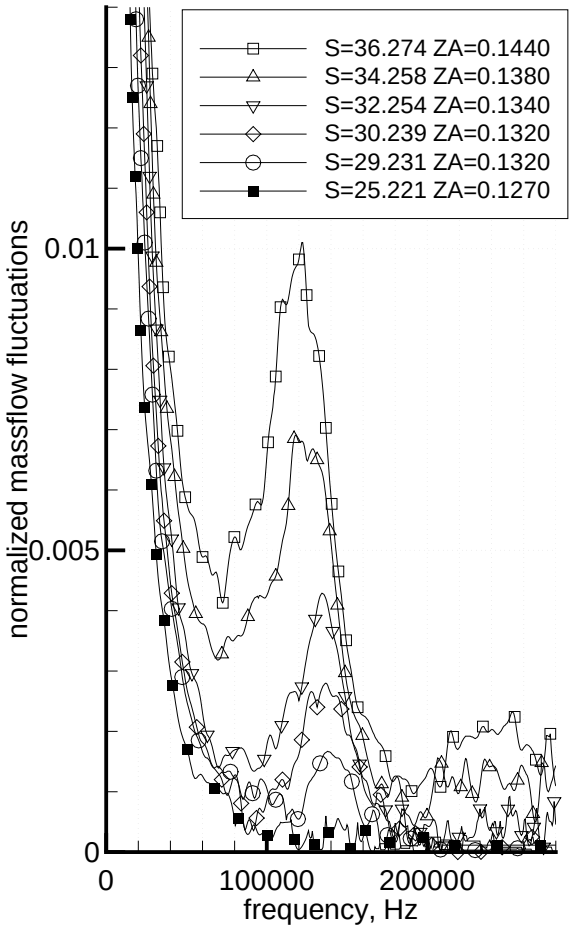

Figure 27: Massflux Spectra for Stetson Blunt Cone

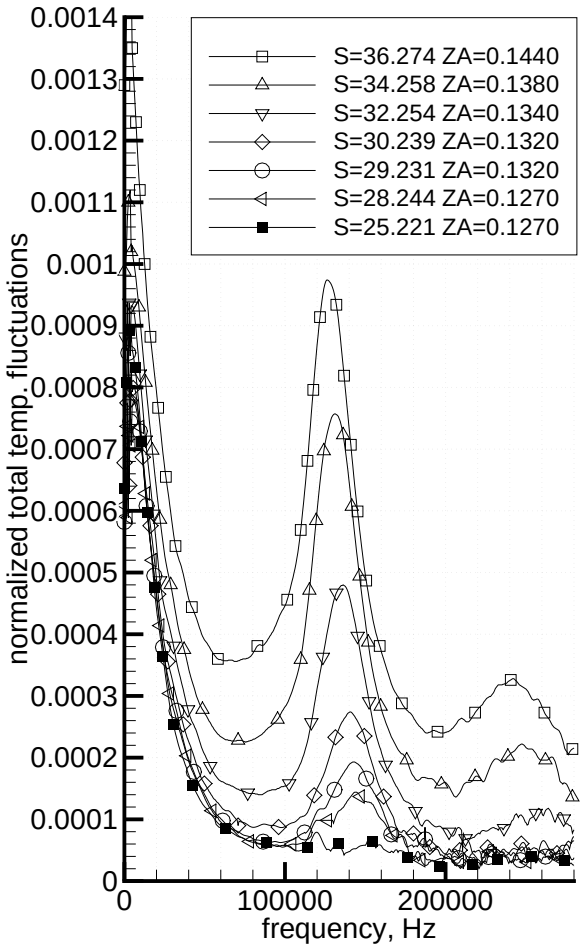

Figure 28: Total Temperature Spectra for Stetson Blunt Cone

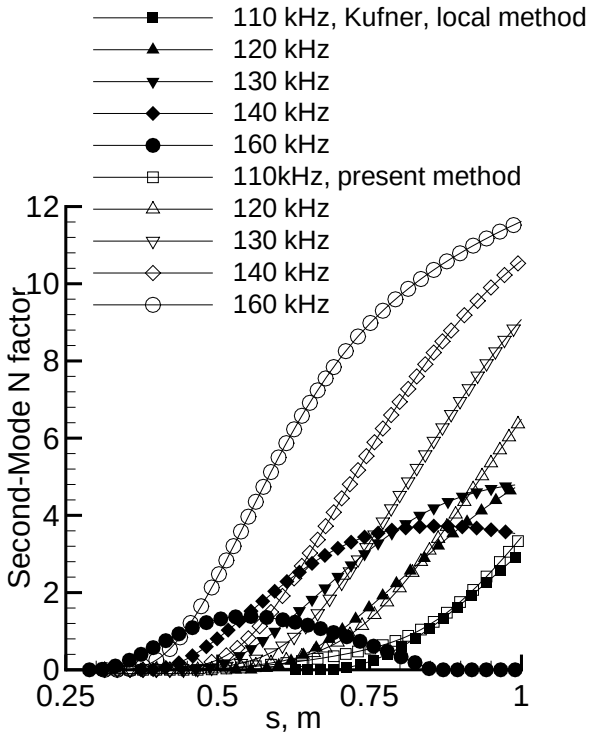

Figure 29: N factors for Blunt Cone Using Two Methods

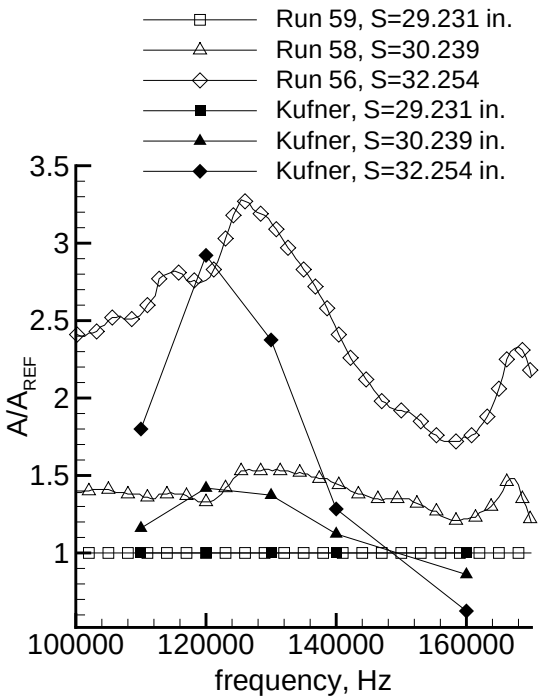

Figure 30: Amplification Ratios for Blunt Cone

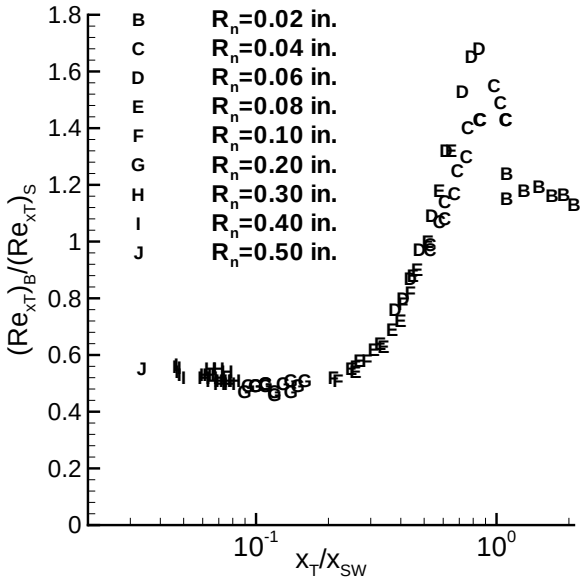

Figure 31: Nondimensional Transition Locations on Blunt Cone at Mach 6

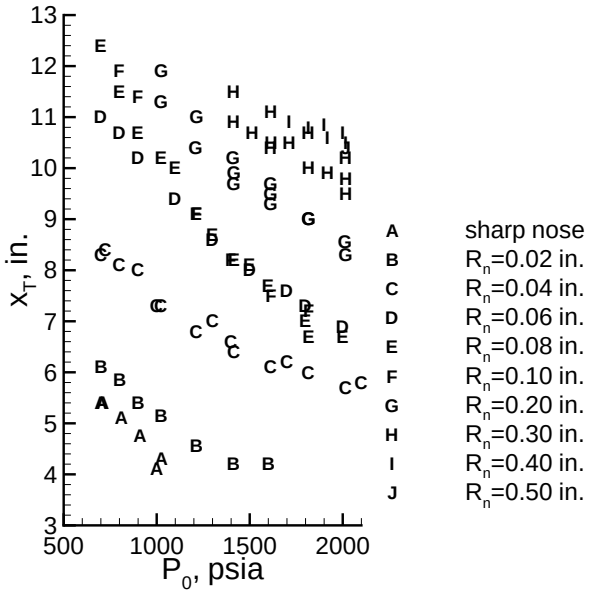

Figure 32: Transition Locations on Blunt Cone at Mach 6

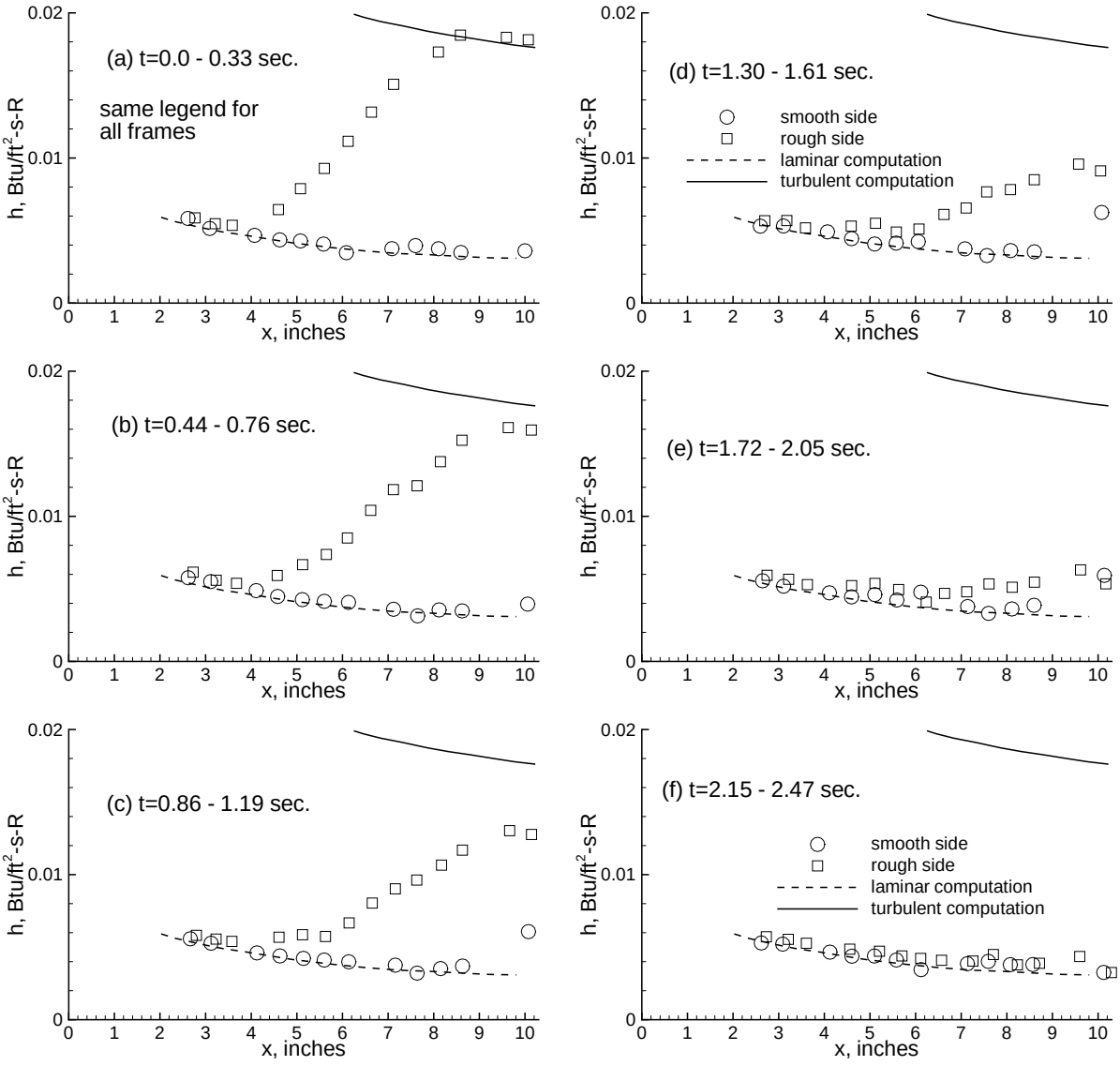

Figure 33: Effect of Nosetip Roughness on Frustum Transition for a Blunt Cone

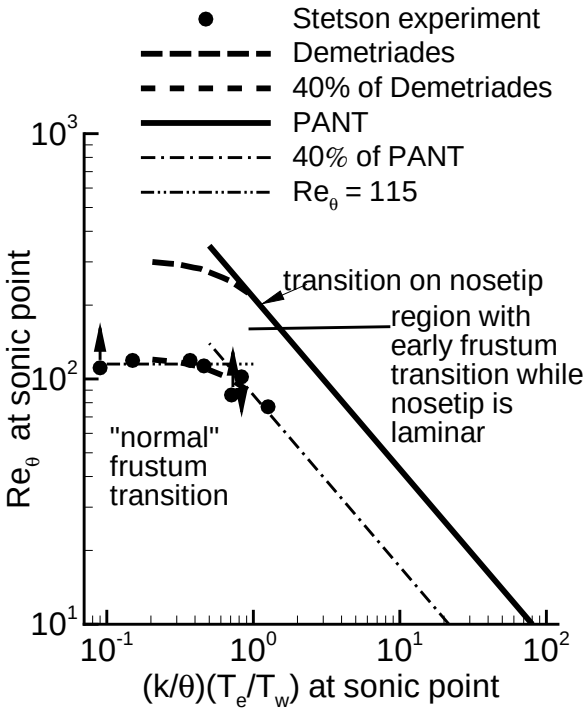

Figure 34: Nosetip Roughness Effect on Cone Frustum Transition

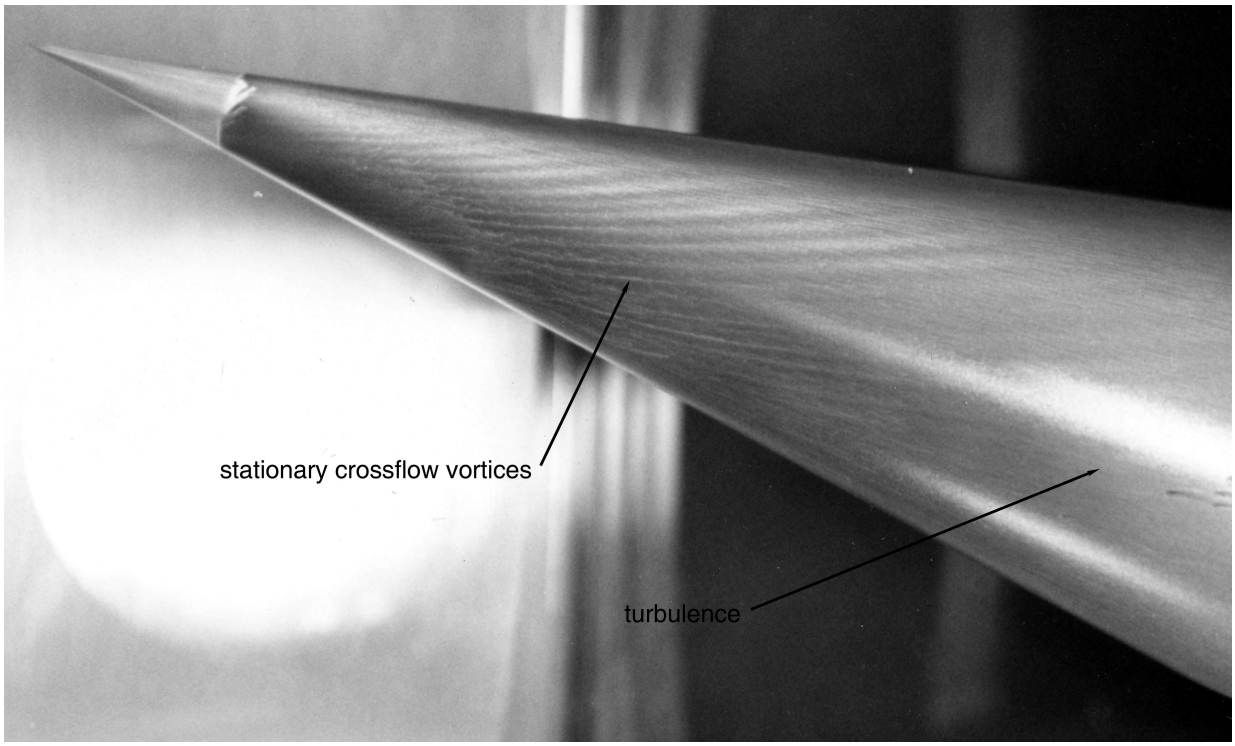

Figure 35: Crossflow Vortices on a Sharp Cone at Angle of Attack

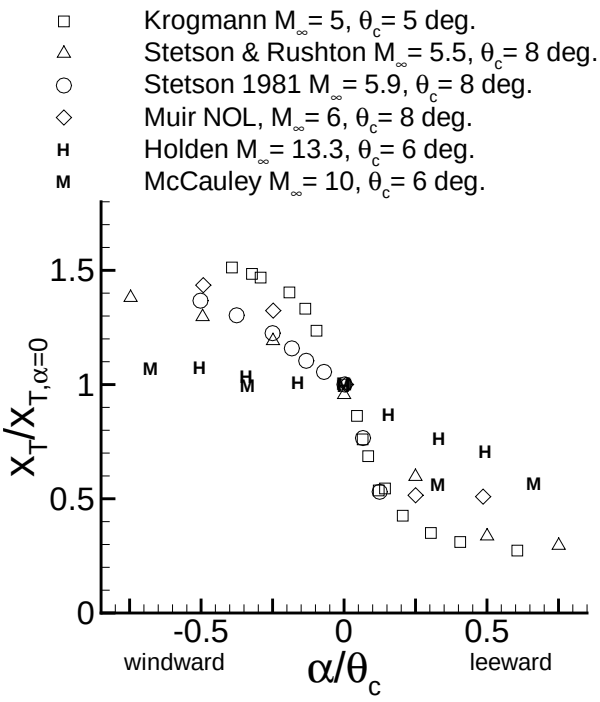

Figure 36: Transition on Sharp Cones at Angle of Attack

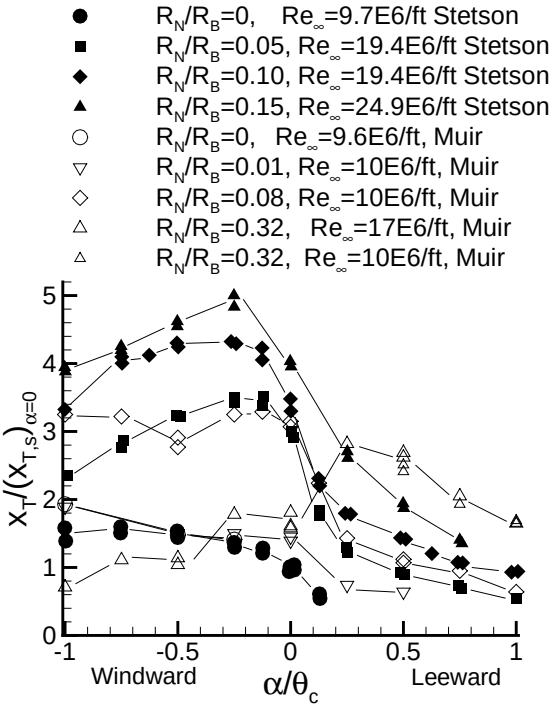

Figure 37: Transition on Blunt Cones at Angle of Attack and Mach 6

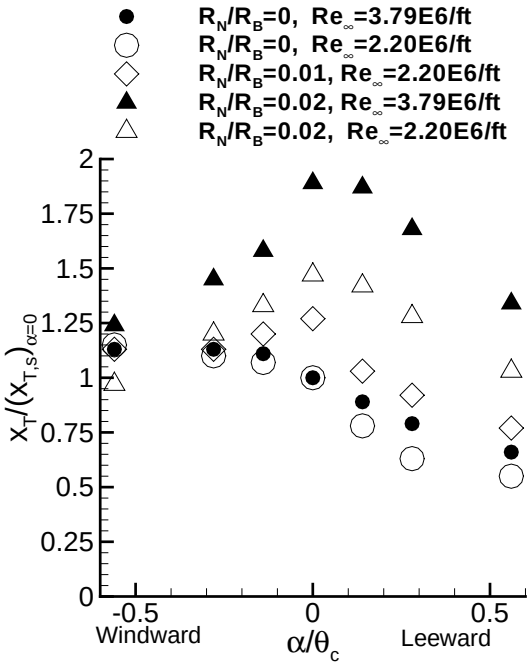

Figure 38: Transition on Blunt Cone at Angle of Attack and Mach 8

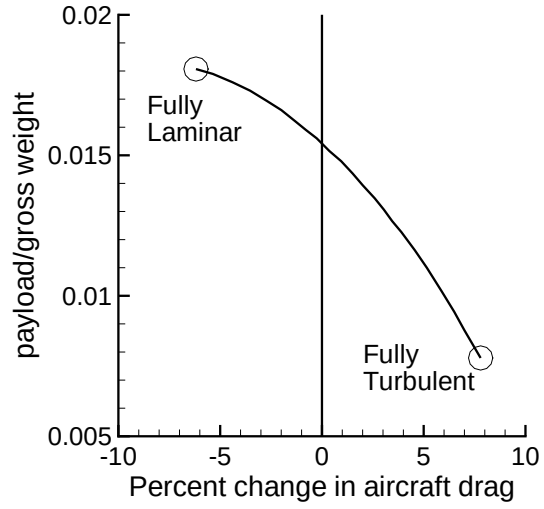

Figure 39: Effect of Transition on NASP Design

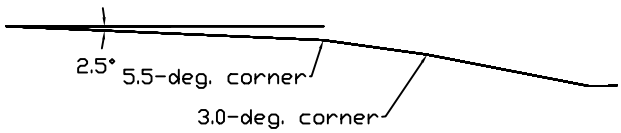

Figure 40: Side View of Hyper2000 Forebody